

DAMAGE ANALYSIS AND ASSESSMENT IN BRIDGE LIKE STRUCTURES
DUE TO
HIGH EXPLOSIVE BLAST LOAD

A THESIS SUBMITTED TO
THE GRADUATE SCHOOL OF NATURAL AND APPLIED SCIENCES
OF
MIDDLE EAST TECHNICAL UNIVERSITY

BY

ÖMER ERDOLU

IN PARTIAL FULFILLMENT OF THE REQUIREMENTS
FOR
THE DEGREE OF MASTER OF SCIENCE
IN
AEROSPACE ENGINEERING

DECEMBER 2016

Approval of the thesis:

**DAMAGE ANALYSIS AND ASSESSMENT IN BRIDGE LIKE
STRUCTURES DUE TO HIGH EXPLOSIVE BLAST LOAD**

submitted by **ÖMER ERDOLU** in partial fulfillment of the requirements for the degree of **Master of Science in Aerospace Engineering, Middle East Technical University** by,

Prof. Dr. Gülbin Dural Ünver
Dean, Graduate School of **Natural and Applied Sciences**

Prof. Dr. Ozan Tekinalp
Head of Department, **Aerospace Engineering**

Prof. Dr. Altan Kayran
Supervisor, **Aerospace Engineering Dept., METU**

Examining Committee Members:

Assoc.Prof. Dr. Demirkan Çöker
Aerospace Engineering Dept., METU

Prof. Dr. Altan Kayran
Aerospace Engineering Dept., METU

Asst. Prof. Dr. Ercan Gürses
Aerospace Engineering Dept., METU

Assoc. Prof. Dr. Ferhat Akgül
Engineering Sciences Dept., METU

Asst. Prof. Dr. Mustafa Kaya
Aeronautical Engineering Dept., YBU

Date: 26.12.2016

I hereby declare that all information in this document has been obtained and presented in accordance with academic rules and ethical conduct. I also declare that, as required by these rules and conduct, I have fully cited and referenced all material and results that are not original to this work.

Name, Last name : Ömer Erdolu

Signature :

ABSTRACT

DAMAGE ANALYSIS AND ASSESSMENT IN BRIDGE LIKE STRUCTURES DUE TO HIGH EXPLOSIVE BLAST LOAD

Erdolu, Ömer

M.Sc., Department of Aerospace Engineering

Supervisor : Prof. Dr. Altan Kayran

December 2016, 132 pages

In recent years, number of explosion attacks on civilian structures is on rise. Fast methods for damage analysis of civilian structures exposed to external blast loads are especially important in the preliminary design stage of structures to implement frequent design changes to come up with more resistant structures. Single degree of freedom (SDOF) approach is a preferable method for fast damage analysis of structures exposed to blast loads. In this thesis, a new damage level calculation tool for external blast loaded bridge-like-structures is developed based on the SDOF approach. The damage assessment tool developed analyzes the blast phenomenon and the subsequent damage induced in three phases. In the first phase, free propagation of the blast wave up to structure is considered. In the

second phase, accurate calculation of the impulsive work on the structure is performed and in the third phase structural response is used to compute the damage level. Free propagation of the blast wave is taken into account by considering height of the burst, the scaled distance and the cases; fully incident wave of close-in explosion, combination of incident wave and Mach Stem and formation of full Mach Stem. Impulsive work on the structure is calculated by considering the spatial variation of the overpressure along the structure as well as the temporal variation of the overpressure. For this purpose, the structure is discretized into several pieces. For the structural response, SDOF methodology is utilized in order to determine the maximum deflection and hinge rotation in the concrete column by means of the DoD response criteria for anti-terrorism design. Case studies are performed for two concrete columns with different cross-sections. For the two columns studied, optimum number of divisions is determined for the calculation of the impulsive work on the structure subjected to the blast load. For the verification of the developed tool, comparison of the results obtained by the tool is performed with the results obtained by the explicit finite element solver AUTODYN and SDOF solver RC BLAST. The modeling in AUTODYN is performed for the fine meshed column and using the Euler domain in order to prevent leakage in the Euler-Lagrange interaction. For the assessment of the damage level in AUTODYN analyses, damage in the element level and damage in the column level are determined respectively. In the element level, damage parameter is computed and when the damage factor is equal to 1, the element is assumed to fail and erode. For column failure, existence of non-eroded elements in any section is checked. If elements are eroded throughout the whole cross-section, the structure is assumed not to sustain any load. Results show that the developed tool and RC Blast yield similar results for the failure explosive mass. It is also seen that

if same side-on overpressure levels are used in the developed tool as determined by the AUTODYN analysis, failure explosive mass predicted by the developed code and AUTODYN agree considerably well.

Keywords: External Blast Loading, Blast Analysis, Concrete Column, Damage Assessment, SDOF

ÖZ

PATLAMA YÜKÜNÜN KÖPRÜ TİPİ YAPILAR ÜZERİNDE OLUŞTURDUĞU HASARIN HESAPLANMASI VE DEĞERLENDİRİLMESİ

Erdolu, Ömer

Yüksek Lisans, Havacılık ve Uzay Mühendisliği Bölümü

Tez Yöneticisi : Prof. Dr. Altan Kayran

Aralık 2016, 132 sayfa

Son yıllarda, sivil yapı hedeflerine karşı gerçekleştirilen patlama saldırılarının sayılarında artış meydana gelmiştir. Patlama yüküne maruz kalmış yapı hedeflerine karşı hızlı bir şekilde hasar analizleri yapmak, özellikle sık tasarım değişikliklerine olanak sağlayarak patlama yüküne daha dayanıklı yapı ön tasarımı için önemlidir. Tek serbestlik dereceli sistem yaklaşımı, patlama yüküne maruz kalmış yapı hedefleri için hızlı hasar analizi yapılması konusunda tercih edilen metottur. Bu tezde, dış patlama yüküne maruz kalmış köprü tipi yapılar için yeni bir hasar hesaplama aracı tek serbestlik dereceli sistem yaklaşımı kullanılarak geliştirilmiştir. Geliştirilen hasar hesaplama aracı patlama yükünü ve bunun yarattığı hasarı üç aşamada hesaplar: İlk aşamada, infilak ile oluşan blast dalgasının yapı hedefine ulaşmadan serbest yayılımı dikkate alınır. İkinci aşamada, blast dalgasının yapı hedefi üzerinde yaptığı impulsif işin yüksek doğrulukta hesaplanması gerçekleştirilir. Üçüncü aşamada, yapı hedefinin impulsif iş üzerindeki yapısal tepkisi hesaplanarak

yapının uğradığı hasar hesaplanır. Blast dalgasının serbest yayılımında, patlama yüksekliği, ölçekli mesafenin bulunması dikkate alınır. Bununla birlikte, hedefe yakın patlama durumunda tamamıyla gelen blast dalgalarından oluşan durum, hedefe uzak patlama durumunda gelen blast dalgalarıyla beraber oluşan Mach Stem ve tamamıyla Mach Stem bölgesinden oluşan durumlar hesaplama aracı tarafından hesaba katılır. Yapı üzerinde yapılan impulsif iş, basıncın yapı üzerindeki değişimi ve zamana göre değişimi dikkate alınarak hesaplanmaktadır. Bu amaçla, yapı hedefi birkaç bölgeye ayrıklaştırılır. Yapısal tepkinin ve hasar miktarının hesaplanması, tek serbestlik derecesi yöntemiyle yapı üzerindeki en yüksek sehim ve destek bölgelerindeki açılma dönüş miktarları belirlenerek, DoD anti terörizm hasar seviyesi kriterlerine göre gerçekleştirilir. Örnek olay incelemesi, farklı kesit alandaki iki betonarme kolon üzerinde yapılmıştır. İki örnek kolon için, yapının maruz kaldığı impulsif işin yüksek doğrulukta hesaplanması için en iyi bölünme sayısı belirlenmiştir. Geliştirilen hasar hesaplama aracının doğrulanması, sonlu eleman çözüm programı AUTODYN ve tek serbestlik derece yöntemini kullanan RC BLAST programının sonuçlarının karşılaştırılması ile yapılmıştır. AUTODYN modellemesi, yüksek eleman sayısı ile kolonun modellenmesi ve Euler-Lagrange etkileşimi esnasında sızıntının olmaması için Euler alanının çözüm ağının oluşturulmasına dikkat edilerek gerçekleştirilmiştir. AUTODYN analizlerinde hasar değerlendirmesi yapılırken, eleman seviyesinde hasar ve kolon seviyesinde hasar sırası ile belirlenmiştir. Eleman seviyesinde, hasar parametresi hesaplanması yapılır ve hasar parametresinin bir olduğu durumda, eleman başarısızlığa uğrayarak erozyona uğrar. Kolon seviyesinde ise, herhangi bir kesit alan üzerinde erozyona uğramamış elemanları varlığı kontrol edilir. Tüm kesit alan boyunca elemanlar erozyona uğramışsa, yapının artık yük taşıyamacağı varsayılmıştır. Sonuçlara bakıldığında, geliştirilen hesaplama aracı ve RC BLAST programının kolonu başarısızlığa uğratabilecek patlayıcı ağırlığı hesaplamasında yakın sonuçlar verdiği görülmüştür. Ayrıca, AUTODYN analizlerindeki gelen dalga basınç değerleri ile geliştirilen kodun basınç değerleri aynı değere getirildiğinde, kolonu başarısızlığa uğratabilecek patlayıcı ağırlığı hesaplamasında geliştirilen kodun ve AUTODYN programının önemli ölçüde uyumlu geldiği görülmüştür.

Anahtar Kelimeler: Dış Patlama Yüğü, Blast Analizi, Betonarme Kolon, Hasar Deęerlendirmesi, Tek Serbestlik Derecesi

To My Family

ACKNOWLEDGEMENTS

The author wishes to express his deepest gratitude to his supervisor Prof. Dr. Altan Kayran and Dr. Hüseyin Emrah Konokman for their guidance, advice, criticism, encouragements and insight throughout the research.

This study was supported by The Scientific and Technological Research Council of Turkey - Defense Industries Research and Development Institute (TÜBİTAK - SAGE).

TABLE OF CONTENTS

ABSTRACT	v
ÖZ.....	viii
ACKNOWLEDGEMENTS.....	xii
TABLE OF CONTENTS.....	xiii
LIST OF TABLES	xv
LIST OF FIGURES.....	xvii
LIST OF SYMBOLS	xxiii
LIST OF ABBREVIATIONS	xxvii
1. INTRODUCTION.....	1
1.1. Literature Survey for Studies of Structures Exposed to Blast Load .	11
1.2. Objective and Outline of the Thesis	19
2. THEORY	21
2.1.....Blast Phenomenon and Propagation in Unconfined Free Air Burst	21
2.2..... Blast Propagation in Unconfined Air Burst and Formation of the Mach Stem	34
2.3.....Impulsive Work on the Structure	40
2.4..... Material Behavior and the Structural Response	51
2.5..... Single Degree of Freedom (SDOF) Method and the Failure Criteria	59

3. DEVELOPMENT OF THE BLAST LOAD INDUCED DAMAGE	
CALCULATION TOOL	67
3.1..... Blast Propagation up to the Structure	
.....	69
3.2..... Interaction of Blast Wave with the Structure	
.....	77
3.3...Material Behavior and the Structural Response Due to Blast Loading	
.....	82
4. RESULTS OF DAMAGE ASSESSMENT OF STRUCTURES	
SUBJECTED TO BLAST LOADING	85
4.1..... Effect of the Number of Divisions on the Results	
.....	88
4.2..... Blast Induced Failure Assessment Using AUTODYN	
.....	93
4.3..... Blast Induced Failure Assessment Using RC BLAST	
.....	100
4.4..... Assessment of the Results	
.....	104
5. CONCLUSION AND FUTURE WORK	119
REFERENCES	123
APPENDICES	129
APPENDIX A: VIEW OF THE DEVELOPED TOOL	129
APPENDIX B: DERIVATION OF MASS AND LOAD FACTOR	130

LIST OF TABLES

Table 1. Effect of Vehicle Bomb Attack on Civilian Areas [3]	3
Table 2. SDOF Method Compared to the Test Results [17].....	17
Table 3. TNT Equivalency Factor For Some Explosives [23]	25
Table 4. KingeryBulmarsh Coefficients for the Calculation of the Side-on Overpressure [29]	30
Table 5. Kingery Coefficients for the Calculation of the Scaled Time of Arrival, Scaled Positive Phase Duration and the Shock Front Velocity [29]	31
Table 6. Blast Loading Categories in Different Propagation Medium [32]	34
Table 7. Scaled Triple Point Height as Function of Scaled Distance for Different Scaled Charge Heights [37]	38
Table 8. Mach Stem Pressure as Function of the Angle of Incidence for Different Scaled Charge Heights [37]	39
Table 9. Kingery Coefficients for the Calculation of the Shock Front Velocity	50
Table 10. Rear Wall Drag Coefficients [23].....	50
Table 11. Dynamic Increase Factor for Far and Close-in Design Ranges [22].....	54
Table 12. Strength Increase Factor Values for Different Materials [42]	54
Table 13. Age Factor for Concrete [19]	54
Table 14. Failure Criteria Published by Department of Defense of the US Army for Antiterrorism Design [23].....	58
Table 15. Load and Mass Factors for Different Boundary Conditions and Loading Used in the SDOF Method [43].....	61
Table 16. Maximum Resistance for Different Loading and Boundary Conditions for a Beam/Column Structure Supported at Both Ends [43]	64
Table 17. Elastic and Plastic Section Modulus for Rectangular Cross Section [44] .	65

Table 18. Stiffness of Beams/Columns for Different Loading and Boundary Conditions [43].....	66
Table 19. Comparison of Side-on Overpressure Calculations	72
Table 20. Comparison of Side-on Overpressure Calculations (Continued)	74
Table 21. Fit Functions Used for the Calculation the Coefficient of Reflection for Side-On Pressures in the Range 200 – 5000 Psi	80
Table 22. Variation of the Required Amount of TNT Explosive Mass [kg] for Failure of Sample Columns with the Number of Divisions	92
Table 23. Explosive masses used in the Wedge Method	94
Table 24. Mesh Density used in Modeling the Concrete Column [7]	96
Table 25. Material Constants for Damage Factor Calculation	98
Table 26. Failure Mass of the Explosive Calculated by RC-BLAST	103
Table 27. First Set of AUTODYN Analysis	105
Table 28. Results of First Set of AUTODYN Analysis.....	108
Table 29. Results of Second Set of AUTODYN Analysis	109
Table 30. Comparison of Explosive Masses Calculated by the Present Study, RC-Blast and AUTODYN.....	111
Table 31. Comparison of Peak Side-on Overpressures Obtained by AUTODYN and the Developed Tool.....	111
Table 32. Comparison of Explosive Masses by the Present Study and AUTODYN	112
Table 33. Comparison of Failure Masses of the TNT Explosive Calculated by AUTODYN and by the Developed Tool at Stand-off Distances 1m and 5 m	117

LIST OF FIGURES

Figure 1. Strain Rate Range for Different Kinds of Loadings [1].....	1
Figure 2. Amplitude vs Frequency Scale for Different Kinds of Loadings [2]	2
Figure 3. A Bridge in Iraq Damaged by an Explosion [2]	4
Figure 4. Difference in Lagrangian (b) and Eulerian (c) Approaches Using Diving Dinosaur (a) Modeling [6]	7
Figure 5. Lagrangian Computation Cycle [4].....	8
Figure 6. Eulerian Computation Cycle [4].....	9
Figure 7. Euler-Lagrange Coupling in AUTODYN [4].....	10
Figure 8. Gauge Placement in the Study of Sherkar et al. (2003) [7]	11
Figure 9. Comparison of Test and Analysis for Large Stand-off Distance [9]	12
Figure 10. Comparison of Test and Analysis for Small Stand-off Distance [9]	12
Figure 11. Comparison of Test and Analysis [10]	13
Figure 12. Comparison of Test and Analysis [11]	13
Figure 13. Effect of Concrete Column Deflection as a Function of the Stand-off Distance [12].....	14
Figure 14. Pressure Variation on the Steel Plate Exposed to Blast Load [14]	14
Figure 15. Principal Plastic Strain Variation on the Deck and the Girder Exposed to Blast Load [16]	15
Figure 16. High Level of Damage [19].....	16
Figure 17. Low Level of Damage [19]	16
Figure 18. Process of Detonation of an Explosive [20]	21
Figure 19. Propagation of the Blast Wave in Air Medium [21]	22
Figure 20. Side-on Pressure as Function of Stand-off Distance [12].....	23

Figure 21. Pressure vs. Time Blast Curve [22]	24
Figure 22. Side-on Overpressure P_{so} and Impulse I_s , Reflected Overpressure P_r and Impulse I_r , Time of Arrival t_a , Time of Duration t_o , Shock Velocity U_s as a Function of the Scaled Distance [22].....	28
Figure 23. Comparison of Blast-Wave Overpressure and Dynamic Pressure [31]	32
Figure 24. Variation of the Dynamic Pressure with the Peak Side-on Overpressure [32].....	33
Figure 25. Categorization of Unconfined Blast Propagation [34]	34
Figure 26. Blast Wave Hitting the Ground and Mach Stem Formation [36]	35
Figure 27. Path of the Triple Point [22].....	36
Figure 28. Mach Stem Formation and its Interaction with the Structure [9]	40
Figure 29. Close-in Explosion and Fully Incident Wave Impinging on the Structure	40
Figure 30. Angle of Incidence with respect to the Different Points on the Structure	41
Figure 31. Comparison of the Face-on and the Side-on Overpressures [38]	42
Figure 32. Variation of the Coefficient of Reflection with the Angle of Incidence for different Side-on Pressures [22]	43
Figure 33. Blast Loading on a Structure [19]	44
Figure 34. Front Wall Blast Loading Overpressure vs. Time Curve [22]	45
Figure 35. Height, Width and Length Definition for Sample Column	46
Figure 36. Sound Velocity as Function of the Peak Side-on Overpressure [23]	46
Figure 37. Overpressure vs. Time Curve for the Rear Wall Loading [23]	47
Figure 38. Rear Wall Loading	48
Figure 39. Equivalent Load Factor CE [32]	49
Figure 40. Girder Type Bridge	51
Figure 41. Components of Girder Type Bridge [18]	52

Figure 42. Strain Rate Effect on the Concrete [40]	53
Figure 43. Elastic, Elastic-Plastic and Plastic Regime.....	55
Figure 44. Plastic Hinge Formation for the Blast Loaded Column [19] and the Beam [43]	56
Figure 45. Maximum Deflection and Support Rotation [23]	57
Figure 46. SDOF Simplification of a Structural System	59
Figure 47. Displacement Characteristics for Different Blast Loading [5]	60
Figure 48. Conversion of the Continous Structural System into Discrete SDOF System	61
Figure 49. Main Flowchart of the Assessment of Blast-Induced Damage	67
Figure 50. Mach Stem Formation.....	70
Figure 51. Analysis of the Blast Wave up to the Structure.....	71
Figure 52. Calculation of the Equivalent Weight of the Explosive	71
Figure 53. Comparison of Side-on Pressures Determined by Tests and Calculated by Kingery's Empirical Formula.....	75
Figure 54. Analysis of the Interaction of the Blast Wave with the Structure	77
Figure 55. Variation of the Scaled Distance Along the Structure	78
Figure 56. Variation of the Scaled Distance with the Height of the Structure	78
Figure 57. Variation of the Scaled Distance Due to Increase in Distance	79
Figure 58. Ratio of the Front Wall Loading to the Rear Wall Loading as a Function of the Scaled Distance	81
Figure 59. Calculation of Dynamic Strength.....	82
Figure 60. Calculation of the Structural Response.....	83
Figure 61. Cross Sections of Sample Columns	88
Figure 62. Sample Column Division with 10 Segments without/with Mach Stem Region (MSR).....	89

Figure 63. Variation of the Required Amount of TNT Explosive for the 1 m Stand-Off Distance to Fail the Sample Columns with the Number of Divisions	90
Figure 64. Variation of the Required Amount of TNT Explosive for the 2.5 m Stand-Off Distance to Fail the Sample Columns with the Number of Divisions	90
Figure 65. Variation of the Required Amount of TNT Explosive for the 5 m Stand-Off Distance to Fail the Sample Columns with the Number of Divisions	91
Figure 66. Variation of the Required Amount of TNT Explosive for the 10 m Stand-Off Distance to Fail the Sample Columns with the Number of Divisions	92
Figure 67. Wedge Modeling of TNT Explosive and Air	93
Figure 68. High Pressurized Gases and Wavefront in Wedge Modeling	94
Figure 69. Mapping of the Pressure and Velocity Information of High Pressurized Gases into 3D Euler Domain	95
Figure 70. Euler and Lagrange Domain for the Interaction	97
Figure 71. Loss of Structural Integrity Utilizing the Failure Erosion Criteria	99
Figure 72. General Member Properties for the Load-Deformation Curve	100
Figure 73. Material and Section Properties for the Load-Deformation Curve.....	101
Figure 74. Sample Output of Moment-Curvature	101
Figure 75. Displacement vs. Time History Curve as a result of explosion of 10 kg of TNT.....	102
Figure 76. Displacement vs. Time History Curve as a result of explosion of 20 kg of TNT.....	103
Figure 77. Displacement vs. Time History Curve as a result of explosion of 25 kg of TNT.....	103
Figure 78. Effect of 45 kg TNT Explosion on the 0.5x0.5x5m Concrete Column..	106
Figure 79. Effect of 60 kg TNT Explosion on the 0.5x0.5x5m Concrete Column..	107
Figure 80. Effect of 50 kg TNT Explosion on the 0.5x0.5x5m Concrete Column..	110
Figure 81. Distribution of the Face on Overpressure along the Structure for a Stand-off Distance of 1 m.....	113

Figure 82. Distribution of the Face on Overpressure along the Structure for a Stand-off Distance of 3 m.....	114
Figure 83. Distribution of the Face on Overpressure along the Structure for a Stand-off Distance of 5 m.....	114
Figure 84. Distribution of the Face on Overpressure along the Structure for a Stand-off Distance of 10 m.....	115
Figure 85. Effect of 450 kg TNT Explosion on the 0.5x0.5x5m Concrete Column	116
Figure 86. Distribution of the Face on Overpressure along the Structure Exposed to 450 kg of TNT Explosive for a Stand-off Distance of 5 m	117

LIST OF SYMBOLS

A	Loaded area
A_v	Area of Reinforcement Bars
b	Effective Width of R/C
c	Damping Coefficient
C	Mass of charge (explosive)
C_D	Drag Coefficient
C_E	Equivalent Uniform Pressure Factor
C_r	Sound Velocity
d	Effective Depth of R/C
D	Damage Factor
F	Uniform or Point Load on Structure
f'_c	Yield Strength of Concrete
f_{dy}	Dynamic Yield Strength of Material
f_{du}	Dynamic ultimate strength of material
f_{dv}	Shear Strength of Steel
f_{du}	Dynamic yield strength of material
f_u	Static ultimate strength of material
f_y	Static yield strength of material
G	Maximum of Height or Width of Structure
H_c^w	Scaled Charge Height
H_T^w	Scaled Triple Point Height
I	Impulse
I_{SDOF}	Impulse of SDOF System
k	Stiffness of SDOF System
L	Length of Structure
L_w	Positive Phase Wave Length
M	Mass of Metal Casing

M_p	Plastic Moment Capacity of Structure
M_{SDOF}	Mass of SDOF System
m	Lumped Mass of Structure in SDOF System
n	Number of Reflective Surface
$P(t)$	External Blast Load as Function of Time
P_O	Ambient Pressure
P_a	Effective Overpressure for Rear Wall
P_{FO}	Face-on (Reflected) Overpressure
P_s	Stagnation Pressure
P_{SO}	Side-on Overpressure
P_R	Face-on (Reflected) Overpressure
q	Dynamic Pressure
R	Stand-off Distance
R_{yield}	Maximum Resistance Force of SDOF System
s	Rebar Spacing
S	Minimum of Height or Width of Structure
S_m	Elastic Section Modulus of Structure
S_x	Distance from nearest free edge to point of interest
t_a	Time of Arrival
t_c	Clearing time
t_d	Positive Phase Duration
t_e	Equivalent Time
t_r	Rise time
T	Period of SDOF System
U_s	Shock Front Velocity
V	Dynamic Reaction of Supports
V_C	Shear Strength of R/C Contributed by Concrete
V_N	Shear Strength of R/C
V_S	Shear Strength of R/C Contributed by Steel Bars
W	Mass of Explosive

$W_{impulse,SDOF}$	Impulsive Work Done on SDOF System
$W_{SDOF,el,max}$	Work Limit for Elastic Deflection of SDOF System
W_e	Equivalent Mass of TNT Explosive
W_U	Uncased Mass of Explosive
Z	Scaled Distance
Z_m	Plastic Section Modulus of Structure

GREEK LETTERS

β	Angle of Incidence
Δ	Deflection
$\Delta\varepsilon^p$	Accumulated plastic strain
Δ_{max}	Maximum Deflection
ε	Angle Criteria for Mach Stem Formation
ε^f	Failure strain
θ	Support Rotation
μ	Ductility Ratio
ρ	Air density of compressed zone

LIST OF ABBREVIATIONS

BC	Boundary Condition
CoR	Coefficient of Reflection
DIF	Dynamic Increase Factor
ft	feet
FW	Front Wall
Ksi	Kilopound-force per square inch
ln	Natural Logarithm
m	meter
NCHRP	National Cooperative Highway Research Program
NoD	Number of Division
Psi	pound-force per square inch
R/C	Reinforced Concrete
RW	Rear Wall
SDOF	Single Degree of Freedom
SIF	Strength Increase Factor
TNT	Trinitrotoluen
TPH	Triple Point Height

CHAPTER 1

INTRODUCTION

Blast is the sudden release of huge amount of energy due to an explosion within very short period of time. A typical blast phenomenon lasts in the range of 0.5 to 1 milliseconds with the loading in the range of several thousands of psi [1]. Blast is a type of dynamic loading. Civilian structures are exposed to dynamic type of loading in nature such as wind and earthquake. Wind, compared to earthquake and blast, is a low intensity loading and does not result in high level of damage, disregarding giant typhoons. On the other hand, earthquakes cause civilian structure to damage moderately or intensely due to the high transmitted energy coming from the ground. Like earthquakes, blast is high intensity loading causing structures to be devastated. Compared to earthquake, however, blast loading lasts in the range of milliseconds while earthquake has a duration of couple of seconds. Therefore, blast loading can be considered as the most disastrous and dangerous threat for civilian structures.

Intensity and duration of the blast load leads to strain rate phenomenon in structures. Comparison of strain rate levels for structures exposed to dynamic loading is given in Figure 1.

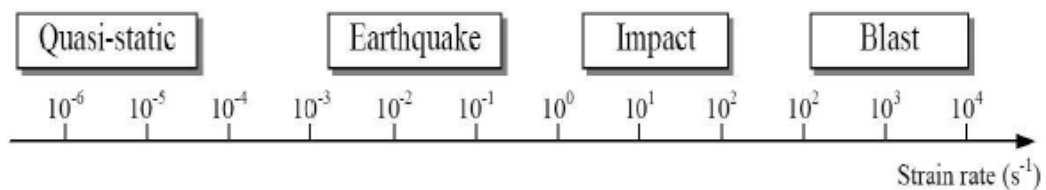


Figure 1. Strain Rate Range for Different Kinds of Loadings [1]

Different types of dynamic loading have different frequency and amplitude and therefore have different effects on the structures. Figure 2 demonstrates the amplitude versus frequency range for different kinds of loading. As seen in Figure 2, blast has the highest amplitude, in other words the highest intensity loading and the frequency range differs in a wide range from low to high.

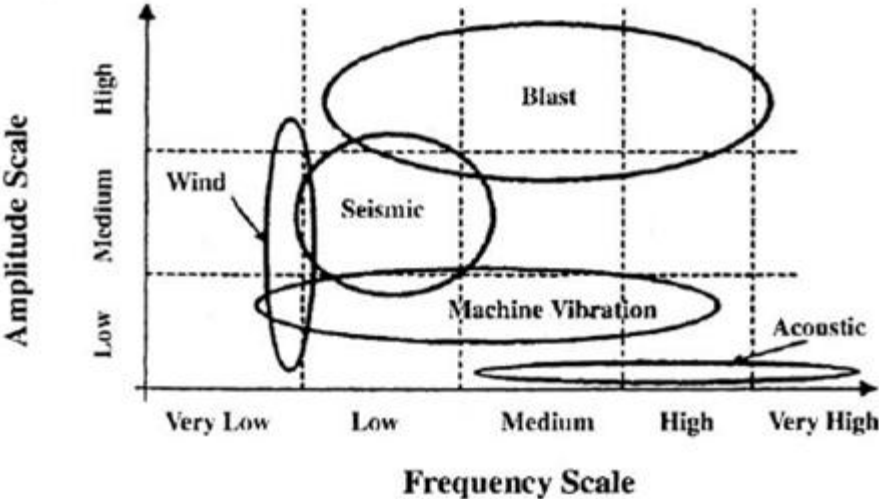
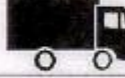
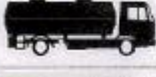


Figure 2. Amplitude vs Frequency Scale for Different Kinds of Loadings [2]

Besides the damage that blast loading causes in the civilian structures, blast loading also causes loss of civilian lives when civilian structures are the targets. Bureau of Alcohol Tobacco Firearms and Explosives, a US federal organization, published a table, given in Table 1, on the damage of vehicle bomb attack in civilian areas [3].

Table 1. Effect of Vehicle Bomb Attack on Civilian Areas [3]

ATF	VEHICLE DESCRIPTION	MAXIMUM EXPLOSIVES CAPACITY	LETHAL AIR BLAST RANGE	MINIMUM EVACUATION DISTANCE	FALLING GLASS HAZARD
	COMPACT SEDAN	500 Pounds 227 Kilos <i>(In Trunk)</i>	100 Feet 30 Meters	1,500 Feet 457 Meters	1,250 Feet 381 Meters
	FULL SIZE SEDAN	1,000 Pounds 455 Kilos <i>(In Trunk)</i>	125 Feet 38 Meters	1,750 Feet 534 Meters	1,750 Feet 534 Meters
	PASSENGER VAN OR CARGO VAN	4,000 Pounds 1,818 Kilos	200 Feet 61 Meters	2,750 Feet 838 Meters	2,750 Feet 838 Meters
	SMALL BOX VAN <i>(14 FT BOX)</i>	10,000 Pounds 4,545 Kilos	300 Feet 91 Meters	3,750 Feet 1,143 Meters	3,750 Feet 1,143 Meters
	BOX VAN OR WATER/FUEL TRUCK	30,000 Pounds 13,636 Kilos	450 Feet 137 Meters	6,500 Feet 1,982 Meters	6,500 Feet 1,982 Meters
	SEMI-TRAILER	60,000 Pounds 27,273 Kilos	600 Feet 183 Meters	7,000 Feet 2,134 Meters	7,000 Feet 2,134 Meters

One of the most highly targeted civilian structures for the blast threat is the bridge structure. Collapse of the bridge due to blast not only causes the loss of structure, but also results in interruption of transportation for some time. Interruption of the transportation in a region disrupts lives of civilians and affects the economic activity significantly. In Figure 3, a damaged bridge in Iraq is seen. The column of the bridge is fully destroyed so that the span of the bridge is collapsed. The bridge cannot function anymore after this attack.



Figure 3. A Bridge in Iraq Damaged by an Explosion [2]

Specialized tools are required to compute damage levels in structures subject to for blast loading. Some finite element solvers such as AUTODYN [4] can handle blast loading and perform damage analysis in the structures exposed to blast loading. However, finite element solvers usually require very long execution times because, due to the highly dynamic nature of the loading, explicit solutions are performed in time domain using very short time intervals. On the other hand, fast responding tools, such as the ones using the SDOF methodology, yield approximate results in couple of seconds. Hence, fast responding tools for damage analysis of bridge like structures subjected to blast loads are important in the preliminary design stage to implement design changes to come up with more resistant structures. There are some tools for this purpose. However, they are either not accessible or restricted to certain scenarios. Fast responding damage assessment tool that is developed within the scope of the thesis allows very fast calculation of damage levels in bridge like structures subject to different blast loading scenarios.

When an explosive detonates, enormous amount of energy is released. High release of energy results in the formation of blast (shock) wave propagating from the detonation point to its surroundings. While the blast wave propagates, the medium is compressed layer by layer. In the compressed zone, pressure rises to very high

values, such as several thousands of psi [1]. Pressure level reached is function of mass of the explosive and the distance from the detonation point to the target, which is known as the stand-off distance. Rise in the pressure level in the compressed zone declines as the blast wave moves away from the detonation point. Depending on the distance and the mass of explosive, the resulting pressure is the key parameter for the damage on the targets.

Predicting the extent of damage incurred in the structures subject to blast loading is very important to develop more resistant structures to blast loading. The blast effect is either observed by conducting series of tests or performing analysis using certain software tools. Conducting tests for blast effects is not practical for three reasons [2]:

- It is troublesome to produce the same blast environment. The temperature, humidity, dust conditions affect the results.
- Due to huge amount of energy release and possible fragment effect, it is difficult to ensure the reliability of sensors and data measurements.
- Experimental blast tests should be conducted in specially designed facilities. Hence, conducting blast tests are costly.

Because of non-practical use of conducting tests, blast analysis is the preferable method to study the blast effects.

In general, there are two main analysis methods for predicting the blast effect on the structures. Finite element method and single degree of freedom analysis method are the two most commonly used methods for the analyzing the response of structures exposed to blast loading. In this thesis, AUTODYN [4] is used as finite element solver whereas RC-BLAST [5] is utilized for SDOF solver to check against the results determined by the fast responding blast loading and damage assessment tool based on SDOF approach which is developed in the thesis study.

AUTODYN is an explicit finite element solver, a hydrocode, mainly used to solve dynamic problems involving high strain rates such as high velocity impact, blast loading etc. Hydrocodes are able to solve time-dependent non-linear problems [6].

Fast-occurring high intensity loading such as impact, blast etc. are high strain rate events [4].

Hydrocodes utilize two methods in order to solve non-linear dynamic problems; Lagrangian and Eulerian approach. Both methods consider the the deformation of the body. In the Lagrangian approach, the finite element mesh is attached to the body and the elements in the body are connected with each other. When the body is deformed by the external forces, elements attached to the body are also get distorted. The flow properties are determined by tracking the motion and properties of the particles in time. Lagrangian approach is commonly applicable to analyze low-strain-rate (less than 10^5) events of solid materials. On the other hand, Eulerian approach is utilized for high-strain-rate events. Fluids are generally modeled using the Eulerian approach. In the Eulerian approach, the fluid properties such as pressure, density and velocity are written as functions of space and time. In this approach, the finite elements are fixed and material flows through the elements. In other words, the elements are not distorted [4]. In Figure 4, Eulerian and Lagrangian approaches are compared for a dinosaur diving event. A dinosaur impacts on the ground. In the Lagrangian approach, in the extremely deformed parts of the dinosaur, such as tail and head, the elements are also extremely deformed. In the Eulerian approach, the elements are fixed and dinosaur itself is deformed and flows through fixed elements.

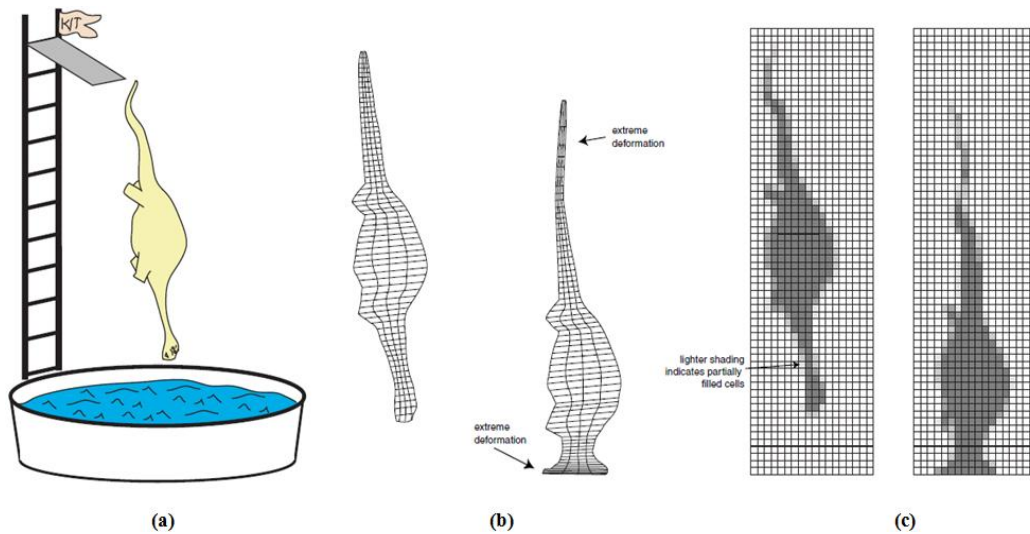


Figure 4. Difference in Lagrangian (b) and Eulerian (c) Approaches Using Diving Dinosaur (a) Modeling [6]

In the Lagrangian computation cycle shown in Figure 5, external force, defined either as boundary condition or interaction, is distributed to the nodes. By using the force-mass relation, nodal forces are converted into nodal accelerations which are integrated to obtain nodal velocities and the displacements. If defined, initial conditions are given as input and using conservation of mass equations, strain rate and density is obtained. Using conservation of energy and equation of state, pressure and internal energy are obtained. Using constitutive relations, deviatoric stresses are found. Finally, using conservation of momentum, nodal forces are determined and one Lagrangian cycle is completed.

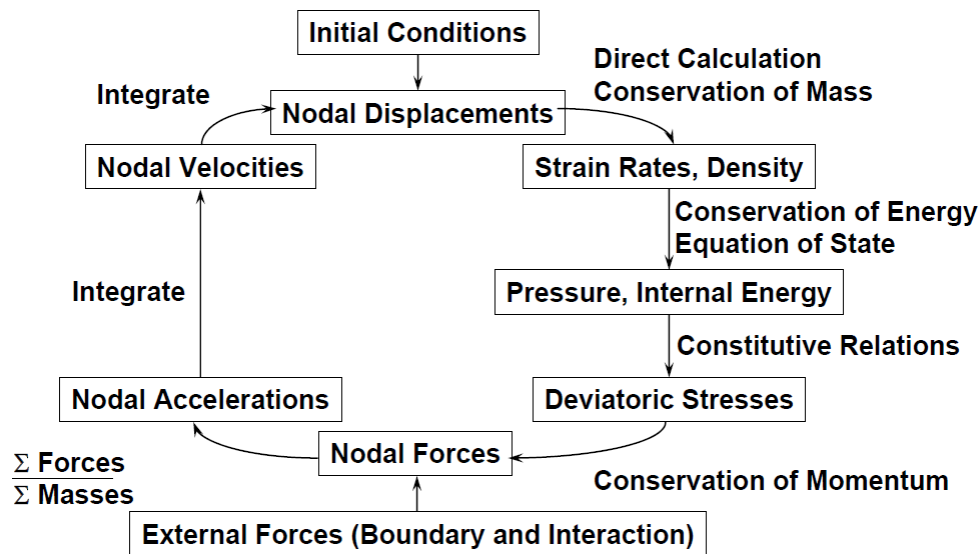


Figure 5. Lagrangian Computation Cycle [4]

In the Eulerian computation cycle shown in Figure 6, external force defined on the boundary is used in order to obtain the face impulses. Face impulse is then converted to nodal accelerations and nodal velocities using momentum-mass relation. Nodal velocities are transported to new cell mass, momentum and energy. Thereafter, using initial conditions, if defined, cell density and strain rates are calculated. Utilizing the conservation of energy and equation of state equations, cell pressure and internal energy are calculated. Then, cell deviatoric stresses are calculated using the constitutive relations. Finally, using the conservation of momentum equations, face impulse is obtained and one Eulerian cycle is completed.

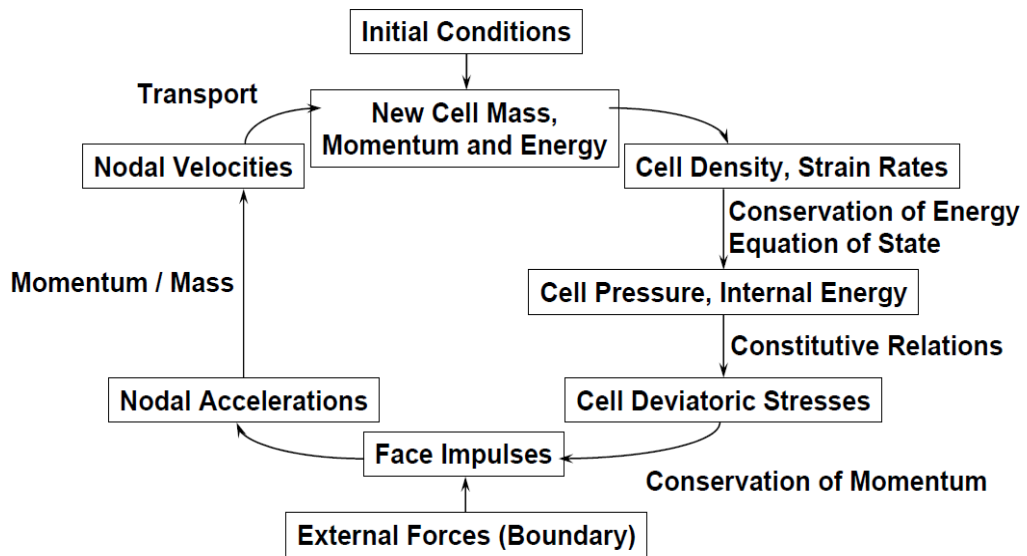


Figure 6. Eulerian Computation Cycle [4]

An AUTODYN analysis can be either Lagrangian or Eulerian or may include Lagrange-Euler coupling. For a bridge-like-structure subjected to blast load studied in this thesis, structure is modeled using the Lagrangian approach whereas the expanded gas led by the shock front is modeled by the Eulerian approach. When the expanded gas led by the shock front impacts the structure, interaction takes place and Euler-Lagrange coupling starts as shown in Figure 7.

Blast wave on a deforming wall (2D)

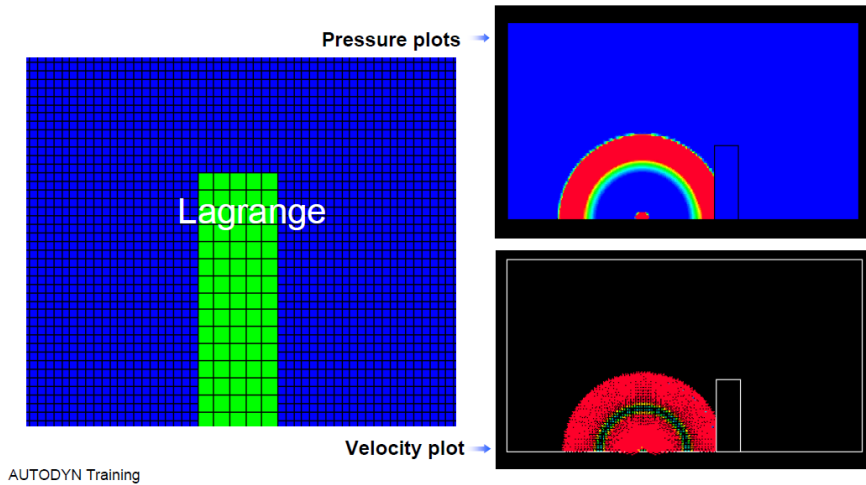


Figure 7. Euler-Lagrange Coupling in AUTODYN [4]

RC Blast [5] is a commercial tool calculating the structural response due to blast loading. It uses Single Degree of Freedom system approach in order to calculate the response. Single Degree of Freedom system simplifies the structure into lumped mass-spring system so that impulsive work input on the system is converted into displacement vs time curve for the given cases. By using the failure criterion written in terms of the displacements of the structure, whether the structure fails or not is determined by RC Blast. The detailed model of the SDOF system is given in Section 2.5.

1.1. Literature Survey for Studies of Structures Exposed to Blast Load

In literature, there are several studies conducting blast analysis and tests for some scenarios. In the study of Sherkar et al. [7] finite element software LS-DYNA [8] is used to investigate the blast resulted pressure on the structure. In this study, three gauges are located on the front face of the concrete column as shown in Figure 8. Pressures after reflection of blast wave on the column are measured. Gauge pressures are compared with the test pressure data.

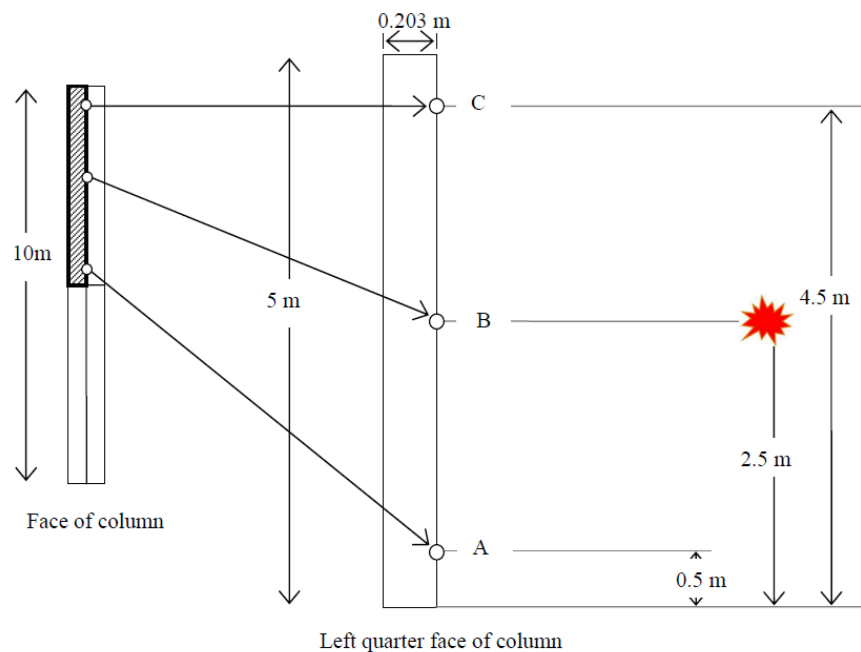


Figure 8. Gauge Placement in the Study of Sherkar et al. (2003) [7]

Williamson et al. [9] conducted experiments and analyses by the finite element software LS-DYNA to study the failure response of a concrete column. Using different explosive masses and different stand-off distances, which is the distance between the detonation point and the target, failure of the concrete column is analyzed. Figure 9 compares the analysis and large stand-off test results of the concrete column that is studied by Williamson et al. [9]. As seen in Figure 9, in the test, damage is observed at bottom of the concrete column and similarly in the analysis; elements at the bottom of the column are seen to erode, as well. In another test group, Williamson conducted small stand-off distance explosion tests. The

results of tests and analyses are compared. For both cases, flexural response of the concrete column is observed as seen in Figure 11. In the analyses, midsection elements are eroded and the concrete column becomes as if it is broken from midsection.

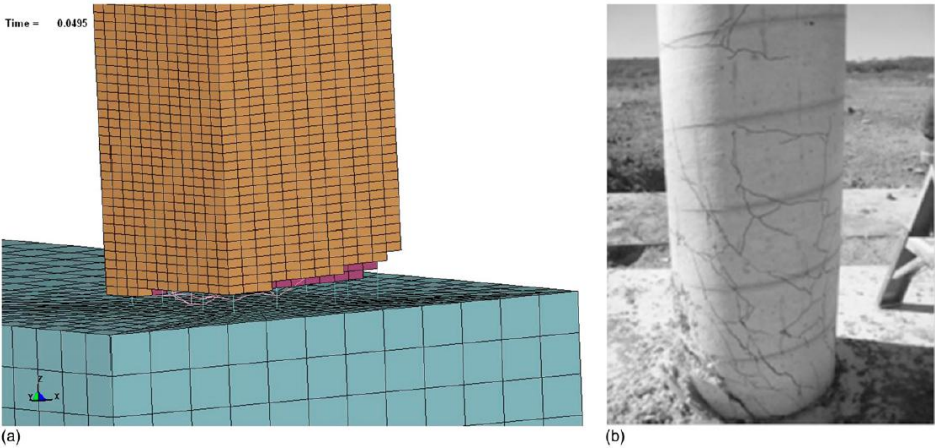


Figure 9. Comparison of Test and Analysis for Large Stand-off Distance [9]

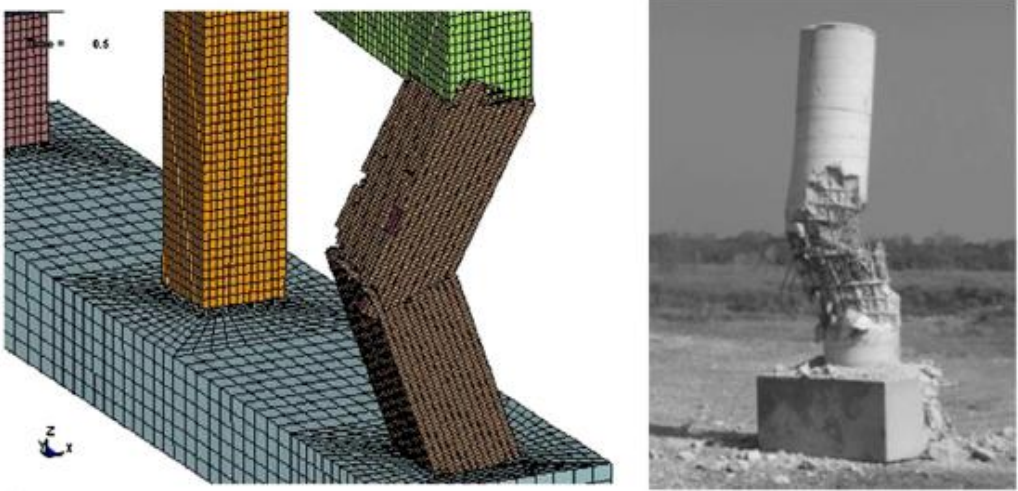


Figure 10. Comparison of Test and Analysis for Small Stand-off Distance [9]

In another study, Fujikara et al. [10] conducted test and performed finite element analysis using LS-DYNA [8] for a concrete column with footing. As seen in Figure 11, shear failure is observed in the footing of the column both in the test and finite element analysis.



Figure 11. Comparison of Test and Analysis [10]

In the study of Matthews et al. [11], finite element simulation LS-DYNA [8] and test results are compared as seen in Figure 12. It is seen that that concrete column tends to be pulled out from the footing due to the stress concentration arising from the cross sectional change between the column and the column cap for the rigidly connected column cap situation.

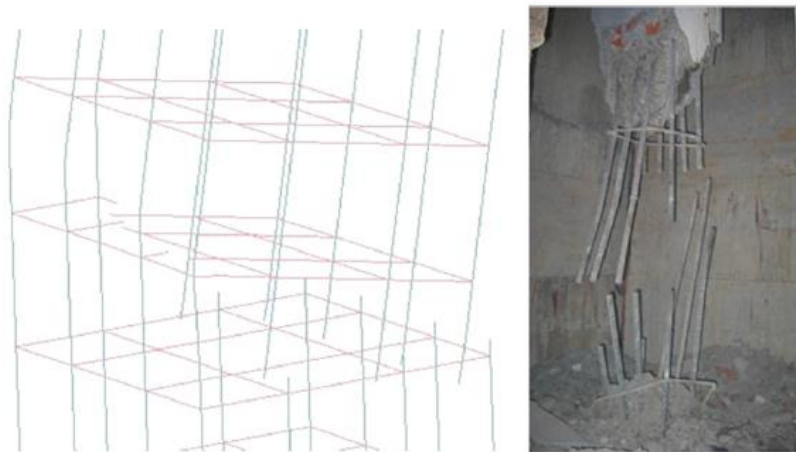


Figure 12. Comparison of Test and Analysis [11]

In the study of Tokal-Ahmed [12], effect of the explosive mass with different stand-off distances is investigated by finite element analysis in ELS software [13]. The change in deflection in the concrete column is observed, as depicted in Figure 13.

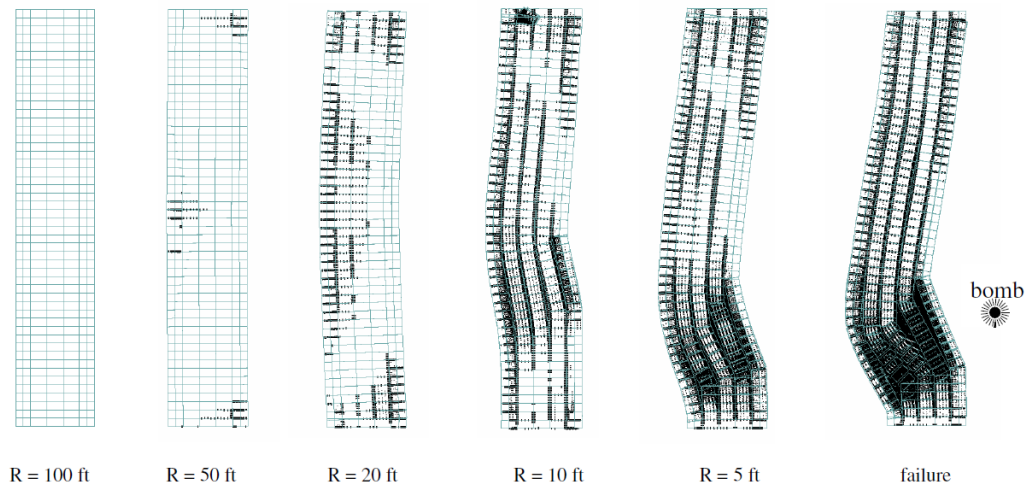


Figure 13. Effect of Concrete Column Deflection as a Function of the Stand-off Distance [12]

Chock [14] used Nastran [15] to calculate the pressure distribution on the steel plate due to the explosion of 20 lb TNT at a stand-off of 24 inches, as shown in Figure 14.

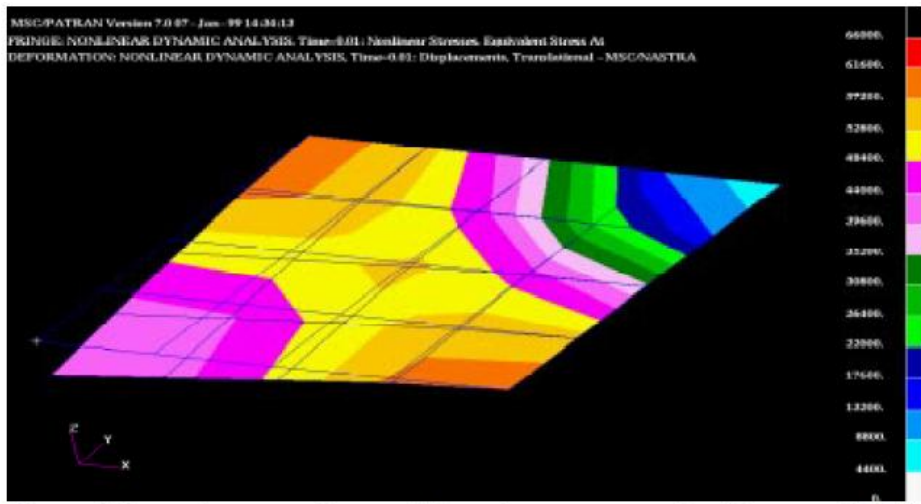


Figure 14. Pressure Variation on the Steel Plate Exposed to Blast Load [14]

Matthews [16] studied the response of a deck and girder assembly which is exposed to the explosion of 250 lb TNT at a stand-off distance of 4 ft. Principal strain distribution on the components is investigated as seen in Figure 15.

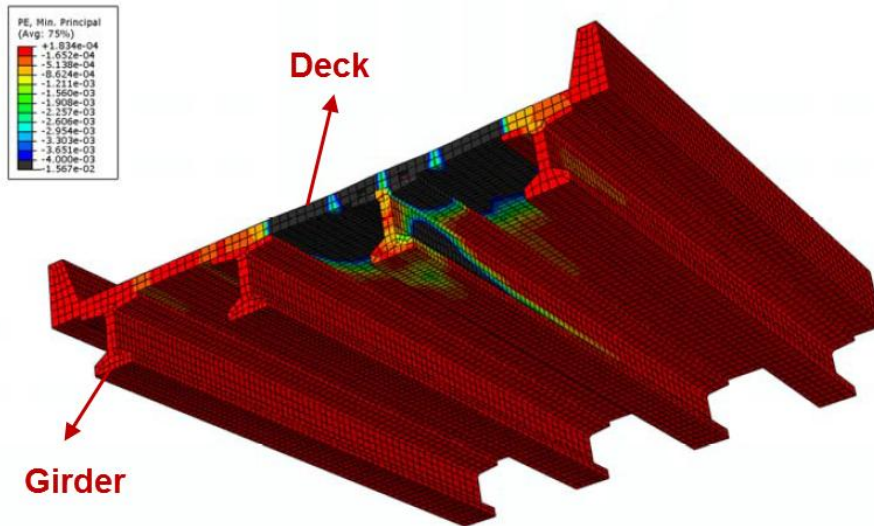


Figure 15. Principal Plastic Strain Variation on the Deck and the Girder Exposed to Blast Load [16]

In addition to blast analysis, results of a series of tests conducted are presented in the NCHRP report [19]. By changing the mass of explosive and the stand-off distance, columns are exposed to the blast loading. As shown in Figure 16, for small stand-off distance test, high level of damage and deflection occur on the column. For large stand-off distance test, low level damage occurs on the column, as shown in Figure 17 and the column does not deflect considerably.



Figure 16. High Level of Damage [19]

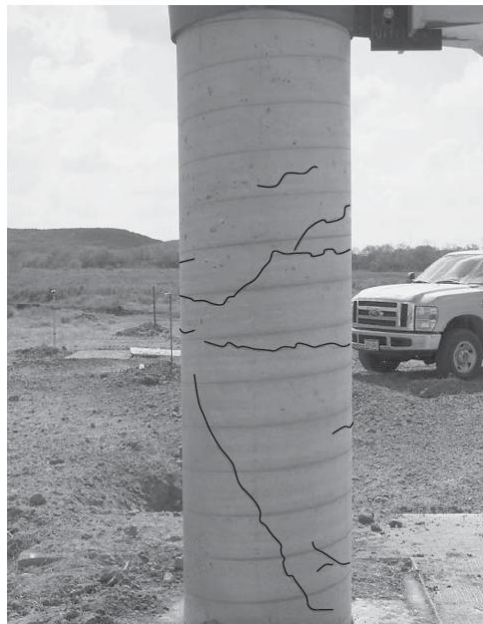


Figure 17. Low Level of Damage [19]

In the study of Oswald et al. [17], series of tests are conducted. In the tests, close-in explosions which have scaled distance less than $1.0 \text{ ft/lb}^{1/3}$ are examined. Moreover, a solver which uses SDOF method is utilized to analyze the response of the structure for the same conditions. Each simply supported concrete slab have 8000 psi compressive strength and 0.66 reinforcement ratio. After conducting the tests, maximum deflection and hinge rotations on the concrete slabs are measured. In addition, maximum deflection and hinge rotation are computed for the same concrete slabs using the SDOF method. Table 2 compares the test and analysis results obtained by the SDOF analysis method. In the last column of Table 2, ratios of the calculated and the measured maximum deformations are given. The ratio ranges from 0.77 to 1.73. In the 6th test, 0.97 ratio is obtained as the best result.

Table 2. SDOF Method Compared to the Test Results [17]

Test No	Length [in]	Thickness [in]	Depth [in]	Max. Measured Deflection [in]	Hinge Rotation [deg]	Calculated Max. Deflection [in]	Ratio of Calculated/Measured
1	250	7.9	6.7	5.2	2.4	4.7	0.90
2	250	7.9	6.7	2.5	1.2	2.1	0.84
3	250	7.9	6.7	0.8	0.4	1.1	1.38
4	250	7.9	6.7	7.9	3.6	11.9	1.51
5	250	7.9	6.7	0.3	0.1	0.5	1.67
6	250	5.3	4.5	2.4	1.1	2.3	0.96
7	250	5.3	4.5	13.4	6.1	23.0	1.72
8	250	5.3	4.5	2.4	1.1	2.7	1.13
9	250	5.3	4.5	11.8	5.4	13.0	1.10
10	250	5.3	4.5	4.9	2.2	3.8	0.78
11	250	5.3	4.5	0.6	0.3	1.0	1.67

As some of the studies taken from the literature show, response of structures exposed to blast loading due to explosion is frequently analyzed by the finite element approach. It should be note that performing blast loading tests is expensive and also dangerous, therefore reliable analysis methods are required to study the response of structures exposed to blast loading in the design stage. However, one drawback of using finite element analysis in studying the response of structures exposed to blast

loading is the high computational cost of the analyses due to the explicit solution method used in the simulation of highly dynamic event such as the explosion. Therefore, there is also a need to develop fast responding tools to obtain approximate solutions for the blast response of the structures. It is considered that approximate solutions can be used to reduce the total number of costly finite element simulations of structures exposed to blast loading significantly. With the approximate solution methods, one can have a baseline design for the structure studied to resist a certain explosion induced loading or can determine an approximate failure explosive mass. Detailed finite element analysis can then be performed utilizing the outcome of the approximate solutions obtained by the fast responding analysis methods.

1.2. Objective and Outline of the Thesis

The main objective of the thesis is to develop a fast-responding tool which is accurate enough for the damage assessment in the columns of bridge structures subjected to blast loading. The objective of the damage assessment could be either the determination of the explosive mass necessary for the complete failure of the column or performing fast preliminary geometric design of concrete columns to withstand the failure for a certain explosive mass. It is also considered that with the developed tool a first estimate of the failure explosive mass can be obtained for detailed AUTODYN analysis and number of AUTODYN trials to determine the failure explosive mass can be reduced in the detailed design and analysis stage.

For this purpose, in this thesis;

- The theory of blast phenomenon is explained in detail in Chapter 2.
- The development of the blast damage tool is explained with aid of flowcharts in Chapter 3.
- Modeling in AUTODYN and RC BLAST is given Section 4.2 and Section 4.3, respectively.
- The results of the developed fast responding tool, AUTODYN and RC BLAST are compared and assessment of the results is presented in Section 0.
- Concluding remarks and future work are given in Chapter 5.
- In Appendix A, a view of the developed tool is given.
- In Appendix B, derivation of load and mass factors used in SDOF conversion is presented.

CHAPTER 2

THEORY

2.1. Blast Phenomenon and Propagation in Unconfined Free Air Burst

Blast is a phenomenon formed by the detonation of an explosive generating enormous energy suddenly. The sudden energy release results in the formation of blast (shock) wave. When an explosive detonates, starting from the detonation point of the explosive, blast wave begins to propagate in the explosive medium first. After reaching the boundary of explosive, blast wave front starts to compress the air layer by layer and continues to propagate. In the compressed air, blast wave moves supersonically. Fast-moving blast wave's velocity drops as it moves away from the detonation point and reaches the speed of sound in the uncompressed air medium [18]. Figure 18 shows the propagation process of the blast wave both inside the explosive and outside the explosive. Led by the shock wave front, expanded gas causes dynamic pressure. Dynamic pressure is defined as the pressure of the resulting air flow of the expanding gas [19].

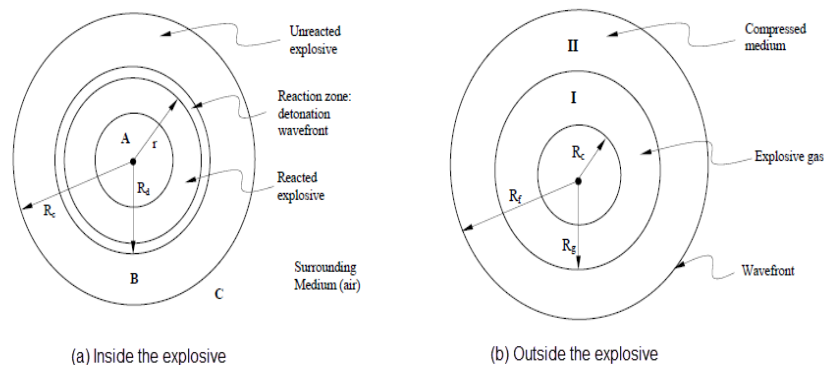


Figure 18. Process of Detonation of an Explosive [20]

As the blast wave propagates through air medium, pressure increases dramatically in the compressed zone. In blast terminology, pressure in the compressed zone is called as “side-on (incident) overpressure”. “Overpressure” term is another usage of the gage pressure, which is the pressure difference between the absolute pressure and the atmospheric ambient pressure. “Side-on overpressure” depends strictly on the mass of the explosive and on the stand-off distance. Stand-off distance is the distance between detonation point and the location where the pressure is to be measured. For instance, in Figure 19, a spherical explosive detonates at the location (0,0) and the blast wave moves in a spherical manner. At time t_1 , blast wave reaches the location (1,0), at time t_2 it is at (2,0), so on. In whatever location, the stand-off distance varies depending on where the pressure is measured.

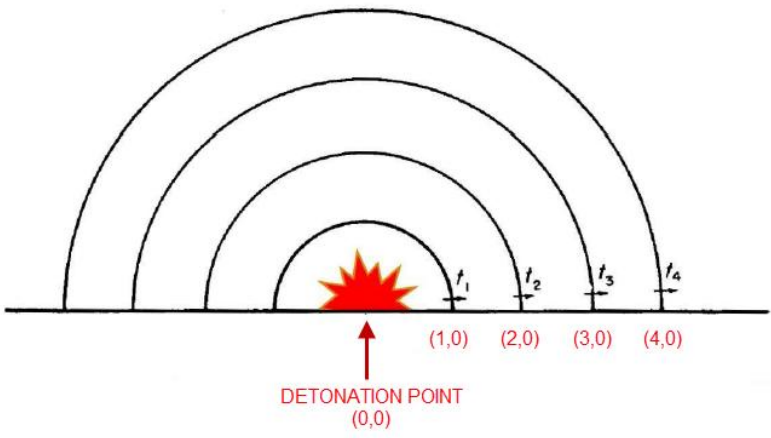


Figure 19. Propagation of the Blast Wave in Air Medium [21]

For fixed mass of the explosive, side-on overpressure varies as function of the stand-off distance exponentially. Figure 20 shows the variation of the side-on overpressure with the stand-off distance. As seen in Figure 20, “side-on overpressure” is 90000 psi at 2 ft, whereas it drops to less than 2000 psi, which is almost 2.2% of the pressure at 2 ft.

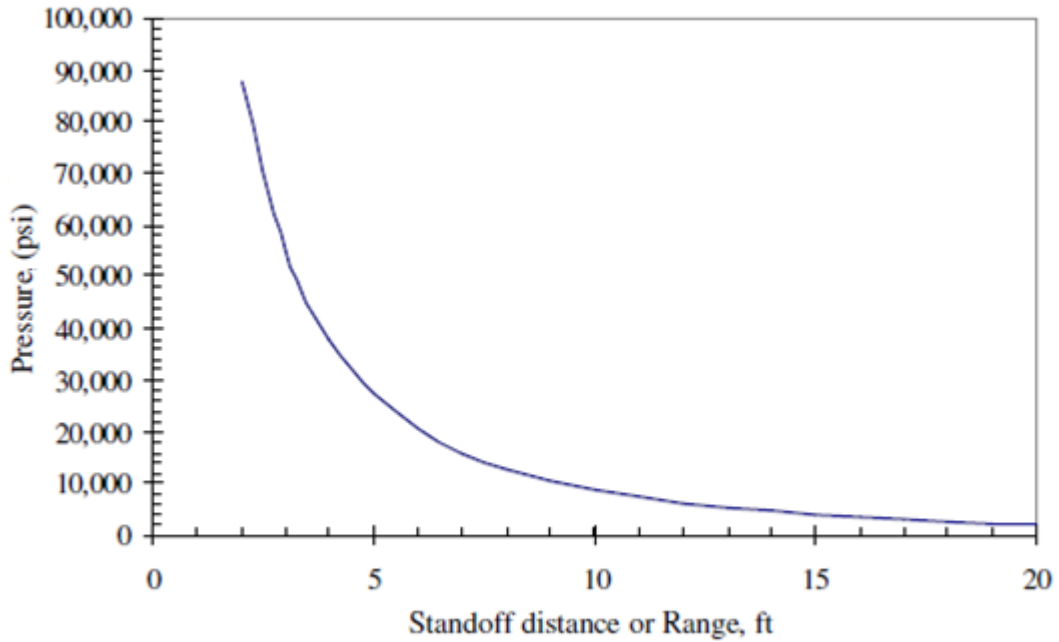


Figure 20. Side-on Pressure as Function of Stand-off Distance [12]

Besides the stand-off distance, side-on overpressure also depends on the mass of the explosive. In blast analysis, the mass of the explosive and the stand-off distance are grouped in the so-called “scaled distance” which is defined by Equation (1),

$$Z = \frac{R}{W_e^{1/3}} \quad (1)$$

where R is the scaled distance [m], W_e is the equivalent mass of the TNT explosive [kg] and Z is the scaled distance [$\text{m}/\text{kg}^{1/3}$]. With the definition of the scaled distance, side-on overpressure depends on the scaled distance. All blast parameters are determined using the scaled distance which combines the stand-off distance and the mass of the explosive in a unique parameter. For some of the blast parameters, one should know how the pressure varies with the time at a fixed point around the explosion. In Figure 21, a characteristic blast curve is shown. At the time of arrival t_a blast wave reaches the fixed point. After reaching to the fixed point, pressure raises suddenly to the peak side-on overpressure P_{SO} . As time passes, pressure drops to the ambient pressure P_0 . The time of duration from the peak value to the ambient value is known as the positive phase duration t_d . The area under pressure versus time curve up to $t_a + t_d$ is the positive impulse/area. Pressure then decreases below the

ambient pressure and increases again until it converges to the ambient pressure value. This region is called the negative phase and the area under the curve is the negative impulse/area [22].

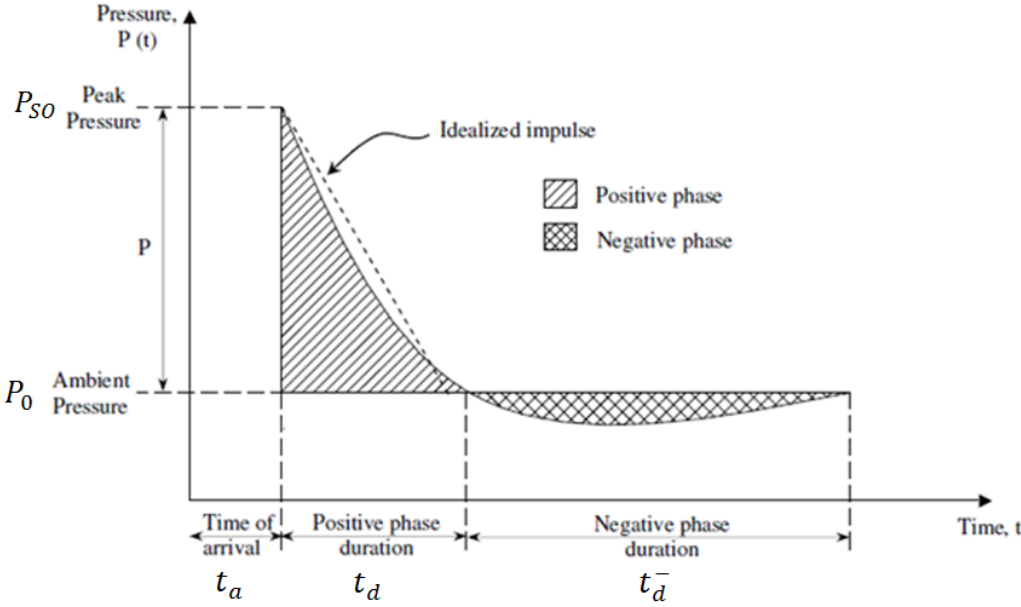


Figure 21. Pressure vs. Time Blast Curve [22]

To determine all the blast parameters caused by the blast pressure using the scaled distance, one should define the mass of explosive for different conditions. In the blast discipline, all explosives are defined in terms of TNT. Mass of the explosive is calculated using the “TNT Equivalency Factor” for other explosives. For instance, tritonal explosive has a TNT equivalency factor of 1.07 for the pressure and 0.96 for the impulse. Table 3 gives the TNT equivalency factor for some explosives. For instance, 100 kg of tritonal equals to 107 kg of TNT for the pressure calculation and 96 kg of TNT for the impulse calculation.

Table 3. TNT Equivalency Factor For Some Explosives [23]

Explosive	Density Mg/m ³	Equivalent Mass for Pressure	Equivalent Mass for Impulse	Pressure Range MPa
Amatol (50/50)	1.59	0.97	0.87	NA ¹
Ammonia Dynamite (50 percent Strength)	NA ¹	0.90	0.90 ²	NA ¹
Ammonia Dynamite (20 percent Strength)	NA ¹	0.70	0.70 ²	NA ¹
ANFO (94/6 Ammonium Nitrate/Fuel Oil)	NA ¹	0.87	0.87 ²	0.03 to 6.90
AFX-644	1.75	0.73 ²	0.73 ²	NA ¹
AFX-920	1.59	1.01 ²	1.01 ²	NA ¹
AFX-931	1.61	1.04 ²	1.04 ²	NA ¹
Composition A-3	1.65	1.09	1.07	0.03 to 0.35
Composition B	1.65	1.11 1.20	0.98 1.30	0.03 to 0.35 0.69 to 6.90
Composition C-3	1.60	1.05	1.09	NA ¹
Composition C-4	1.59	1.20 1.37	1.19 1.19	0.07 to 1.38 1.38 to 20.70
Cycloid (75/25 RDX/TNT)	1.71	1.11	1.26	NA ¹
(70/30)	1.73	1.14	1.09	0.03 to 0.35
(60/40)	1.74	1.04	1.16	NA ¹
DATE	1.80	0.87	0.96	NA ¹
Explosive D	1.72	0.85 ²	0.81	0.01 to 0.30
Gelatin Dynamite (50 percent Strength)	NA ¹	0.80	0.80 ²	NA ¹
Gelatin Dynamite (20 percent Strength)	NA ¹	0.70	0.70 ²	NA ¹
H-6	1.76	1.38	1.15	0.03 to 0.70
HBX-1	1.76	1.17	1.16	0.03 to 0.14
HBX-3	1.85	1.14	0.97	0.03 to 0.17
HMX	NA ¹	1.25	1.25 ²	NA ¹
LX-14	NA ¹	1.80	1.80 ²	NA ¹
MINOL II	1.82	1.20	1.11	0.02 to 0.14
Nitrocellulose	1.65 to 1.70	0.50	0.50 ²	NA ¹
Nitroglycerine Dynamic (50 percent Strength)	NA ¹	0.90	0.90 ²	NA ¹
Nitroglycerine (NQ)	1.72	1.00	1.00 ²	NA ¹
Nitromethane	NA ¹	1.00	1.00 ²	NA ¹

Explosive	Density Mg/m ³	Equivalent Mass for Pressure	Equivalent Mass for Impulse	Pressure Range MPa
Octol (75/25 HMX/TNT)	1.81	1.02	1.06	NA ¹
(70/30)	1.14	1.09	1.09 ²	0.01 to 0.30
PBX-9010	1.80	1.29	1.29 ²	0.03 to 0.21
PBX-9404	1.81	1.13	1.13 ²	0.03 to 0.69
		1.70	1.70	0.69 to 6.90
PBX-9502	1.89	1.00	1.00	NA ¹
PBXC-129	1.71	1.10	1.10 ²	NA ¹
PBXN-4	1.71	0.83	0.85	NA ¹
PBXN-107	1.64	1.05 ²	1.05 ²	NA ¹
PBXN-109	1.67	1.05 ²	1.05 ²	NA ¹
PBXW-9	NA ¹	1.30	1.30 ²	NA ¹
PBXW-125	1.80	1.02 ²	1.02 ²	NA ¹
Pentolite. (Cast)	1.64	1.42	1.00	0.03 to 0.69
	1.68	1.38	1.14	0.03 to 4.14
	NA ¹	1.50	1.00	0.69 to 6.90
PETN	1.77	1.27	1.27 ²	0.03 to 0.69
Picrotol (52/48 Ex D/TNT)	1.63	0.90	0.93	0.03 to 4.10
RDX	NA ¹	1.10	1.10 ²	NA ¹
RDX/Wax (98/2)	1.92	1.16	1.16 ²	NA ¹
RDX/AL/Wax (74/21/5)	NA ¹	1.30	1.30 ²	NA ¹
TATB	NA ¹	1.00	1.00 ²	NA ¹
Tetryl	1.73	1.07	1.07 ²	0.02 to 0.14
Tetrytol (75/25 Tetryl/TNT)	1.59	1.06	1.06 ²	NA ¹
TNETB	1.69	1.13	0.96	0.03 to 0.69
TNETB/AL (90/10)	1.75	1.23	1.11	0.03 to 0.69
(78/22)	1.18	1.32	1.32 ²	NA ¹
(65/35)	1.23	1.38	1.38 ²	NA ¹
TNT	1.63	1.00	1.00	Standard
Torpex	1.85	1.23	1.28	0.01 to 0.30
Tritonal (80/20 TNT/AL)	1.72	1.07	0.96	0.03 to 0.69

¹NA - Data not available.

²Value is estimated.

Apart from the TNT equivalency factor, another factor which affects the mass of the explosive is the casing factor. If the explosive is filled into a metal casing, like a warhead, the effectiveness of the explosive decreases since the energy generated from the detonation of the explosive should fracture the casing first and then release its energy to the atmosphere. For this situation, considering tests of explosive with casing, Fano proposed Equation (2) for the calculation of the uncased mass of the explosive [24]

$$W_U = W \left[0.6 + \frac{0.4}{1 + 2 \frac{M}{C}} \right] \quad (2)$$

where W_U is the uncased mass of explosive [kg], W is the mass of explosive [kg], M is the mass of the metal casing [kg], C is the explosive mass [kg]. Considering both the TNT equivalency factor and the casing factor, one can define the equivalent mass of TNT explosive, W_e [kg], as,

$$W_e = W \left[0.6 + \frac{0.4}{1 + 2 \frac{M}{C}} \right] * TNTEquivalencyFactor \quad (3)$$

Using the equivalent mass of the explosive, one can then properly define the scaled distance corresponding to a stand-off distance. Once the scaled distance is determined, one can get the time of arrival, peak side-on overpressure, positive phase duration etc. using Figure 22 which was generated by combining the test results of series of experiments during 1960's.

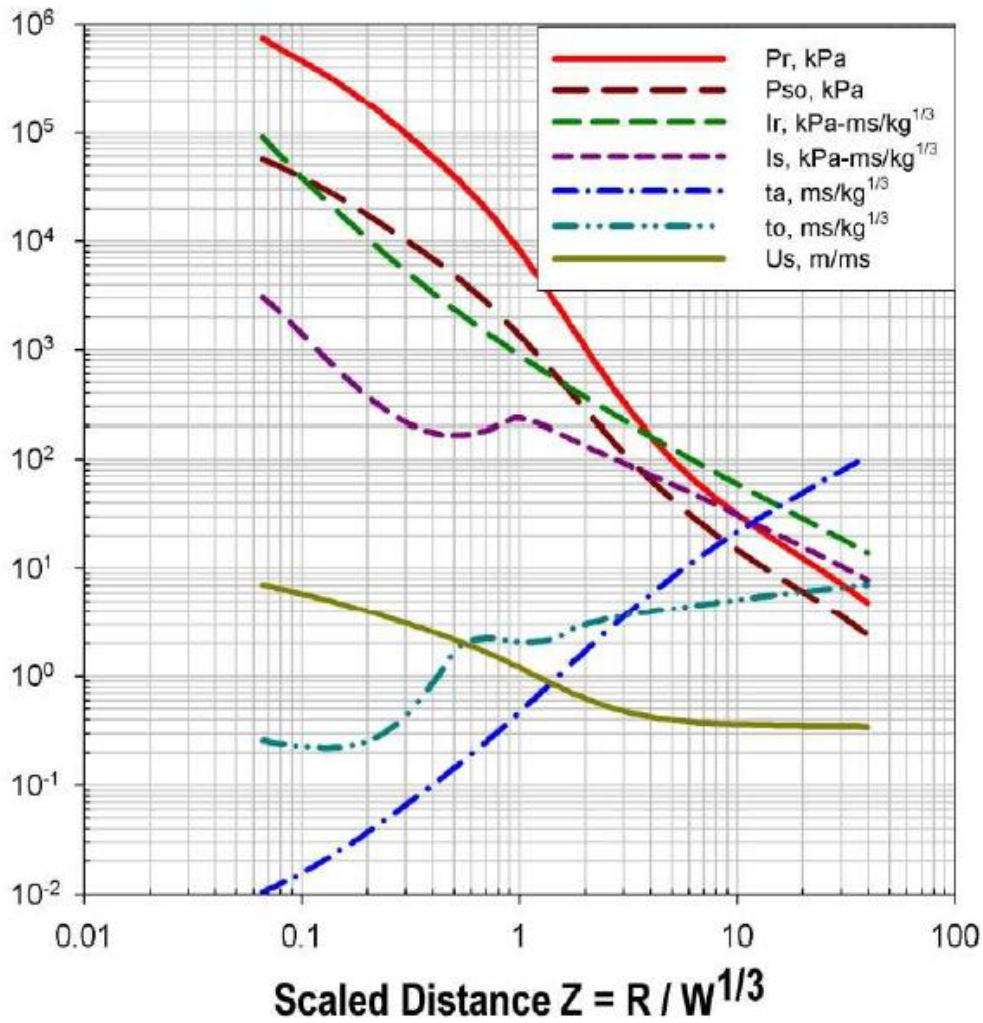


Figure 22. Side-on Overpressure P_{so} and Impulse I_s , Reflected Overpressure P_r and Impulse I_r , Time of Arrival t_a , Time of Duration t_o , Shock Velocity U_s as a Function of the Scaled Distance [22]

Besides the test data, there are some empirical formulae for the calculation of the blast parameters, especially for the calculation of the peak side-on overpressure. Kinney proposed Equation (4) for the calculation of the peak side-on pressure P_{so} [25].

$$P_{so} = P_0 * \frac{808 \left[1 + \left(\frac{Z}{4.5} \right)^2 \right]}{\sqrt{1 + \left(\frac{Z}{0.048} \right)^2} \sqrt{1 + \left(\frac{Z}{0.32} \right)^2} \sqrt{1 + \left(\frac{Z}{1.35} \right)^2}} \quad (4)$$

where P_0 is the ambient pressure [kPa], Z is the scaled distance [$\text{m}/\text{kg}^{1/3}$].

Brode suggested Equation (5) for the peak side-on pressure P_{so} in different ranges of the overpressure [26]

$$P_{so} = \frac{6.7}{Z^3} + 1 \text{ for } P_{so} > 10 \text{ bar} \quad (5)$$

$$P_{so} = \frac{0.975}{Z} + \frac{1.455}{Z^2} + \frac{5.85}{Z^3} - 0.019 \text{ for } 0.1 < P_{so} < 10 \text{ bar}$$

where the scaled distance Z is in [$\text{m}/\text{kg}^{1/3}$], side-on overpressure P_{so} is in [bar]

Newmark proposed Equation (6) for the peak side-on overpressure P_{so} ,

$$P_{so} = 6784 \frac{W_e}{R^3} + 93 \sqrt{\frac{W_e}{R^3}} \quad (6)$$

where equivalent mass of the TNT explosive W_e is in [tons], stand-off distance R is in [m] and side-on overpressure P_{so} is in [bar].

Mills introduced Equation (7) for the peak side-on pressure P_{so} [28],

$$P_{so} = \frac{1772}{Z^3} - \frac{114}{Z^2} + \frac{108}{Z} \quad (7)$$

where the scaled distance Z is in [$\text{m}/\text{kg}^{1/3}$] and the side-on overpressure P_{so} is in [kPa].

Sadovski proposed Equation (8) for the peak side-on pressure P_{so} [30],

$$P_{so} = 0.84 \frac{W_e^{1/3}}{R} + 2.7 \frac{W_e^{2/3}}{R^2} + 7 \frac{W_e}{R^3} \quad (8)$$

where the equivalent mass of the explosive W_e is in [kg], stand-off distance W_e is in [m] and side-on overpressure P_{so} is in [atm].

Kingery and Bulmash defined a function given by Equation (9) for the determination of the side-on peak pressure for different ranges of the scaled distance Z. As seen in Equation (9), Kingery and Bulmash used sixth degree polynomial and exponential function in order to fit the experimental data shown in Figure 22 accurately.

$$Function = e^{A+B(\ln Z)+C(\ln Z)^2+D(\ln Z)^3+E(\ln Z)^4+F(\ln Z)^5+G(\ln Z)^6} \tag{9}$$

In Equation (9), A-G are the coefficients defined for different ranges of the scaled distance Z [m/kg^{1/3}], Table 4 gives the coefficients A-G used for the calculation of the peak side-on overpressure.

Table 4. KingeryBulmash Coefficients for the Calculation of the Side-on Overpressure [29]

Side-on Overpressure [kPa]							
Range of Z [m/kg ^{1/3}]	A	B	C	D	E	F	G
0.2-2.9	7.2106	-2.1069	0.3229	0.1117	0.0685	0	0
2.9-23.8	7.5938	-3.0523	0.40977	0.0261	-0.01267	0	0
23.8-198.5	6.0536	-1.4066	0	0	0	0	0

Equation (9), proposed by Kingery and Bulmash, can also be used for the calculation of the time of arrival, positive phase duration and the shock front velocity.

Table 5 gives the the coefficients A-G used for the calculation of the time of arrival, positive phase duration and the shock front velocity for different range of the scaled distance Z.

Table 5. Kingery Coefficients for the Calculation of the Scaled Time of Arrival, Scaled Positive Phase Duration and the Shock Front Velocity [29]

Scaled Time of Arrival [ms/kg ^{1/3}]							
Range of Z [m/kg ^{1/3}]	A	B	C	D	E	F	G
0.06-1.50	-0.7604	1.8058	0.1257	-0.0437	-0.0310	-0.00669	0
1.50-40	-0.7137	1.5732	0.5561	-0.4213	0.1054	-0.00929	0
Scaled Positive Phase Duration [ms/kg ^{1/3}]							
Range of Z [m/kg ^{1/3}]	A	B	C	D	E	F	G
0.2-1.02	0.5426	3.2299	-1.5931	-5.9667	-4.0815	-0.9149	0
1.02-2.80	0.5440	2.7082	-9.7354	14.3425	-9.7791	2.8535	0
2.80-40	-2.4608	7.1639	-5.6215	2.2711	-0.44994	0.03486	0
Shock Front Velocity [km/s]							
Range of Z [m/kg ^{1/3}]	A	B	C	D	E	F	G
0.06-1.50	0.1794	-0.956	-0.0866	0.109	0.0699	0.01218	-
1.50-40	0.2597	-1.326	0.3767	0.0396	-0.0351	0.00432	

Dynamic pressure resulting from the air flow due to the blast pressure is calculated by Equation (10) [18],

$$q = \frac{1}{2} \rho U_s^2 \quad (10)$$

where q is the dynamic pressure in [Pa], ρ is density of compressed air [kg/m³], U_s is the shock front velocity in [m/s]. Figure 23 compares the variation of the blast wave overpressure and the dynamic pressure with the time at a fixed point. It is noted that in the negative phase zone, dynamic pressure is always greater than the atmospheric pressure whereas the side-on overpressure is less than the atmospheric pressure.

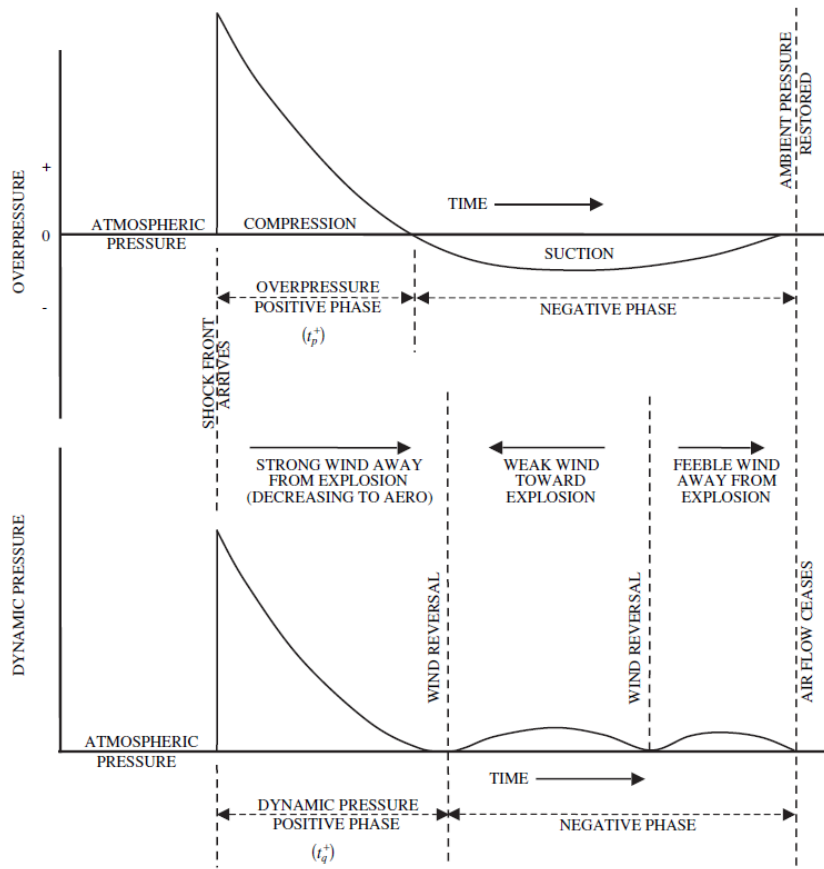


Figure 23. Comparison of Blast-Wave Overpressure and Dynamic Pressure [31]

Figure 24 shows the variation of the dynamic pressure q with the side-on overpressure. This relation is obtained by experiments then fitted to a formula in Equation (11),

$$q = \frac{5P_{so}^2}{2(P_{so} + 7P_0)} \quad (11)$$

where peak side-on overpressure P_{so} and ambient pressure P_0 are in [kPa].

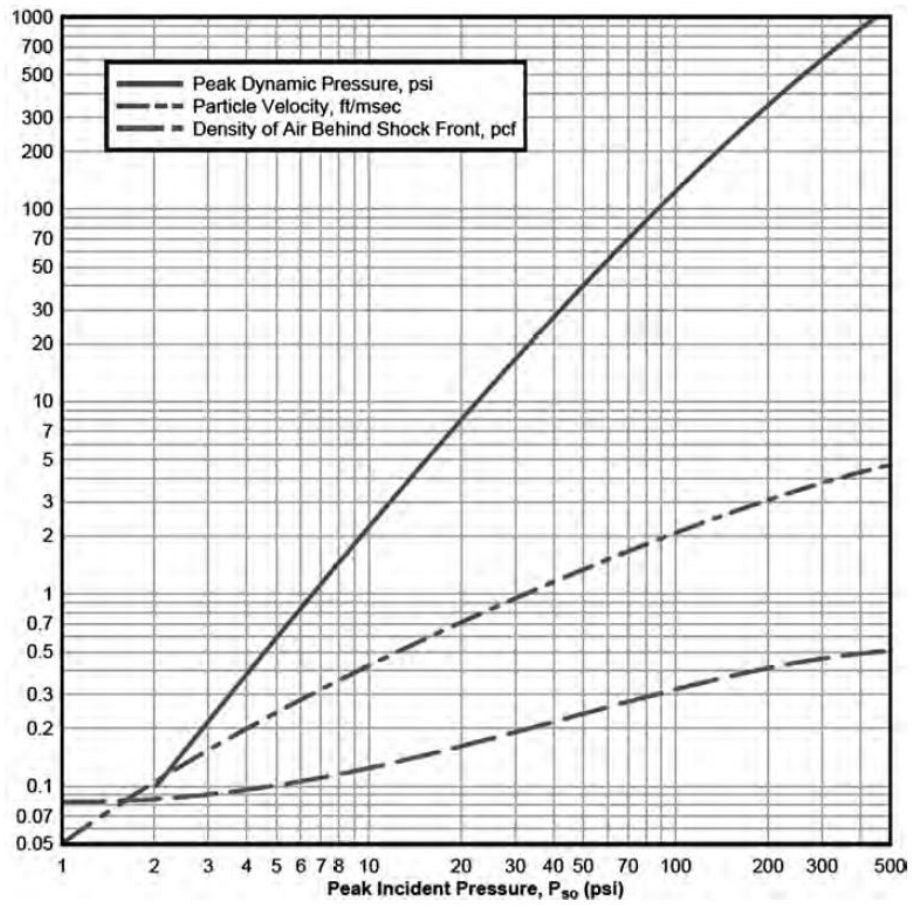


Figure 24. Variation of the Dynamic Pressure with the Peak Side-on Overpressure [32]

2.2. Blast Propagation in Unconfined Air Burst and Formation of the Mach Stem

In section 2.1, blast propagation in free air burst is examined. Blast loading in different propagation medium is categorized and tabulated in Table 6 [12].

Table 6. Blast Loading Categories in Different Propagation Medium [32]

BLAST LOADING CATEGORIES		
Explosive Confinement	Category	Pressure Loads
Unconfined Explosions	Free Air Burst	Unreflected
	Air Burst	Reflected
	Surface Burst	Reflected
Confined Explosions	Fully Vented	Internal Shock
		Leakage
	Partially Confined	Internal Shock
		Internal Gas
		Leakage
	Fully Confined	Internal Shock
Internal Gas		

Blast loading for bridge-like-structures is external and unconfined. Depending on the height of burst, blast loading could be classified as either free air burst, air burst or surface burst, as shown in Figure 25. If the explosive detonates on the surface, this is called as unconfined surface burst.

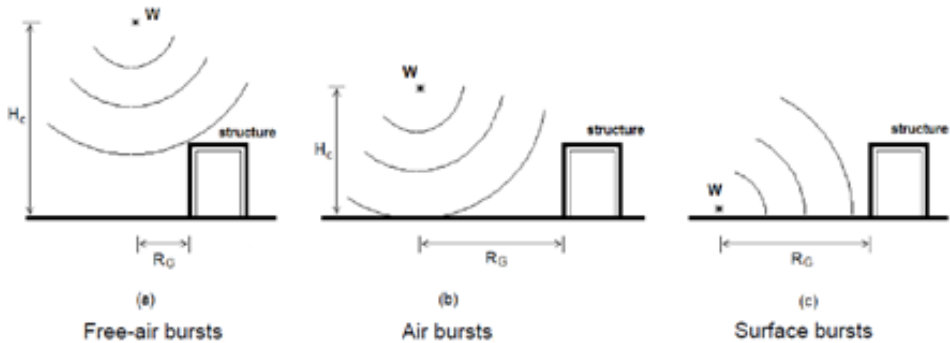


Figure 25. Categorization of Unconfined Blast Propagation [34]

As shown in Figure 25b and Figure 25c, blast wave propagates in a spherical manner without encountering any reflecting surface for some time before it impacts the ground. After impacting the ground, the wave is reflected and moves in the air spherically. The wave reflecting from ground, known as the “reflected blast (shock) wave”, moves faster than the original incident blast wave and after a while reaches the incident wave [35]. Incident blast wave and the reflected blast wave merge. This merging point is called as the “Triple Point”. Merging waves form the so-called Mach Stem wave which does not propagate spherically anymore but rather makes a planar move. Moreover, Mach Stem has pressure greater than incident wave since it is the combination of ground reflected wave and the incident wave. Figure 26 shows the incident and the reflected waves and the formation of the Mach Stem. β is the angle of incidence, which is the angle between normal vector of the propagating incident wave and the surface normal. Angle of incidence is one of the critical parameters for the formation of Mach Stem. Angle of incidence should be greater than a certain critical angle, in order to have Mach Stem formation.

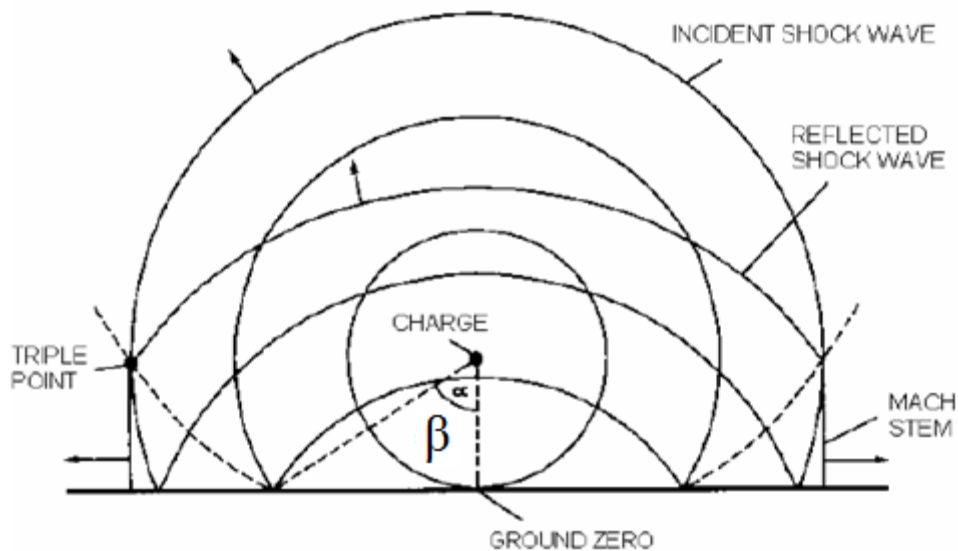


Figure 26. Blast Wave Hitting the Ground and Mach Stem Formation [36]

After merging of the incident and the reflected waves at the triple point, Mach Stem grows and draws a path. This path is called as the path of the triple point and Figure 27 shows the path of the triple point and the growth of the Mach Stem.

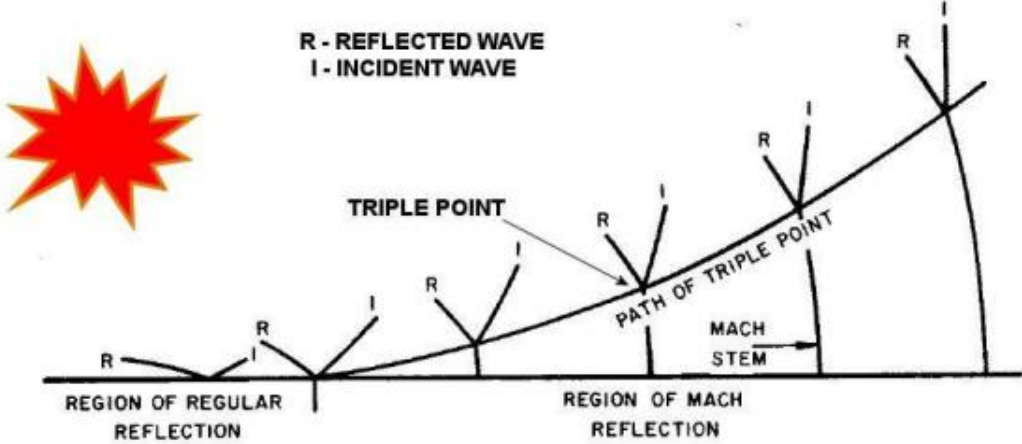


Figure 27. Path of the Triple Point [22]

In general, for blast waves reflecting from the surface, the magnification of the explosion is defined in terms of magnification in the mass of the explosive [18]. Equation (12) gives equivalent mass of the TNT explosive W_e if reflecting surfaces exist,

$$W_e = 2^n \tag{12}$$

where n is number of reflective surface(s).

For the unconfined surface burst, ground is the reflective surface and mass of explosive should be doubled to calculate the scaled distance. If an explosive detonates at the corner with two reflective surfaces and the mass of explosive is multiplied by 4. In calculating the mass of the explosive, surface is assumed to fully reflect the blast wave and it is assumed that no energy is absorbed by the ground or transmitted through the ground. Some studies were performed in order to find the transmitting energy fraction and blast energy loss through the ground. Regarding this loss, instead of using a magnification factor of 2, 1.7-1.8 is recommended. Mass of

explosive is found accordingly and then the scaled distance and the correlated blast parameters are computed [36].

Besides the magnification factor used for the mass of the explosive, increasing pressure effect of Mach Stem formation scenario is modeled by Miller [37]. In order to find the triple point height just before it impacts the structure and the corresponding Mach Stem pressure, by means of tests and analyses, Miller defined new terms to calculate these parameters. A parameter ε , given by Equation (13), is defined to decide on whether the Mach Stem forms or not.

$$\varepsilon = \frac{P_0}{P_{so} + P_0} \quad (13)$$

In Equation (13), ambient pressure P_0 and side-on overpressure P_{so} are in kPa. Using the parameter ε , critical angle for Mach Stem formation is determined using Equation (14).

$$\alpha_{critical} = \frac{40.02 - 76.81\varepsilon + 61.01\varepsilon^2 - 23.26\varepsilon^3}{1 - 1.79\varepsilon + 1.02\varepsilon^2 - 0.22\varepsilon^3} \quad (14)$$

If the angle of incidence β (Figure 26) is greater than $\alpha_{critical}$, then Mach Stem forms [37]. After deciding on the Mach Stem formation, triple point height and Mach Stem pressure should be determined with a series of computations. For the triple point height, scaled charge height should be determined first using Equation (15). As all “scaled” blast parameters, “scaled” means division by cube root of equivalent mass of TNT explosive.

$$H_c^w = \frac{\text{Height of Burst}}{W_e^{1/3}} \quad (15)$$

In Equation (15), H_c^w is the scaled charge height [ft/lb^{1/3}], height of burst is in [ft], W_e is the equivalent mass of TNT explosive in [lb].

To determine the scaled triple point height, Miller divides the scaled charge height into intervals of 1, 1.5, 2, 2.5, 3, 3.5, 4, 5, 6, 7. For all intervals, scaled triple point height is defined as function of the scaled distance. For instance, for the scaled charge height of 1, scaled triple point height is given by Equation (16).

$$H_T^w = -0.001Z^4 + 0.0199Z^3 + 0.0146Z^2 + 0.1183Z \quad (16)$$

For other scaled charge height parameter, Table 7 gives the scaled triple point height as function of the scaled distance for different scaled charge heights. For any scaled charge height parameter, interpolation could be performed. Note that parameters in Table 7 are in British Unit System.

Table 7. Scaled Triple Point Height as Function of Scaled Distance for Different Scaled Charge Heights [37]

Scaled Triple Point Height, H_T^w (ft/lb ^{1/3}); (H_c^w (ft/lb ^{1/3}))	
$H_c^w = 1$	$H_T^w = -0.001z^4 + 0.0199z^3 + 0.0146z^2 + 0.1183z$
$H_c^w = 1.5$	$H_T^w = -7.0 \times 10^{-5} z^6 + 2.2 \times 10^{-3} z^5 - 0.0266z^4 + 0.1566z^3 - 0.3638z^2 + 0.3982z$
$H_c^w = 2$	$H_T^w = \frac{-5.513 \times 10^{-3} + 1.466 \times 10^{-2} z + 1.828 \times 10^{-2} z^2}{1 - 0.1273z + 1.068 \times 10^{-2} z^2 - 3.241 \times 10^{-4} z^3}$
$H_c^w = 2.5$	$H_T^w = \frac{-5.539 \times 10^{-3} + 5.889 \times 10^{-3} z + 3.692 \times 10^{-3} z^2 - 8.038 \times 10^{-5} z^3}{1 - 0.2982z + 3.927 \times 10^{-2} z^2 - 2.339 \times 10^{-3} z^3 + 5.167 \times 10^{-5} z^4}$
$H_c^w = 3$	$H_T^w = \frac{5.385 \times 10^{-4} - 0.2295z + 5.934 \times 10^{-2} z^2}{1 + 0.1211z - 3.345 \times 10^{-3} z^2}$
$H_c^w = 3.5$	$H_T^w = \frac{1.838 \times 10^{-3} + 1.524 \times 10^{-2} z + 1.379 \times 10^{-3} z^2}{1 - 0.156z + 1.002 \times 10^{-2} z^2 - 2.242 \times 10^{-4} z^3}$
$H_c^w = 4$	$H_T^w = \frac{-1.343 \times 10^{-3} - 1.075 \times 10^{-2} z + 5.559 \times 10^{-3} z^2}{1 - 0.07748z + 2.674 \times 10^{-3} z^2}$
$H_c^w = 5$	$H_T^w = \frac{-1.617 \times 10^{-3} + 2.83 \times 10^{-3} z + 1.433 \times 10^{-3} z^2}{1 - 0.08417z + 2.307 \times 10^{-3} z^2}$
$H_c^w = 6$	$H_T^w = \frac{-2.30 \times 10^{-3} + 9.116 \times 10^{-3} z - 8.267 \times 10^{-4} z^2}{1 - 0.1745z + 9.455 \times 10^{-3} z^2 - 1.734 \times 10^{-4} z^3}$
$H_c^w = 7$	$H_T^w = \frac{7.525 \times 10^{-4} + 8.725 \times 10^{-3} z - 7.177 \times 10^{-4} z^2}{1 - 0.1239z + 3.45 \times 10^{-3} z^2}$

Scaled charge height is function of the height of burst and the equivalent mass of TNT explosive, scaled triple point height is function of the scaled charge height and the scaled distance. Thus, scaled triple point height is function of the stand-off distance, equivalent mass of explosive and the height of burst.

Mach Stem pressure is determined according to different scaled charge height intervals. Miller gives formulae for the Mach Stem pressure in his thesis for the scaled charge height values of 0.8, 1.9, 3, 5.3, 7.2, as shown in Table 8. Mach Stem pressure is dependent on the scaled charge height and the angle of incidence β , which depends on the height of burst and the stand-off distance. Since scaled charge height depends on the height of burst and the equivalent mass of explosive, Mach Stem pressure is function of the stand-off distance, height of burst and the equivalent mass of the TNT explosive.

Table 8. Mach Stem Pressure as Function of the Angle of Incidence for Different Scaled Charge Heights [37]

Mach Pressure, P_{mach} (psi): (H_c^w (ft/lb ^{1/3}), β_1 (°))	
$H_c^w = 0.8$	$P_{mach} = 11323 + 4.601\beta_1 - 8.718\beta_1^2 + 0.13\beta_1^3 - 5.469 \times 10^{-4}\beta_1^4$
$H_c^w = 1.9$	$P_{mach} = 1559 + 4.4\beta_1 - 1.609\beta_1^2 + 0.07331\beta_1^3 - 2.848 \times 10^{-3}\beta_1^4 - 6.67071 \times 10^{-5}\beta_1^5 - 8.729 \times 10^{-7}\beta_1^6 + 5.9304 \times 10^{-9}\beta_1^7 - 1.6574 \times 10^{-11}\beta_1^8$
$H_c^w = 3$	$P_{mach} = 483.5 - 11.39\beta_1 + 0.05746\beta_1^2 + 2.601 \times 10^{-4}\beta_1^3 - 1.704 \times 10^{-6}\beta_1^4$
$H_c^w = 5.3$	$P_{mach} = 72.48 + 0.7531\beta_1 - 0.04146\beta_1^2 + 1.862 \times 10^{-4}\beta_1^3 + 9.5714 \times 10^{-7}\beta_1^4$
$H_c^w = 7.2$	$P_{mach} = 34.86 + 0.6254\beta_1 - 4.35 \times 10^{-3}\beta_1^2 - 1.433 \times 10^{-4}\beta_1^3 + 1.5338 \times 10^{-6}\beta_1^4$

2.3. Impulsive Work on the Structure

Blast wave which impacts the structure, may be composed of either fully incident wave, fully Mach Stem or mixed depending on the height of burst and the scaled distance. In Figure 28, shelter is exposed to fully Mach Stem since the triple point at the location of the shelter is greater than the height of the shelter.

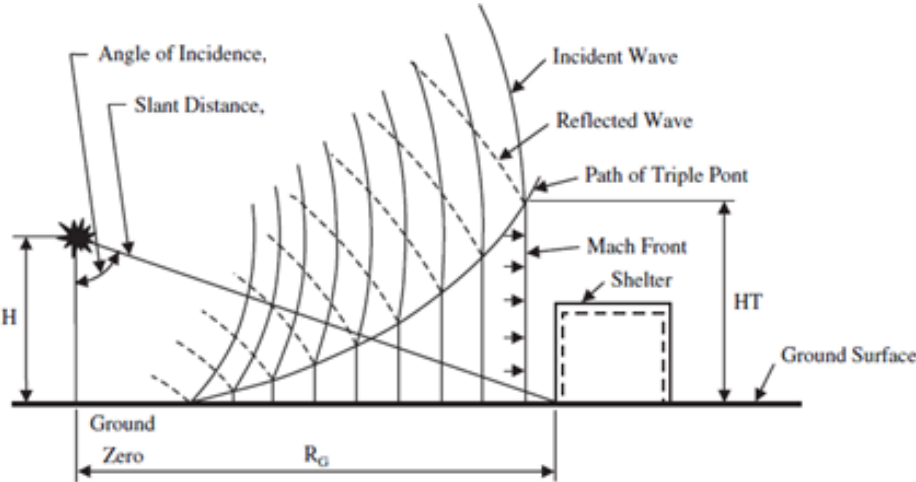


Figure 28. Mach Stem Formation and its Interaction with the Structure [9]

If explosion occurs at a closer location, as shown in Figure 29, blast wave is a fully incident wave. If the explosion location is neither close enough to be fully incident nor far enough to be fully Mach Stem, mixed condition may occur.



Figure 29. Close-in Explosion and Fully Incident Wave Impinging on the Structure

When the blast wave impacts on the structure, it makes an angle with the structure. For instance, Figure 30 shows a spherical blast wave impacting on the column. The explosion is close enough to the column so that it is a fully incident wave. The incident wave has different angle of incidence with respect to different parts of the column. The arrows emerging from the explosion point demonstrate the normal direction of the spherical blast wave. Vector R1 makes an angle of β_1 with the surface normal of the column. Vectors R2, R3, R4 have angles of incidence $\beta_2, \beta_3, \beta_4$ respectively.

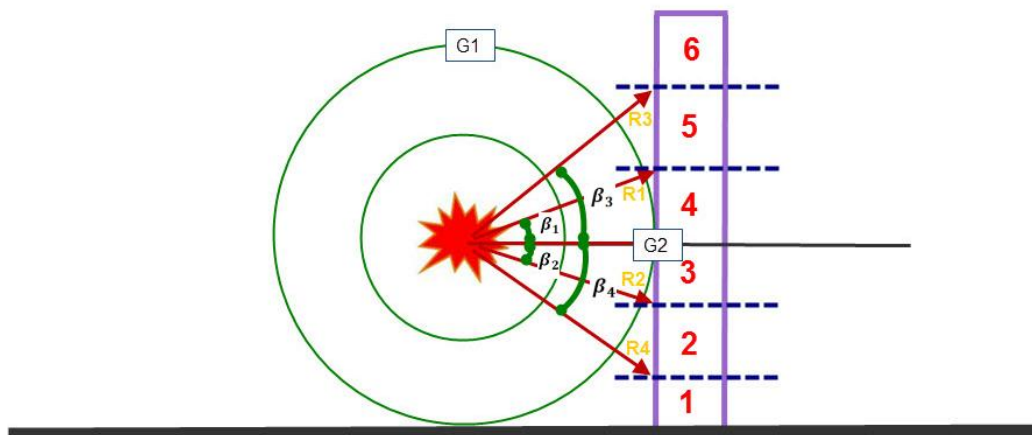


Figure 30. Angle of Incidence with respect to the Different Points on the Structure

Side-on (incident) overpressure impacting on the structure at an angle of incidence is magnified by a factor of “coefficient of reflection” and the resulting pressure is named as the “face-on (reflected) overpressure” in blast terminology [22]. Referring to Figure 30, pressure at the location G1 is the side-on overpressure whereas at the same stand-off distance pressure at the location G2, just next to the structure is the face-on overpressure. Figure 31 compares the side-on and the face-on pressures and how they are measured with the pressure probes.

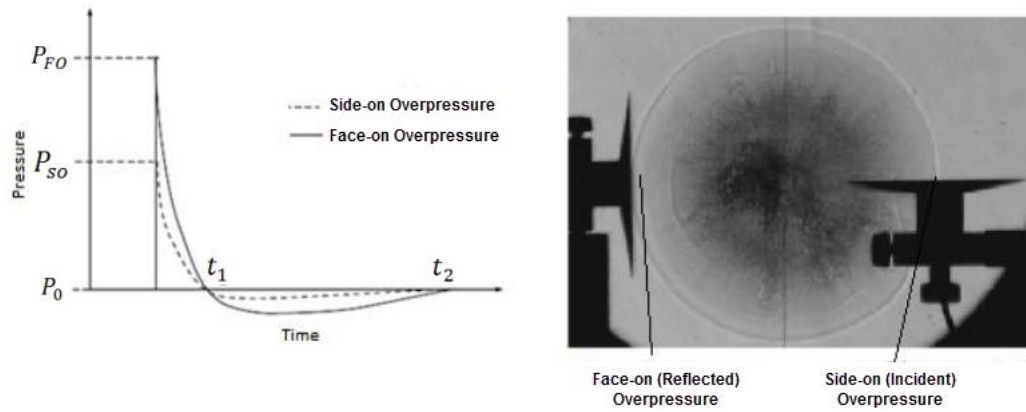


Figure 31. Comparison of the Face-on and the Side-on Overpressures [38]

The relation between the face-on overpressure and the side-on overpressure is given by Equation (17) [12],

$$P_{FO} = CoR * P_{SO} \quad (17)$$

where P_{FO} is the face-on pressure and the coefficient of reflection (CoR) is a function of the side-on overpressure intensity and the angle of incidence. With series of experiments performed in 1960's, gauges were inserted at the same stand-off distance but with different configurations, as shown in Figure 31. Test data for the variations of the face-on with the side-on overpressure were recorded, and it was observed that coefficient of reflection varies between 1 and 12.25. Figure 32 shows the variation of the coefficient of reflection with the angle of incidence for different side-on pressures. Angle of incidence "0" means that wave is fully reflected whereas angle of incidence "90" means that incident wave is not reflected at all. Therefore, for the incidence angle of 90, coefficient of reflection is 1 for all side-on pressure values. Intermediate values of the incidence angle are for "oblique reflection" [22].

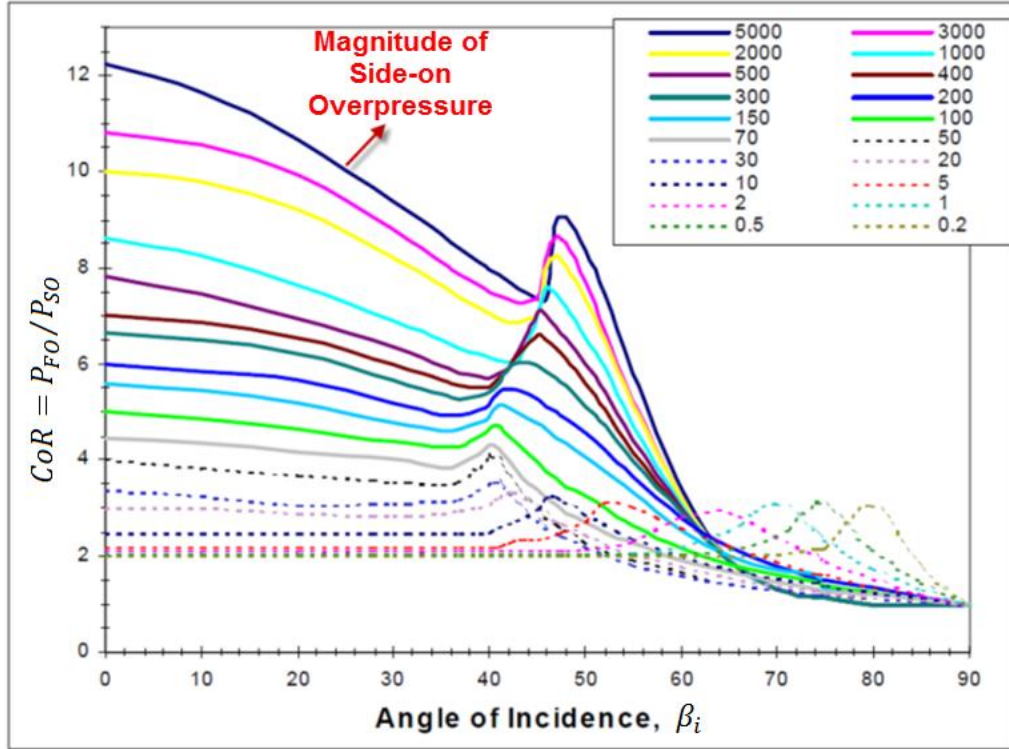


Figure 32. Variation of the Coefficient of Reflection with the Angle of Incidence for different Side-on Pressures [22]

When blast wave interacts with the structure, structure is subjected to the face-on pressure which varies with time as shown in Figure 31. In addition to the face-on overpressure, impulse has significant role on the damage incurred on the structure. The area under the face-on overpressure - time curve is the impulse per unit area. Impulse per unit area could be found using different approaches. By means of conducted tests, an empirical formula is proposed by Driels for the impulse per unit area [18]. Pressure variation in time was recorded by gauges and impulse/area is computed. The results are correlated to the scaled distance with formula fits. Equation (18) gives the impulse per unit area proposed by Driels,

$$\frac{I}{A} = \frac{0.067 * [1 + \left(\frac{Z}{0.23}\right)^4]^{1/2}}{Z^2 * [1 + \left(\frac{Z}{1.55}\right)^3]^{1/3}} \quad (18)$$

where Z is the scaled distance in $[m/kg^{1/3}]$, I/A is the impulse/area $[kPa.ms]$.

In Equation (18), only the positive phase impulse is taken into account. It should be noted that although the negative phase has a longer duration than the positive phase, difference in the peak overpressure values for the positive and the negative phases is very high so that negative phase impulse is ignored [22].

In Figure 33, loading of a blast-exposed-structure is given. Structure is subjected to the face-on overpressure on the front wall, side-on overpressure on the sides, roof and the rear wall. Side-on overpressures on the sides cancel each other; thus, net loading is

$$Net\ Loading = FW\ Loading - RW\ Loading \tag{19}$$

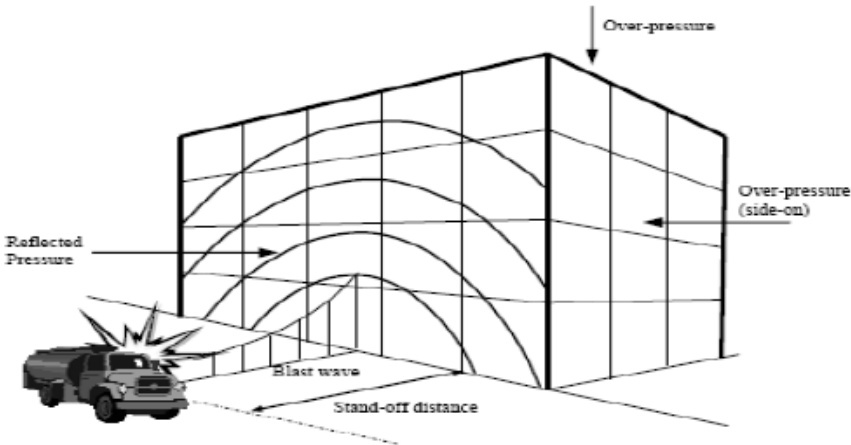


Figure 33. Blast Loading on a Structure [19]

In the report prepared by the U.S. Department of the Army [22], overpressure versus time curve for a blast-exposed-structure is simplified and exponentially decaying function of the face-on pressure shown in Figure 31 is converted into trapezoid and triangular pulses. Figure 34 shows the simplified front wall loading of a structure.

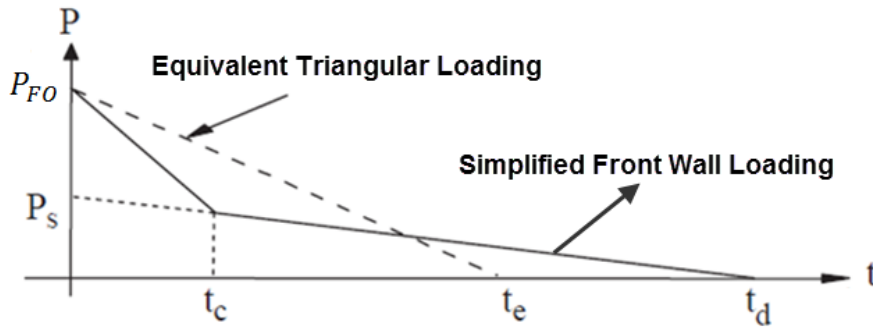


Figure 34. Front Wall Blast Loading Overpressure vs. Time Curve [22]

In Figure 34, P_{FO} is the face-on overpressure, P_S is the stagnation pressure which is combination of the side-on overpressure and the dynamic pressure, t_d is the positive phase duration, t_e is the equivalent time in which same impulse/area is calculated as the simplified loading given in Figure 34. t_c is clearing time in which clearing effect occurs. Face-on overpressure along the structure varies since the scaled distance and the angle of incidence change. During the clearing effect period, face-on overpressure relieves toward the lower pressure zones at free edges. This forms a relief wave propagating from the low to the high pressure zones.

Clearing time is determined using Equation (20). Instead of the shock front velocity, sound velocity in the compressed zone as function of the peak side-on overpressure is utilized as shown in Figure 36 [23],

$$t_c = \frac{4S}{\left(1 + \frac{S}{G}\right) C_r} \quad (20)$$

where S is the minimum of width or height of the structural member [ft], G is the maximum of width or height [ft], C_r is the sound velocity in [ft/ms] and t_c is the clearing time in [ms]. Figure 35 demonstrates front and top view of a sample structural member in which width, height and lengths are defined. For this case, since height is greater than width, S is the width of the structural member while G is the height of the structural member.

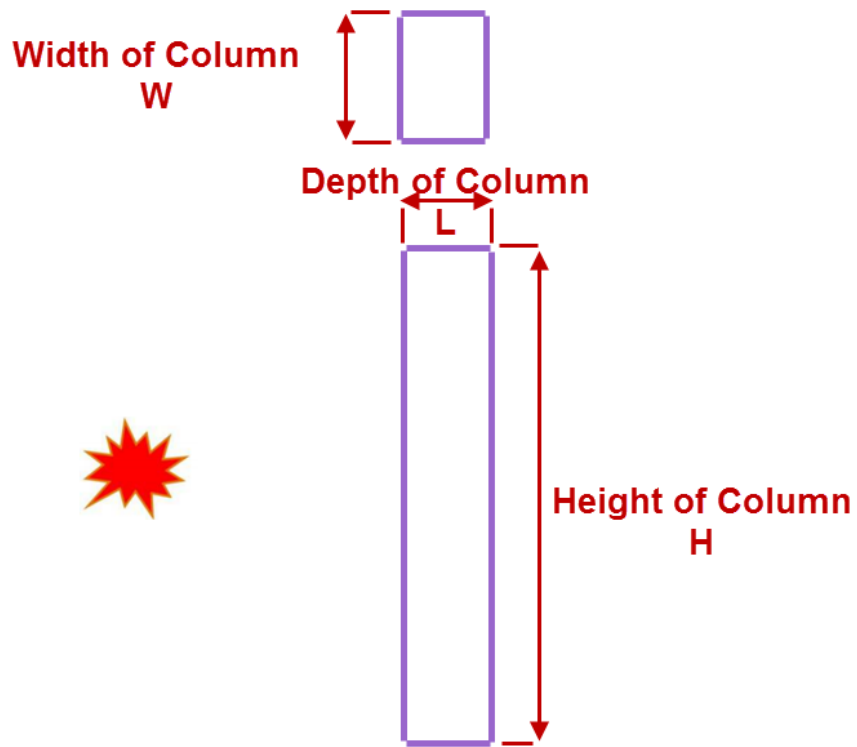


Figure 35. Height, Width and Length Definition for Sample Column

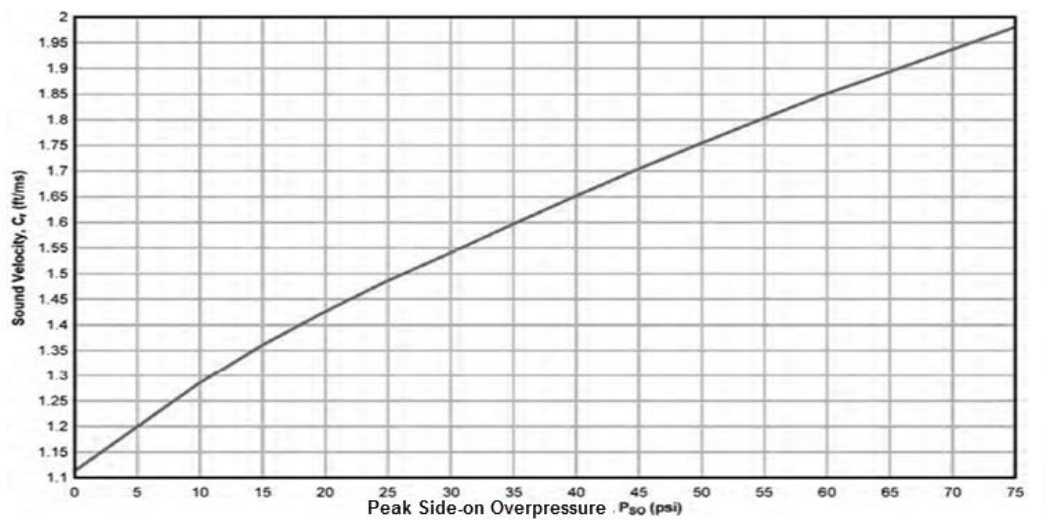


Figure 36. Sound Velocity as Function of the Peak Side-on Overpressure [23]

Stagnation overpressure P_s is calculated by Equation (21) [23],

$$P_s = P_{so} + C_D q \quad (21)$$

where C_D is the drag coefficient and its recommended value is 1 for front wall loading [23]. After determining the face-on overpressure, stagnation overpressure, positive phase duration and the clearing time, impulse/area is computed as the area under the simplified front wall loading curve shown in Figure 34. Utilizing the known the impulse/area of the simplified front wall loading, equivalent time for the equivalent triangular loading is calculated using Equation (22),

$$t_e = \frac{2\left(\frac{I}{A}\right)}{P_{FO}} \quad (22)$$

where P_{FO} is the face-on overpressure in [kPa], I/A is the impulse/area in [kPa-ms], t_e is the equivalent time in [ms].

Rear wall loading is similar to the side wall and roof loading [23]. Equivalent rear wall loading is a triangular pulse as shown in Figure 32 which gives the variation of the effective side-on overpressure P_a with respect to time. The gauge pressure is assumed to become zero at time $t_r + t_d$, which is the sum of the rise time t_r and positive phase duration t_d .

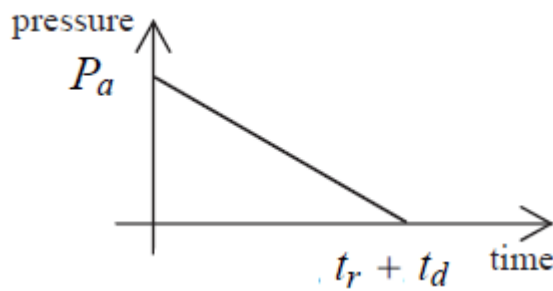


Figure 37. Overpressure vs. Time Curve for the Rear Wall Loading [23]

Effective overpressure P_a , which is the combination of dynamic pressure and side-on overpressure at rear side, is determined using Equation (23) [13],

$$P_a = C_E P_{SO} + C_D q \tag{23}$$

where C_E is the equivalent uniform pressure factor, which is defined as the reduction factor of side-on overpressure at the rear wall in [psi], C_D is the drag coefficient, P_{SO} is the side-on overpressure in [psi], q is the dynamic pressure in [psi]. A schematic figure for the rear loading is shown in Figure 38. Blast wave with a wavelength of L_w surpasses through the rear wall.

Equivalent uniform pressure factor C_E is determined with aid of the graph presented in Figure 39 in which equivalent uniform pressure factor is given as a function of the ratio of the blast wave length L_w to the span length L which is length of rear side of the structural member as shown in Figure 38.

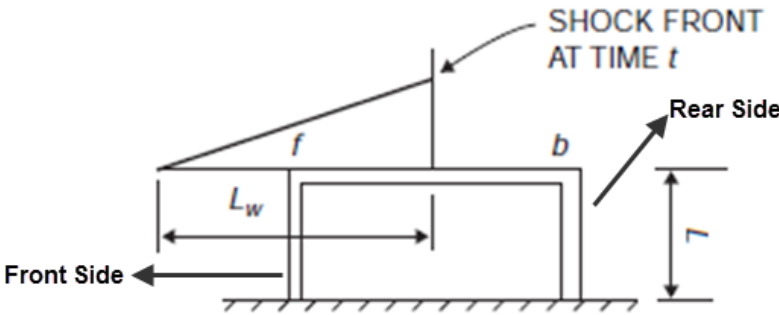


Figure 38. Rear Wall Loading

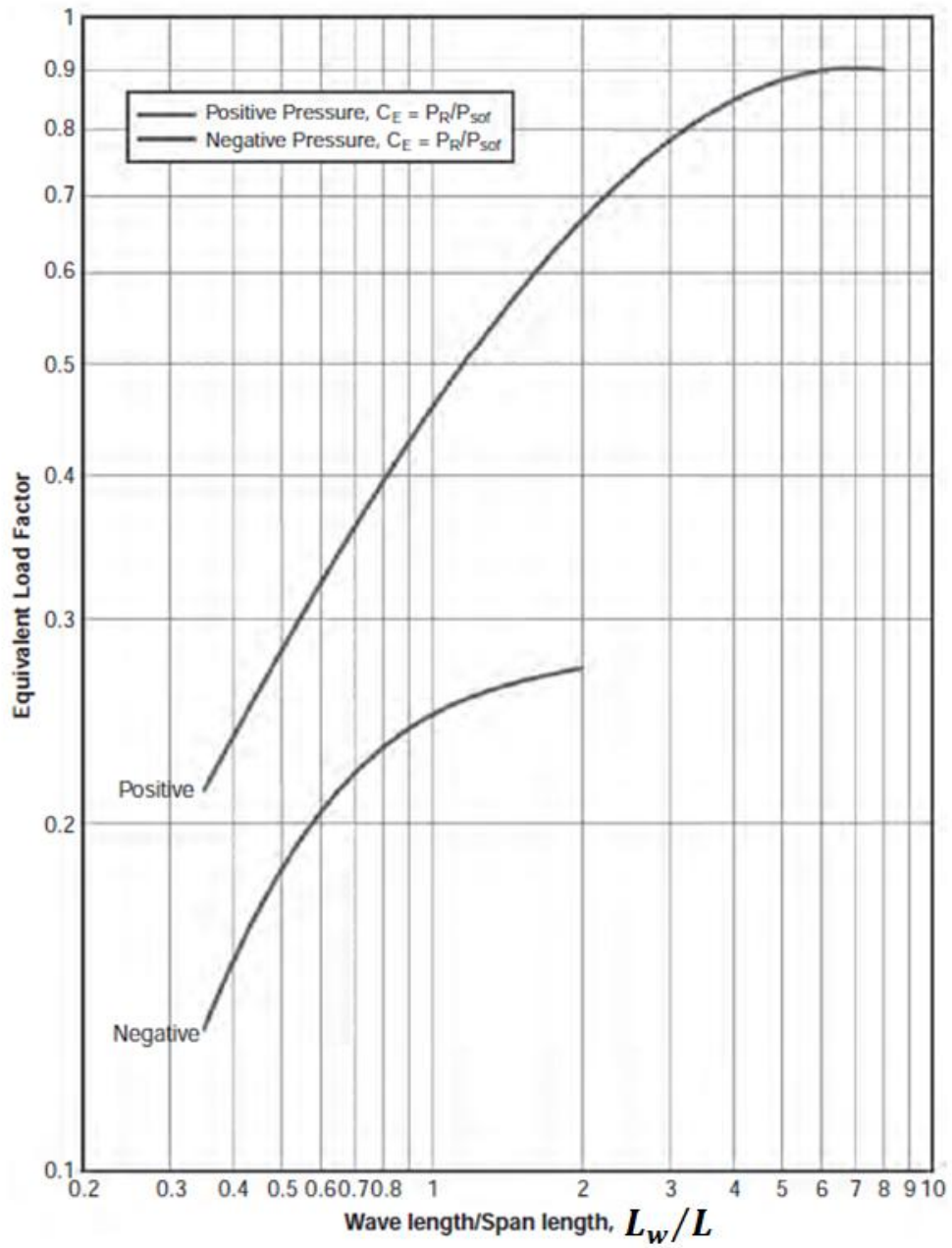


Figure 39. Equivalent Load Factor C_E [32]

Blast wave length L_w is determined by [23],

$$L_w = U_s t_d \quad (24)$$

where t_d is the positive phase duration in [ms], U_s is the shock front velocity in [km/s], L_w is blast wave length in [m]. Shock front velocity U_s is calculated by evaluating the function given in Equation (9) using the Kingery coefficients, which is the 1960's experimental data fit for the shock front velocity. Table 9 gives the Kingery coefficients used for the calculation for the shock front velocity.

Table 9. Kingery Coefficients for the Calculation of the Shock Front Velocity

Shock Front Velocity [km/s]							
Range Z [m/kg ^{1/3}]	A	B	C	D	E	F	G
0.06-1.50	0.1794	-0.956	-0.0866	0.109	0.0699	0.01218	0
1.50-40	0.2597	-1.326	0.3767	0.0396	-0.0351	0.00432	0

Drag coefficient for the rear loading is determined using the data given in Table 10.

Table 10. Rear Wall Drag Coefficients [23]

Peak dynamic pressure	Drag coefficient
0-25 psi	-0.40
25-50 psi	-0.30
50-130 psi	-0.20

Rise time t_r is determined by Equation (25) [18],

$$t_r = S/U_s \quad (25)$$

where S is minimum of height or width of the rear side of the structure in [ft], U_s is the shock front velocity in [ft/ms].

2.4. Material Behavior and the Structural Response

Structures like columns, beams, slabs etc. experience static loading because of carrying dead loads like their mass. In addition, as mentioned in Chapter 1, blast loading is categorized as the dynamic type of loading. Unlike static loading, dynamic loading includes inertia and damping effects. Moreover, dynamic loading in a very short period of time causes material to behave differently compared to its behavior under static loading. During the blast loading, structure is exposed to enormous loading in a very short period of time and material is subjected to strain rate effects. Blast loading has a strain rate in the range 10^2 - 10^4 [s^{-1}]. Since concrete and steel are the materials mostly used in bridge-like-structures, in this study material behavior of bridge-like-structures is examined. Girder bridge, shown in Figure 40, is selected for further examination since it is mostly used in the highways or used over the rivers due to its convenience.



Figure 40. Girder Type Bridge

Figure 41 shows components of the girder type bridge. A typical girder type of bridge consists of pier (column), bent (horizontal beam), girder (longitudinal beam) and deck (slab). Piers, which are the main carriers, support bents from below. Piers are generally made up of reinforced concrete. Bents and girders carry upper parts of

the girder bridge. Bents are made from reinforced concrete whereas girders can be from either reinforced concrete or steel [18].

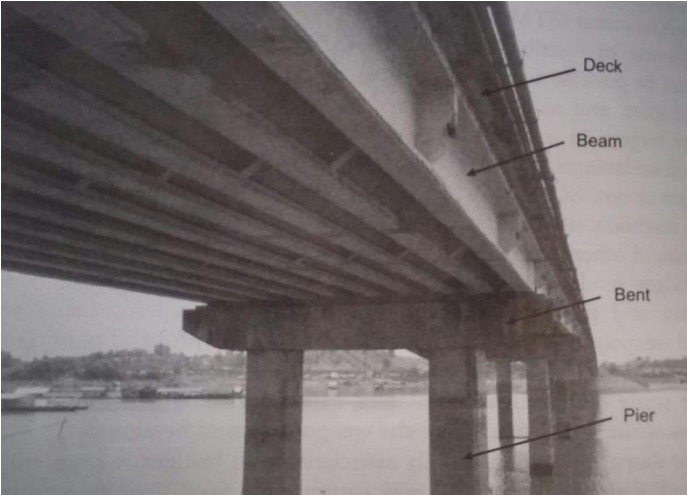


Figure 41. Components of Girder Type Bridge [18]

When a girder bridge is subjected to blast loading, either reinforced concrete or steel components experience strain rate effects. Strain rate due to blast loading increases the strength of the materials several times. This “several times” increase in strength due to strain rate hardening is named as “Dynamic Increase Factor” (DIF). In Figure 42, strain rate effect on the concrete is seen. Since the blast loading has a strain rate range of 10^2 - 10^4 [s^{-1}], in tension, strength of the concrete is multiplied by a factor of 8, while the strength of the concrete becomes four times the static strength in compression.

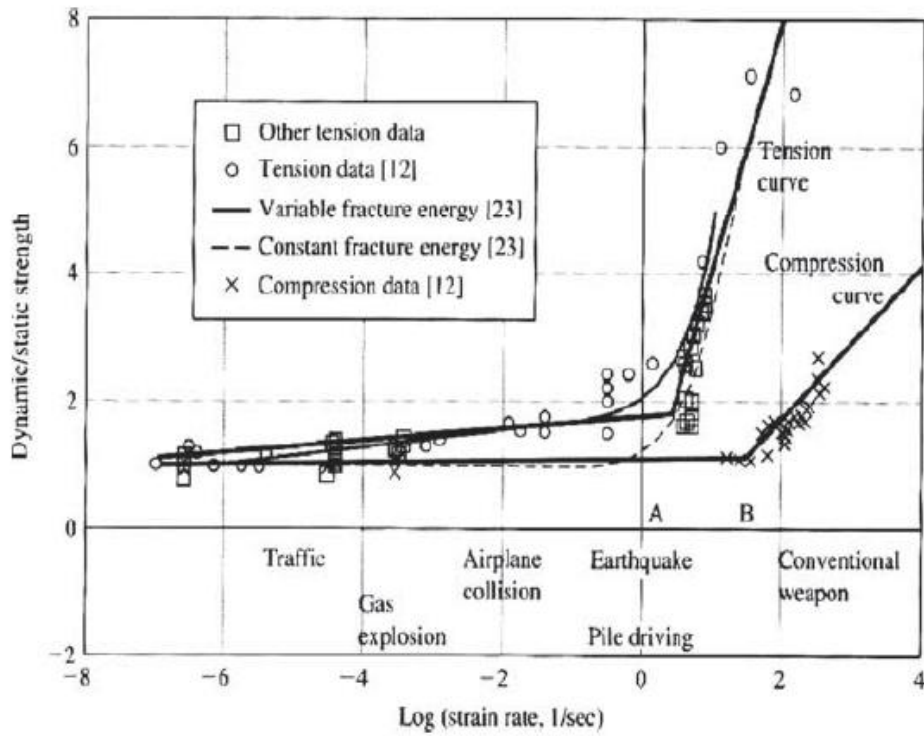


Figure 42. Strain Rate Effect on the Concrete [40]

Dynamic increase factor for steels, on the other hand, is calculated by using Equation (26) [41],

$$DIF = \left(\frac{\text{Strain Rate}}{10^{-4}} \right)^a \quad (26)$$

and,

$$a = 0.074 - 0.040 \frac{f_y}{414} \text{ for yield strength} \quad (27)$$

$$a = 0.019 - 0.009 \frac{f_u}{414} \text{ for ultimate strength}$$

where f_y is the static yield strength of the material in [ksi], f_u is the static ultimate strength in [ksi]. In another resource, dynamic increase factor is tabulated in terms of the stand-off distance and the type of failure. Table 11 gives the dynamic increase factor for concrete and steel depending on the type of failure and the stand-off distance [22].

Table 11. Dynamic Increase Factor for Far and Close-in Design Ranges [22]

Stress Type	Far Design Range				Close-in Design Range			
	Steel		Concrete		Steel		Concrete	
	DIF for Ultimate	DIF for Yield	DIF for Ultimate	DIF for Yield	DIF for Ultimate	DIF for Yield	DIF for Ultimate	DIF for Yield
Flexure	1.05	1.17	1.19	1.19	1.05	1.23	1.25	1.25

*Far design range : $Z \geq 2.5 \text{ ft/lb}^{1/3}$, close-in design range: $Z < 1 \text{ ft/lb}^{1/3}$

In addition to the dynamic increase factor which is due to the strain rate effect, another factor to consider for the material behavior in blast loading is the “Strength Increase Factor” (SIF). The mechanical properties obtained from standard tests are generally the minimum values. On the contrary, these properties are higher than specified values [19]. Regarding this fact, strength increase factor is a multiplication factor to be used in dynamic seismic and blast loading of structures in order to represent the actual strength of materials. For steel and steel contained materials, strength increase factor values are tabulated in Table 12 [42] .

Table 12. Strength Increase Factor Values for Different Materials [42]

Material	SIF
Structural Steel ($f_y \leq 50 \text{ ksi}$)	1.1
Reinforcing Steel ($f_y \leq 60 \text{ ksi}$)	1.1
Cold-Formed Steel	1.21
Concrete	1.0

For concrete, age factor is another strength increase factor which multiplies the strength of the material. Recommended values for the age factor of the concrete is tabulated in Table 13 [19]

Table 13. Age Factor for Concrete [19]

Age of Concrete	Age Factor
Less than 6 months	1.15
Greater than 6 months	1.1

Structures are exposed to huge impulsive loading due to blast. Exposed to considerable impulsive loading, structure is deflected as if it is rotated about some hinge points and “flexural deformation” occurs. Depending on the impulsive work done by the blast loading, structure, at first, deforms elastically and then undergoes

through the elastic-plastic regime. Finally, the structure is plastically deformed, as shown in Figure 43.

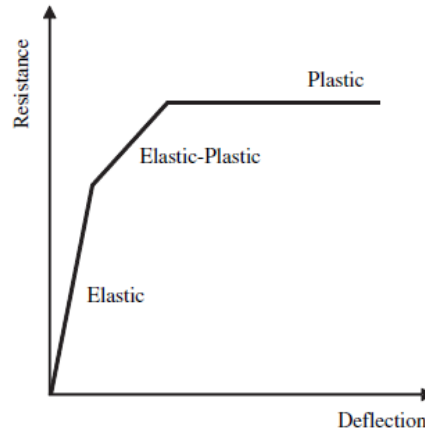


Figure 43. Elastic, Elastic-Plastic and Plastic Regime

Plastic hinges occur at the vicinity of the end supports and at the closest stand-off distance along the structure. For instance, if height of burst is half of the height of the column, hinges are observed at end points and at the midpoint, which is closest section of the structure to detonation point as shown in Figure 44 which also shows the formation of the plastic hinges in the blast loaded column and the beam. Assuming that the closest stand-off distance is at the midpoint of the structure, at the hinge locations, bending moment, known as plastic moment, is maximized. Plastic moment is the critical parameter to calculate damage in the structure [19].

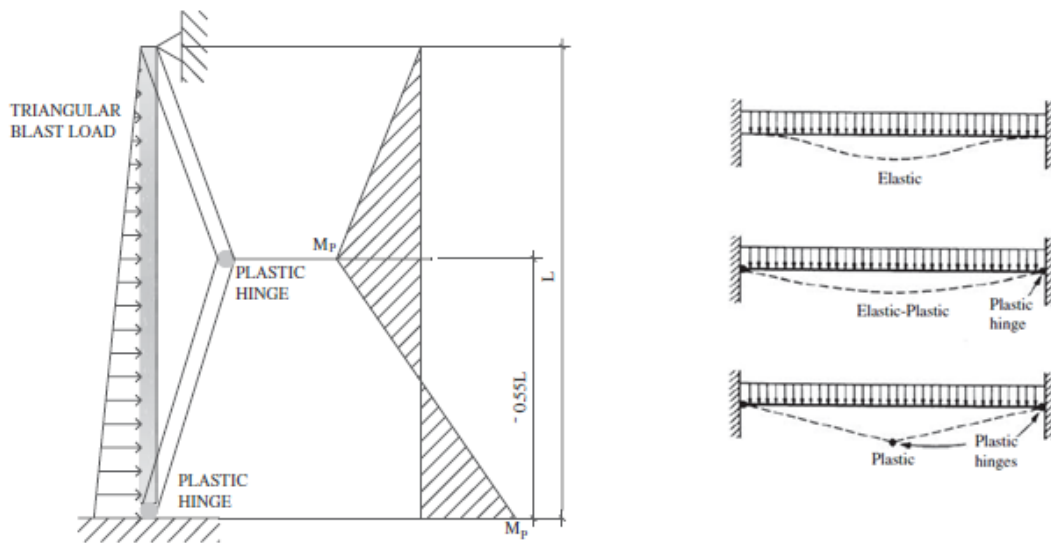


Figure 44. Plastic Hinge Formation for the Blast Loaded Column [19] and the Beam [43]

Maximum deflection of the structure, ductility ratio and the rotation of the structure about the hinge points are the significant parameters to decide whether the structure fails or not. Deflection of the column is related to the “ductility ratio” μ given by [22],

$$\mu = \frac{\Delta_{max}}{\Delta_{elastic}} \quad (28)$$

where Δ_{max} is maximum deflection of the blast loaded structure, $\Delta_{elastic}$ is allowable elastic deflection of the structure. In Figure 45, blast-loaded beam is deflected such that the beam looks like as if it is broken and rotated about hinge points. Maximum deflection Δ_{max} and support rotation parameters are shown in Figure 45.

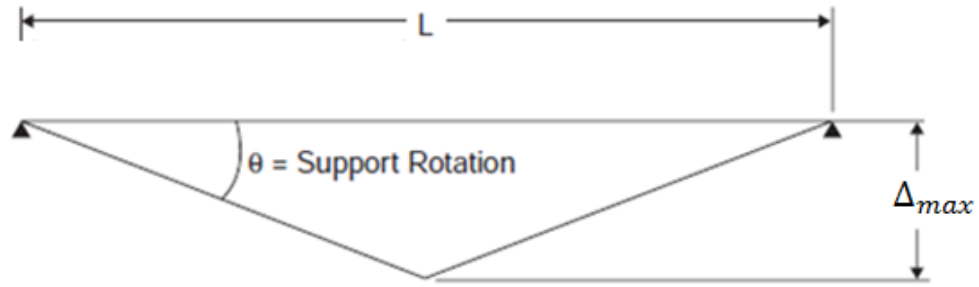


Figure 45. Maximum Deflection and Support Rotation [23]

Hinge (support) rotation, which is function of maximum deflection, is computed as,

$$\theta_{max} = \tan^{-1}\left(\frac{\Delta_{max}}{L/2}\right) \quad (29)$$

After the calculation of the maximum deflection and the hinge rotation, whether the structure fails or not is decided depending on the maximum deflection and the hinge rotation. Department of Defense in United States published a table, given in Table 14, for the assessment of damage based on the maximum deflection and the hinge rotation. In Table 14, structural members are categorized as reinforced concrete, prestressed concrete, masonry and steel structures. Component damage is divided into 4 zones. From superficial to hazardous, damage level rises in the structure. Hazardous damage level is considered as the limit just before the failure of the structure. For some structure and damage level, ductility ratio is not given or vice versa. In the present study, by referencing Table 14, for the reinforced concrete, 10 degree of hinge rotation is considered to cause failure of the structure such that it cannot function anymore. For steel-made-structures, the limit is taken as 20 degrees.

**Table 14. Failure Criteria Published by Department of Defense of the US Army
for Antiterrorism Design [23]**

Element Type		Superficial		Moderate		Heavy		Hazardous	
		Ductility Ratio	Max Hinge Rotation [deg]	Ductility Ratio	Max Hinge Rotation [deg]	Ductility Ratio	Max Hinge Rotation [deg]	Ductility Ratio	Max Hinge Rotation [deg]
Reinforced Concrete	Single-reinforced slab or beam	1	-	-	2	-	5	-	10
	Double-reinforced slab or beam without shear	1	-	-	2	-	5	-	10
	Double-reinforced slab or beam with shear	1	-	-	4	-	6	-	10
Structural Steel (hot-rolled)	Beam with compact section	1	-	3	3	12	10	25	20
	Beam with noncompact section	0.7	-	0.85	-	1	-	1.2	
	plate bent about weak axis	4	1	8	2	20	6	40	12
Cold-formed steel	Girt or purlin	1	-	-	3	-	10	-	20
	Stud with sliding connection at top	0.5	-	0.8	-	0.9	-	1	-

2.5. Single Degree of Freedom (SDOF) Method and the Failure Criteria

Single degree of freedom simplifies the structural system into a lumped mass and spring system. Damping effect is also included in the SDOF method. Figure 46 shows the SDOF simplification of a structural system.

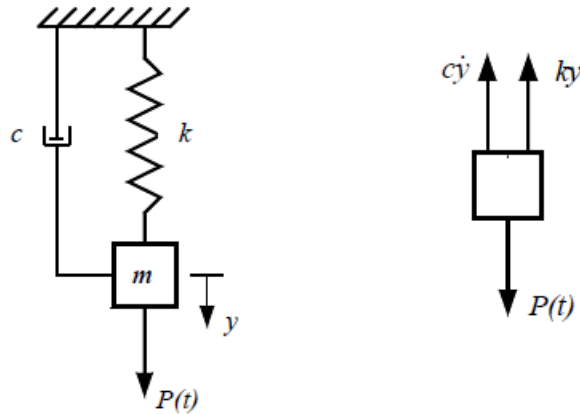


Figure 46. SDOF Simplification of a Structural System

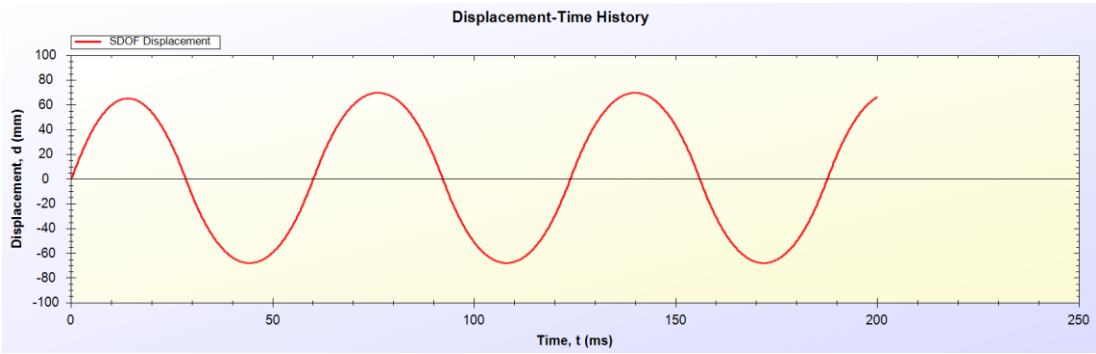
The equation of motion for such a SDOF system is given by,

$$m\ddot{y} + c\dot{y} + ky = P(t) \quad (30)$$

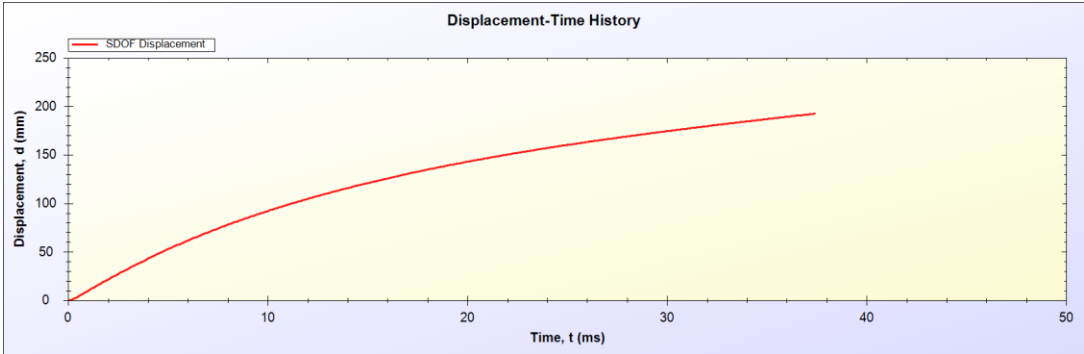
where m is total lumped mass, c is the damping, k is the stiffness of the structural system. SDOF methodology is extensively used in order to find maximum deflection and rotation of the structure exposed to the blast load. With the knowledge of the maximum deflection and rotation of the structure, failure analysis of the structure can be performed.

In the SDOF method, the impulsive work due to blast pressure as function of time is given as input to the structural system and the deflection and rotation of the system as function of time is the output. Depending on the magnitude of the impulsive work on the structure, structure, represented by the lumped mass, spring and damper, either has sinusoidal displacement curve or an increasing and converging displacement curve, as depicted in Figure 47. In RC-BLAST software, a 0.5x0.5x5 m concrete column is modeled and exposed to blast load of 20 kg and 30 kg of TNT at a stand-off distance 1m [5]. For the first case, lumped mass has a fluctuating

displacement history as seen in Figure 47a and has a maximum deflection of 62 mm. Structure is damaged but survives in this case. On the other hand in the second case, structure is subjected to the blast loading due to the explosion of 30 kg of TNT at 1 m, and it is seen that the structure has an increasing displacement with a decreasing slope, as seen in Figure 47b. In the second case, deflection converges to the allowable deflection limit and the structure fails [5].



(a)



(b)

Figure 47. Displacement Characteristics for Different Blast Loading [5]

In the SDOF method, lumped mass of the structural system is taken as the total mass of the structure. Lumped mass is exposed to the net loading given by Equation

(19). Blast loading is a time-dependent impulsive loading. In the calculation of the impulsive work on the structure, lumped mass and the load are multiplied by factors determined by Biggs [43]. Biggs tabulated load and mass factors depending on the end conditions and the type of loading. Table 15 gives the load and mass factors in

order to convert the continuous structural system to the discrete SDOF system, as depicted in Figure 48.

Table 15. Load and Mass Factors for Different Boundary Conditions and Loading Used in the SDOF Method [43]

	Strain Range	Load Factor K_L	Mass Factor K_M
Fixed-Fixed & Uniformly Loaded	Elastic	0.53	0.41
	Elastic-Plastic	0.64	0.50
	Plastic	0.50	0.33
Fixed-Fixed & Point Load	Elastic	1.0	1.0
	Plastic	1.0	1.0
Simply Supported & Uniformly Loaded	Elastic	0.64	0.50
	Plastic	0.50	0.33
Simply Supported & Point Load	Elastic	1.0	1.0
	Plastic	1.0	1.0

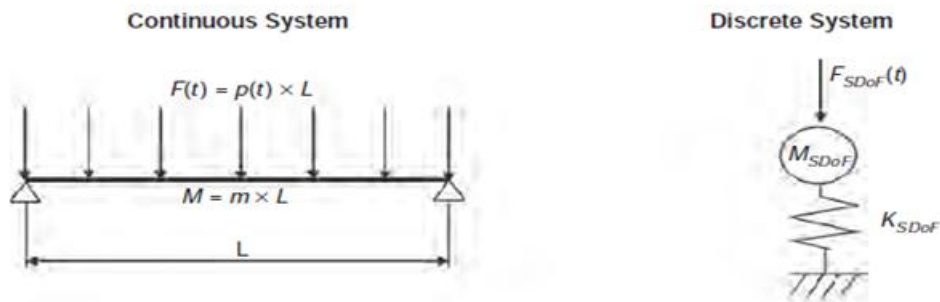


Figure 48. Conversion of the Continuous Structural System into Discrete SDOF System

Using load and mass factors given by Biggs [43], SDOF conversion process is made as follows:

- Lumped mass M is multiplied by mass factor to obtain the mass of the SDOF system M_{SDOF} .
- Blast load F is multiplied by the load factor to obtain blast load of the SDOF system F_{SDOF} .
- Stiffness of the structure K is multiplied by the load factor to obtain stiffness of the SDOF system K_{SDOF} .
- Resistance force R_{yield} exerted by the structure is multiplied by load factor to obtain the resistance force exerted by the spring of the SDOF system $R_{yield,SDOF}$.
- Impulse of blast load I is multiplied by load factor to obtain impulse of discrete SDOF system I_{SDOF} .
- Impulsive work done on the structure is multiplied by the load factor to obtain impulsive work done on the discrete SDOF system.

During the positive phase duration, lumped mass of SDOF system is exposed to impulse, which is equal to change in momentum of the lumped mass. Since velocity of the lumped mass $v(t)$ is zero at time zero, the relation between the momentum and the impulse is given by Equation (31).

$$M_{SDOF}v = I_{SDOF} \quad (31)$$

Impulse of blast load is converted to the kinetic energy of the lumped mass, which is equal to the impulsive work done on the SDOF system. Thus,

$$W_{impulse,SDOF} = \frac{1}{2}M_{SDOF}v^2 \quad (32)$$

Substituting v from Equation (31) into Equation (32) yields the impulsive work done on the SDOF system $W_{impulse,SDOF}$, which is given by Equation (33) [23],

$$W_{impulse,SDOF} = \frac{I_{SDOF}^2}{2M_{SDOF}} \quad (33)$$

where M_{SDOF} is the lumped mass of the SDOF system, I_{SDOF} is the impulse exerted to the SDOF system. The impulsive work on the SDOF system causes the structure to deflect. For a spring-mass system as shown in Figure 48, maximum resistance force R_{yield} exerted by the spring on the lumped mass M_{SDOF} occurs at the time of maximum deflection. Impulsive work on the SDOF system I_{SDOF} is simply equivalent to resistance of the spring R_{yield} multiplied by maximum deflection Δ_{max} . Hence, maximum deflection of the system is calculated as [23],

$$\Delta_{max} = \frac{W_{impulse,SDOF}}{R_{yield,SDOF}} \quad (34)$$

For a beam/column, resistance force R_{yield} is tabulated by Biggs depending on the loading type and boundary conditions in Table 16 [43].

Table 16. Maximum Resistance for Different Loading and Boundary Conditions for a Beam/Column Structure Supported at Both Ends [43]

	Strain Range	R_{yield}
Fixed-Fixed & Uniformly Loaded	Elastic	$\frac{12M_p}{L}$
	Elastic-Plastic	$\frac{8M_p}{L}$
	Plastic	$\frac{8M_p}{L}$
Fixed-Fixed & Point Load	Elastic	$\frac{4M_p}{L}$
	Plastic	$\frac{4M_p}{L}$
Simply Supported & Uniformly Loaded	Elastic	$\frac{8M_p}{L}$
	Plastic	$\frac{8M_p}{L}$
Simply Supported & Point Load	Elastic	$\frac{4M_p}{L}$
	Plastic	$\frac{4M_p}{L}$

A structure subjected to blast load is deflected as shown in Figure 44 and enormous bending moment is exerted by means of blast load. Depending on the geometry of the structure, plastic moment capacity M_p , which is the allowable bending moment capacity, is determined by using Equation (35) [23],

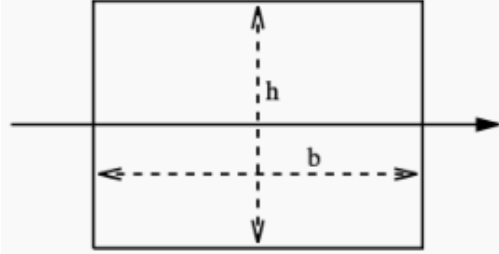
$$M_p = \frac{S_m + Z_m}{2} f_{dy} (if \mu < 3) \quad (35)$$

$$M_p = Z_m f_{dy} (if \mu > 3)$$

where μ is the ductility ratio, S_m is the elastic section moduli, Z_m is the plastic section moduli, f_{dy} is the yield strength of the structure. Section modulus is geometric property of the cross section of the beams, columns, or flexural members. Depending on the deformation type, section modulus is computed for the elastic and the plastic deformation separately. Elastic and plastic section moduli of the beam/column cross-sections are listed in Table 17.

Table 17. Elastic and Plastic Section Modulus for Rectangular Cross Section

[44]

	
Elastic Section Modulus S_m	$S_m = \frac{bh^2}{6}$
Plastic Section Modulus Z_m	$Z_m = \frac{bh^2}{4}$

To check whether the structure is in the elastic or plastic regime, maximum elastic work on the SDOF system should be calculated. At its elastic limit, impulsive work done on the SDOF system is given by Equation (36).

$$W_{SDOF,el,max} = \frac{1}{2} K_{SDOF} \Delta_{el}^2 \quad (36)$$

Since the resistance force at the yield point is the stiffness of SDOF system K_{SDOF} multiplied by deflection at elastic limit deflection Δ_{el} , maximum impulsive work for elastic deformation $W_{SDOF,el,max}$ is calculated as [23],

$$W_{SDOF,el,max} = \frac{R_{yield,SDOF}^2}{2K_{SDOF}} \quad (37)$$

If the impulsive work done on the SDOF system is greater than the maximum elastic work on the system, the impulsively loaded structure is in the plastic regime.

To justify the impulsive loading assumption, it is recommended to satisfy the following inequality [23],

$$\frac{t_d}{T} < 0.1 \quad (38)$$

where t_d is the positive phase duration and T is the period of the SDOF system. Period of SDOF system T is determined by [23],

$$T = 2\pi \sqrt{\frac{M_{SDOF}}{K_{SDOF}}} \quad (39)$$

where M_{SDOF} is the lumped mass of SDOF system, K_{SDOF} is the stiffness of SDOF system. For beams/columns supported at both ends, stiffness of the converted SDOF system, K_{SDOF} , is listed by Biggs in Table 18 [43].

Table 18. Stiffness of Beams/Columns for Different Loading and Boundary Conditions [43]

	Strain Range	K_{SDOF}
Fixed-Fixed & Uniformly Loaded	Elastic	$\frac{384EI}{L^3}$
	Elastic-Plastic	$\frac{384EI}{5L^3}$
	Plastic	-
Fixed-Fixed & Point Load	Elastic	$\frac{192EI}{L^3}$
	Plastic	-
Simply Supported & Uniformly Loaded	Elastic	$\frac{384EI}{5L^3}$
	Plastic	-
Simply Supported & Point Load	Elastic	$\frac{48EI}{L^3}$
	Plastic	-

CHAPTER 3

DEVELOPMENT OF THE BLAST LOAD INDUCED DAMAGE

CALCULATION TOOL

In this chapter, the methodology for predicting the blast-induced damage in bridge-like-structures is explained in detail. Based on the methodology described in Chapter 2, a fast-responding tool is developed for the prediction of blast-induced damage in bridge-like structures. In Chapter 2, the underlying theory for the relevant steps for the prediction of blast-induced damage is presented. In this chapter, with aid of flowcharts, the whole process of blast-induced damage is explained to aid the understanding of the capability of the developed fast-responding tool. The main process of assessing the blast-induced damage is shown in the flowchart given in Figure 49.

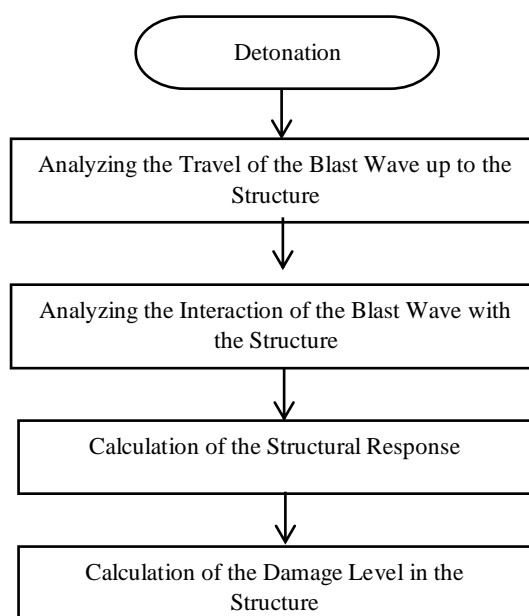


Figure 49. Main Flowchart of the Assessment of Blast-Induced Damage

After the detonation of the explosive, blast wave is formed and it propagates up to the structure. Then, blast wave impacts the structure and interacts with it. Depending on the impulsive work on the structure, structure is deflected and damaged. With the use of relevant failure criteria, the damage level in the structure is predicted. The main process of the damage assesement due to blast loading is explained in detail in sections 3.1, 3.2, 3.3.

3.1. Blast Propagation up to the Structure

Figure 50 shows the flowchart which gives the analysis of the blast wave up to the structure. When the blast wave propagates up to the structure; there are three different cases that one has to consider.

- Height of burst is high enough so that there is no Mach Stem formation. In this case, blast wave is fully incident (side-on) wave.
- Height of burst is at a certain height so that Mach Stem is formed. However, triple point height is less than the height of the structure. In this case, the structure is divided into two regions. First region is exposed to the Mach Stem wave. Second region is exposed to the incident wave.
- Height of burst is so low that Mach Stem is formed and triple point height is higher than the height of structure. In this case, all the structure is subjected to the Mach Stem.

Blast wave interactions for all three cases are shown with a flowchart in Figure 51.

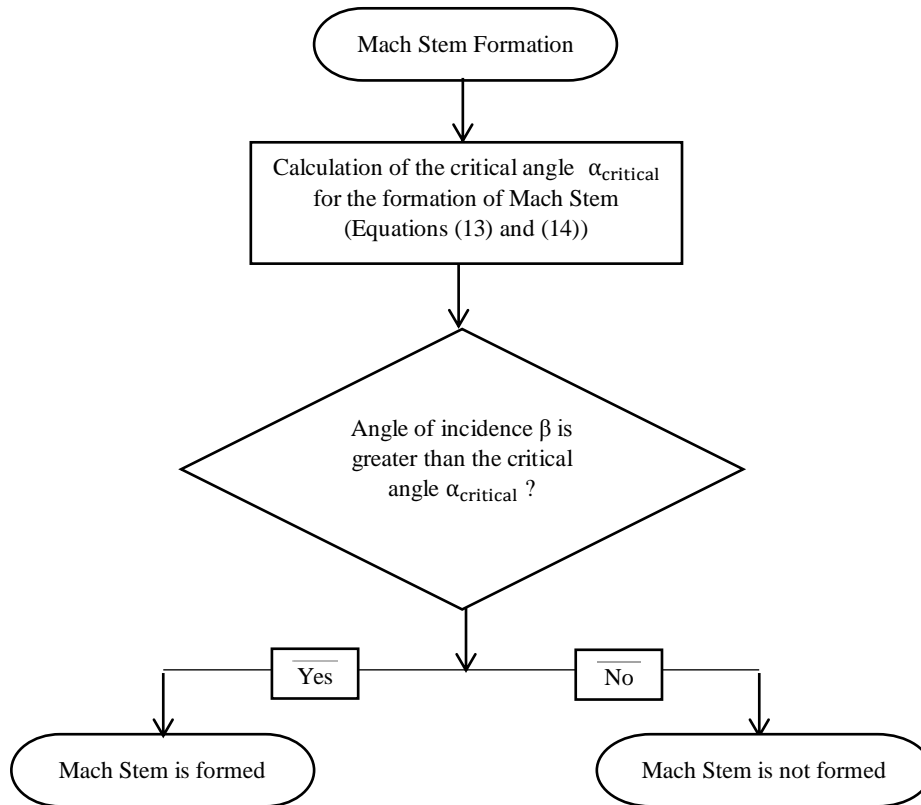


Figure 50. Mach Stem Formation

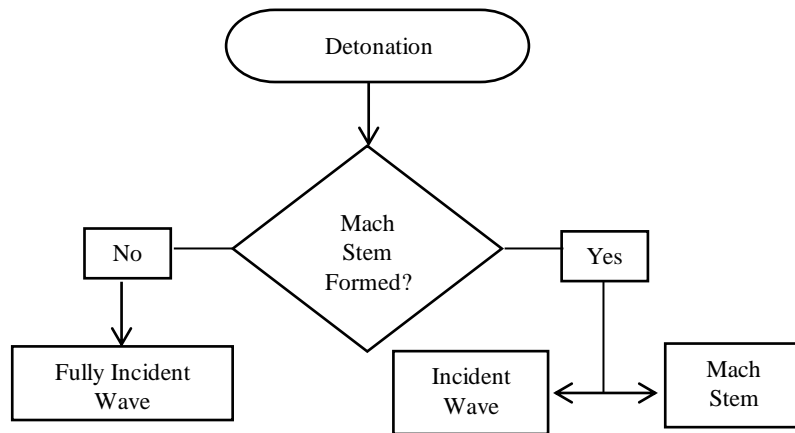


Figure 51. Analysis of the Blast Wave up to the Structure

In all three cases, side-on overpressure should be calculated. Side-on overpressure is calculated using the equivalent mass of the explosive. The process of calculating the equivalent mass of the explosive is explained with the flowchart in Figure 52.

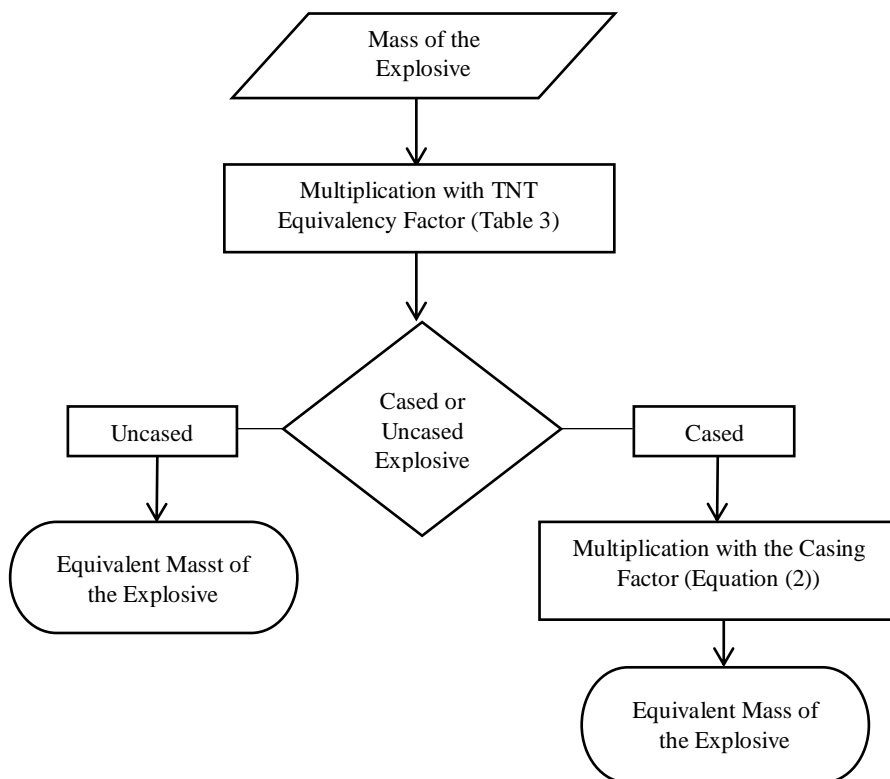


Figure 52. Calculation of the Equivalent Weight of the Explosive

After determining the equivalent mass of explosive, scaled distance should be calculated in order to find blast parameters such as side-on overpressure, positive phase duration etc. Most important parameter to be determined in a typical blast curve, given by Figure 21, is the side-on overpressure. There are several approaches followed in the literature to calculate the side-on overpressure. Equations (4), (5), (6), (7), (8), (9) given in Chapter 2 are different formulae that are used for the calculation of the side-on pressure. In order to find the best method to calculate the side-on overpressure accurately, six different approaches are compared with the test results obtained in 1960s and presented in Figure 22 in Chapter 2. For the comparison purpose, test data in Figure 22 is transferred to the digital environment. Side-on overpressures calculated by different approaches are compared with the experimental results in Table 19 and Table 20.

Table 19. Comparison of Side-on Overpressure Calculations

Scaled Distance [m/kg ^{0.33}]	Side-on Overpressure [kPa]						
	Test Results	Kinney Equation (2)	Difference [%]	Brode Equation (3)	Difference [%]	Newmark Equation (4)	Difference [%]
0.07	56091.30	47194.19	15.86%	2349953.35	-4089.51%	2396730.90	-4172.91%
0.08	48471.80	41678.54	14.01%	1419516.51	-2828.54%	1450748.49	-2892.97%
0.09	42360.50	37165.63	12.26%	932642.30	-2101.68%	955205.72	-2154.94%
0.10	37860.50	32824.96	13.30%	612762.98	-1518.48%	629237.30	-1561.99%
0.11	33460.70	29683.55	11.29%	445323.21	-1230.88%	458386.25	-1269.92%
0.13	28915.40	25794.07	10.79%	292603.37	-911.93%	302315.43	-945.52%
0.15	24708.40	22208.32	10.12%	192273.55	-678.17%	199563.62	-707.68%
0.17	21113.60	19314.84	8.52%	132881.66	-529.37%	138586.52	-556.39%
0.19	18245.50	16784.43	8.01%	93401.58	-411.92%	97941.82	-436.80%
0.22	15074.40	14270.33	5.33%	63493.44	-321.20%	67048.89	-344.79%
0.25	13026.70	11928.07	8.43%	42454.85	-225.91%	45224.15	-247.17%
0.29	10642.40	9546.60	10.30%	26558.61	-149.55%	28638.45	-169.10%
0.33	8694.55	7929.59	8.80%	18381.72	-111.42%	20047.15	-130.57%
0.38	7103.20	6406.62	9.81%	12314.48	-73.37%	13623.31	-91.79%
0.44	5803.11	4924.82	15.13%	7730.30	-33.21%	8718.43	-50.24%
0.51	4794.52	3923.43	18.17%	5284.36	-10.22%	6067.43	-26.55%
0.62	3384.90	2724.54	19.51%	2979.24	11.98%	3524.99	-4.14%
0.71	2673.74	2072.12	22.50%	1991.63	25.51%	2409.50	9.88%
0.84	1908.96	1454.48	23.81%	1223.59	35.90%	1518.53	20.45%

1.00	1393.90	1017.97	26.97%	778.70	44.14%	983.21	29.46%
1.16	984.08	721.26	26.71%	523.98	46.75%	663.24	32.60%
1.37	710.54	499.78	29.66%	360.44	49.27%	447.07	37.08%
1.54	513.03	381.32	25.67%	283.01	44.84%	339.00	33.92%
1.78	358.15	271.81	24.11%	218.23	39.07%	243.25	32.08%
2.05	258.60	196.06	24.18%	177.67	31.29%	178.78	30.86%
2.43	178.51	132.87	25.57%	146.92	17.70%	125.33	29.79%
2.81	131.82	95.48	27.57%	130.31	1.14%	93.25	29.26%
3.30	93.06	66.84	28.18%	118.62	-27.46%	67.88	27.06%
3.76	71.08	50.97	28.28%	112.65	-58.50%	53.22	25.12%
4.32	56.14	38.51	31.41%	108.31	-92.92%	41.17	26.67%
4.94	42.40	29.87	29.55%	105.55	-148.95%	32.40	23.59%
5.56	35.03	24.22	30.86%	103.90	-196.61%	26.39	24.65%
6.61	27.06	18.15	32.91%	102.32	-278.17%	19.64	27.39%
7.52	21.37	14.88	30.37%	101.57	-375.28%	15.85	25.82%
8.51	18.06	12.44	31.09%	101.09	-459.79%	12.95	28.27%
9.84	14.92	10.20	31.66%	100.70	-574.97%	10.24	31.38%
11.32	12.19	8.51	30.18%	100.46	-724.20%	8.19	32.82%
13.47	9.63	6.88	28.52%	100.27	-941.47%	6.23	35.31%
15.75	8.14	5.73	29.54%	100.17	-1131.30%	4.88	40.05%
18.22	6.35	4.87	23.43%	100.11	-1475.44%	3.89	38.74%
21.80	5.19	4.00	22.94%	100.06	-1827.51%	2.95	43.08%
25.36	4.44	3.40	23.27%	100.04	-2155.16%	2.34	47.15%
31.20	3.31	2.74	17.30%	100.02	-2919.31%	1.71	48.38%
36.70	2.62	2.32	11.48%	100.01	-3722.04%	1.34	48.93%
39.25	2.31	2.16	6.52%	100.01	-4224.50%	1.21	47.81%

Table 20. Comparison of Side-on Overpressure Calculations (Continued)

Scaled Distance [m/kg ^{0.33}]	Side-on Overpressure [kPa]						
	Test Results	Mills Equation (5)	Difference [%]	Sadovski Equation (6)	Difference [%]	Kingery Equation (7)	Difference [%]
0.07	56091.30	6190161.17	-10935.87%	2551416.40	-4448.68%	-	-
0.08	48471.80	3736621.47	-7608.86%	1548459.91	-3094.56%	-	-
0.09	42360.50	2453360.13	-5691.62%	1022009.78	-2312.65%	-	-
0.10	37860.50	1610664.73	-4154.21%	675010.25	-1682.89%	-	-
0.11	33460.70	1169777.09	-3395.97%	492775.91	-1372.70%	-	-
0.13	28915.40	767864.66	-2555.56%	325959.08	-1027.29%	-	-
0.15	24708.40	504010.15	-1939.83%	215845.21	-773.57%	-	-
0.17	21113.60	347932.35	-1547.91%	150323.79	-611.98%	-	-
0.19	18245.50	244258.83	-1238.73%	106535.78	-483.90%	18172.11	0.40%
0.22	15074.40	165786.47	-999.79%	73159.90	-385.33%	15305.89	-1.54%
0.25	13026.70	110640.24	-749.33%	49505.93	-280.03%	12847.50	1.38%
0.29	10642.40	69022.88	-548.56%	31464.23	-195.65%	10471.21	1.61%
0.33	8694.55	47642.97	-447.96%	22083.74	-154.00%	8883.77	-2.18%
0.38	7103.20	31799.14	-347.67%	15045.80	-111.82%	7375.48	-3.83%
0.44	5803.11	19846.37	-242.00%	9651.51	-66.32%	5865.07	-1.07%
0.51	4794.52	13479.09	-181.14%	6725.22	-40.27%	4801.91	-0.15%
0.62	3384.90	7489.20	-121.25%	3908.56	-15.47%	3460.91	-2.25%
0.71	2673.74	4927.86	-84.31%	2668.65	0.19%	2689.83	-0.60%
0.84	1908.96	2939.05	-53.96%	1676.33	12.19%	1926.76	-0.93%
1.00	1393.90	1788.49	-28.31%	1079.64	22.55%	1366.02	2.00%
1.16	984.08	1130.02	-14.83%	723.37	26.49%	974.72	0.95%
1.37	710.54	706.91	0.51%	483.42	31.96%	677.99	4.58%
1.54	513.03	506.09	1.35%	364.04	29.04%	518.12	-0.99%
1.78	358.15	337.40	5.79%	258.90	27.71%	370.05	-3.32%
2.05	258.60	230.99	10.68%	188.73	27.02%	267.83	-3.57%
2.43	178.51	149.24	16.40%	131.20	26.50%	183.04	-2.54%
2.81	131.82	104.18	20.97%	97.13	26.32%	133.36	-1.17%
3.30	93.06	71.50	23.17%	70.58	24.16%	94.77	-1.84%
3.76	71.08	54.14	23.83%	55.44	21.99%	73.27	-3.09%
4.32	56.14	40.88	27.19%	43.15	23.14%	56.19	-0.08%
4.94	42.40	31.87	24.82%	34.30	19.10%	44.13	-4.08%
5.56	35.03	26.06	25.60%	28.29	19.23%	36.09	-3.02%
6.61	27.06	19.86	26.61%	21.58	20.24%	27.25	-0.71%
7.52	21.37	16.51	22.75%	17.82	16.64%	22.37	-4.68%

8.51	18.06	14.00	22.49%	14.93	17.31%	18.67	-3.41%
9.84	14.92	11.66	21.87%	12.21	18.13%	15.22	-2.01%
11.32	12.19	9.87	19.01%	10.14	16.81%	12.60	-3.36%
13.47	9.63	8.12	15.70%	8.12	15.69%	10.05	-4.35%
15.75	8.14	6.85	15.81%	6.68	17.83%	8.23	-1.20%
18.22	6.35	5.88	7.53%	5.61	11.71%	6.86	-7.92%
21.80	5.19	4.89	5.90%	4.55	12.41%	5.47	-5.43%
25.36	4.44	4.19	5.55%	3.82	13.79%	4.51	-1.67%
31.20	3.31	3.40	-2.72%	3.03	8.49%	3.42	-3.34%
36.70	2.62	2.89	-10.59%	2.54	3.09%	2.72	-4.05%
39.25	2.31	2.71	-17.03%	2.36	-1.92%	2.47	-6.63%

The results show that Kingery's results have the best fit with test results given in Figure 22. Side-on overpressures determined by the tests and calculated by the Kingery's empirical formula are compared in the graph given in Figure 53.

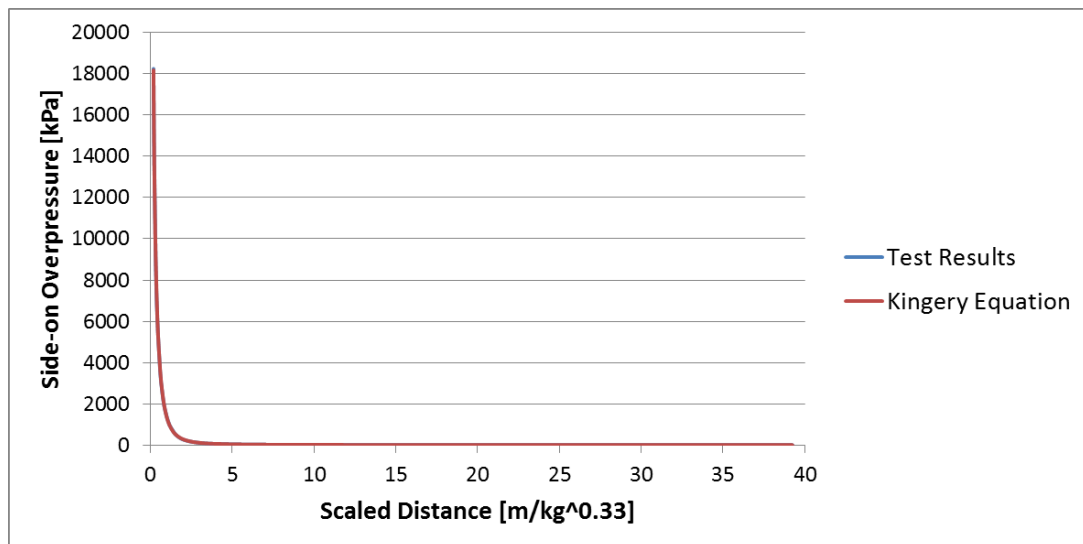


Figure 53. Comparison of Side-on Pressures Determined by Tests and Calculated by Kingery's Empirical Formula

It is seen that empirical formulae other than Kingery's have narrow ranges that fit good. At this point there are two alternatives to follow for the calculation of the side-on pressure. Either the side-on overpressure will be defined according to the scaled distance range using different formulae or Kingery's equation will be used for all

scaled distances. Looking at the percent differences given in Table 19 and Table 20, even the narrow ranges of different formulae has higher percent difference from the test results compared to the side-on pressure calculated by the Kingery's formula. It should be noted that unlike other empirical formulae, Kingery divided the considered three different ranges of the scaled distance to fit experimental data well. For positive phase duration and the shock front velocity, Kingery's approach is used in the tool developed within the scope of the thesis. For the positive phase duration and shock front velocity, Kingery coefficients are listed in Table 5 in Chapter 2.

3.2. Interaction of Blast Wave with the Structure

Blast wave propagates through the air in a spherical manner and once it reaches the structure, blast wave impacts the structure. At this point, second phase of the blast analysis, which is the interaction of the blast wave with the structure, begins. In Figure 54, main process for interaction with structure is explained via the flowchart.

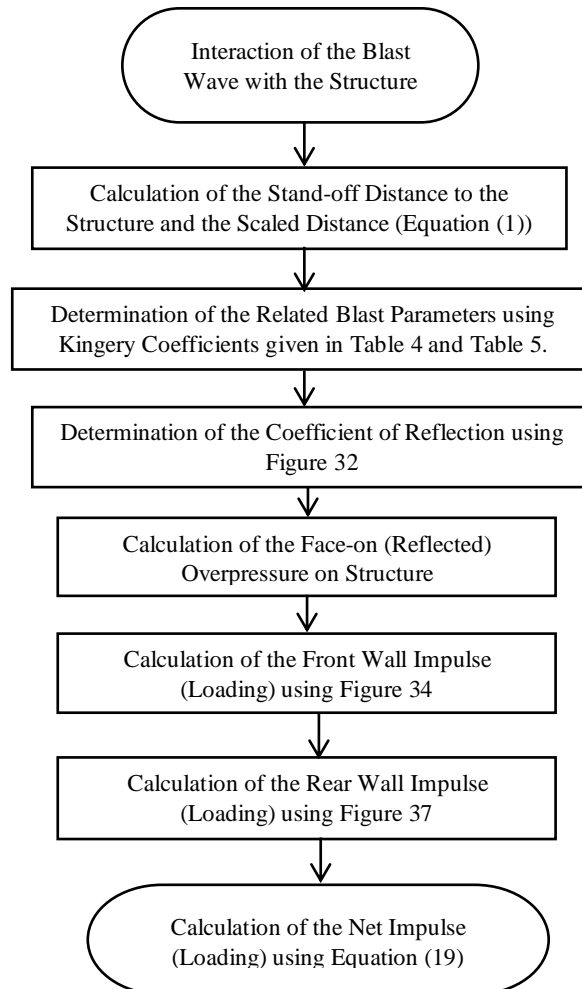


Figure 54. Analysis of the Interaction of the Blast Wave with the Structure

Using the stand-off distance to the structure, scaled distance has to be calculated. Scaled distance of a fixed mass of the explosive, or the stand-off distance, varies along the structure. Figure 55 shows how the scaled distance varies along the structure. Depending on the location of the explosive with respect to the structure and the length of the structure, scaled distance changes. In Figure 55, the top point

has a scaled distance of Z_1 whereas the midpoint has a scaled distance of Z_4 , and bottom point has a scaled distance of Z_7 .

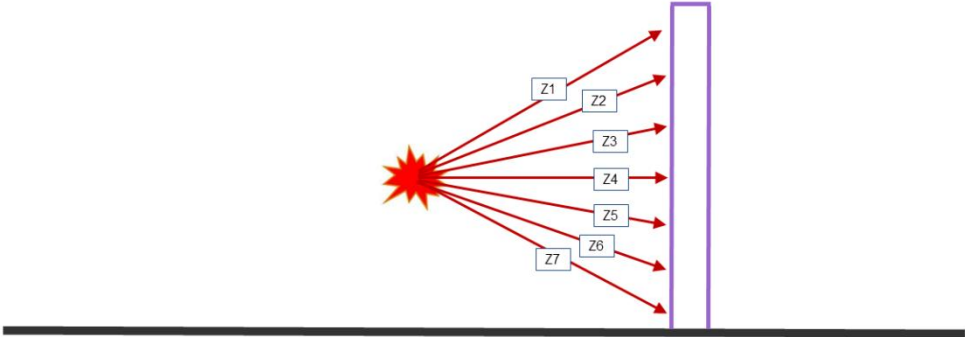


Figure 55. Variation of the Scaled Distance Along the Structure

Variation of the scaled distance along the structure depends on the height of the structure and the position of the explosive with respect to the structure. In Figure 56, two different structures with two different heights are seen. For both structures, structure is divided into 7 segments. As shown in Figure 56, when the height of structure increases, its effect on the scaled distance is higher compared to a structure with low height.

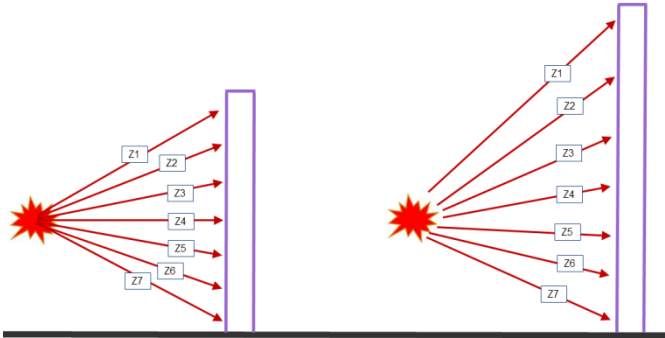


Figure 56. Variation of the Scaled Distance with the Height of the Structure

In Figure 57, two structures with same height are shown. One of the structures is exposed to near-field explosion, whereas the other structure is exposed to far-field explosion. As shown in Figure 57, as the distance from the explosion location to the structure increases, changes in the scaled distance at different segments in the structure diminish.

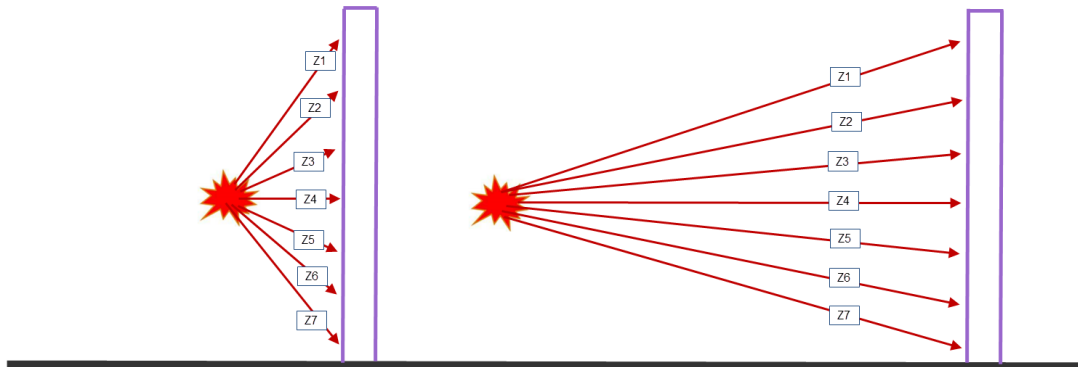


Figure 57. Variation of the Scaled Distance Due to Increase in Distance

After calculating the scaled distances for each segment along the structure, side-on overpressures for different segments are calculated. Following the calculation of the side-on overpressures, utilizing the coefficient of reflection graph given in Figure 32, and the angle of incidence given in Figure 30, face-on overpressure is computed. In order to use Figure 32 for the calculation of the coefficient of reflection for different side-on pressures automatically, the curves are divided into several regions so that appropriate curve fits could be performed. In Table 21, fit functions are given for for different side-on overpressures and different angle of incidence intervals. For intermediate side-on pressures, the developed tool uses interpolation to calculate the coefficient of reflection.

**Table 21. Fit Functions Used for the Calculation the Coefficient of Reflection
for Side-On Pressures in the Range 200 – 5000 Psi**

Side-on Overpressure [psi]	Angle of Incidence [deg]	Fit Function
5000 psi	0-45	$y = -0.0011773701x^2 - 0.0600908395x + 12.2816227670$
	46-52	$y = 0.0637034115x^3 - 9.4710081001x^2 + 468.7638751907x - 7,715.3712492941$
	53-85	$y = -0.0002951941x^3 + 0.0714568037x^2 - 5.7540106851x + 155.1177909063$
	86-90	1
3000 psi	0-43	$y = -0.0017772559x^2 - 0.0127160201x + 10.8444264516$
	44-52	$y = -0.0839470084x^2 + 7.9779657893x - 181.2190159583$
	53-85	$y = -0.0002948220x^3 + 0.0695927606x^2 - 5.4767818525x + 144.9631400256$
	86-90	1
2000 psi	0-43	$y = -0.0015412155x^2 - 0.0128817509x + 10.0266771658$
	44-51	$y = -0.0040936284x^3 + 0.5020435095x^2 - 19.9451749237x + 261.3722933939$
	52-85	$y = -0.0002965972x^3 + 0.0689801503x^2 - 5.3600800346x + 140.5430074971$
	86-90	1
1000 psi	0-43	$y = -0.0005300796x^2 - 0.0417335535x + 8.6495782176$
	44-53	$y = 0.0110070728x^3 - 1.6505526939x^2 + 82.1116322599x - 1,348.5379263807$
	54-85	$y = -0.0002311970x^3 + 0.0544859734x^2 - 4.2898844349x + 114.2248415517$
	86-90	1
500 psi	0-42	$y = -0.0002920896x^2 - 0.0407200922x + 7.8389110727$
	42-53	$y = 0.0088228860x^3 - 1.2985379395x^2 + 63.3793658801x - 1,019.5566890884$
	54-85	$y = -0.0001897874x^3 + 0.0451890592x^2 - 3.5992499994x + 97.2063024550$
	86-90	1
400 psi	0-40	$y = -0.0008672048x^2 - 0.0065661565x + 6.9840495122$
	41-50	$y = -0.0399925756x^2 + 3.6383806227x - 76.3138891658$
	51-85	$y = -0.0001327854x^3 + 0.0323332372x^2 - 2.6441672834x + 73.8652252463$
	86-90	1
300 psi	0-39	$y = -0.0007431326x^2 - 0.0089131298x + 6.6160424347$
	40-50	$y = -0.0288564900x^2 + 2.5616439755x - 50.9107027162$
	51-85	$y = -0.0000872903x^3 + 0.0225575165x^2 - 1.9499414737x + 57.4337143452$
	86-90	1
200 psi	0-37	$y = -0.0007967835x^2 - 0.0003832897x + 5.9353381333$
	38-50	$y = -0.0213043454x^2 + 1.8155750911x - 33.3009141972$
	51-85	$y = -0.0000503870x^3 + 0.0133640838x^2 - 1.2000410961x + 37.5386360980$
	86-90	1

Following calculation of the face-on overpressure, front and rear wall impulse/area are calculated. It should be noted that, side-loading is not taken into account since these loadings cancel each other. In the rear wall loading calculation, equivalent load factor is defined in a certain range, as seen in Figure 39. Equivalent load factor cannot be calculated for scaled distances less than $0.5 \text{ m/kg}^{1/3}$. In order to compare the front and the rear wall loading, ratio of the front wall loading to the rear wall loading is calculated for the $0.5 \times 0.5 \times 5 \text{ m}$ column. Then, a curve is fit to data points as shown in Figure 58. Calculation range of the scaled distance is taken up to $5 \text{ m/kg}^{1/3}$ because for scaled distances greater than $5 \text{ m/kg}^{1/3}$, no damage occurs in the structure [19].

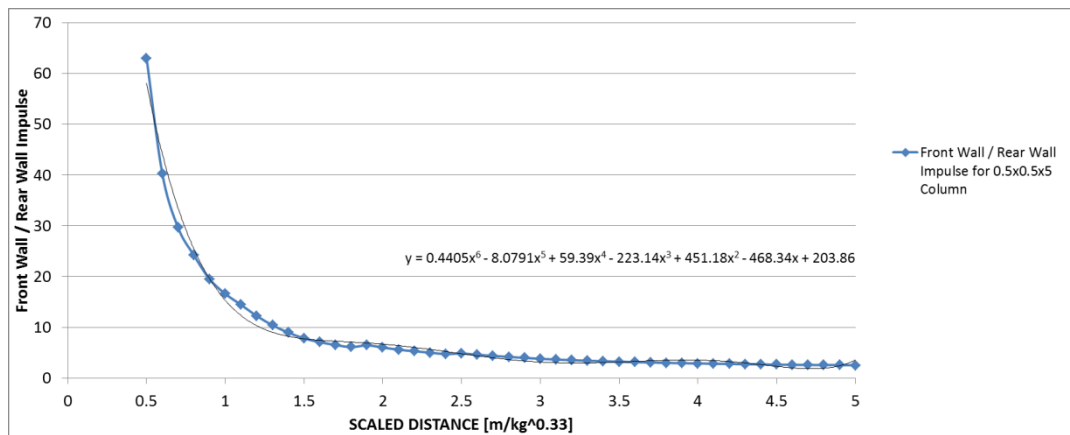


Figure 58. Ratio of the Front Wall Loading to the Rear Wall Loading as a Function of the Scaled Distance

For scaled distances less than $0.5 \text{ m/kg}^{1/3}$, rear wall loading cannot be calculated. However as seen in Figure 58, front wall loading is very dominant over the rear wall loading for low scaled distances. Therefore, in the developed tool, rear wall loading is ignored for scaled distances less than $0.5 \text{ m/kg}^{1/3}$.

3.3. Material Behavior and the Structural Response Due to Blast Loading

As mentioned before, blast loading is a type of dynamic loading. Unlike other dynamic loadings, such as wind and earthquakes, blast loading is an intensive loading which occurs in a very short period of time. Consequently, materials subjected to blast loading strengthen. In Figure 59, calculation of the dynamic strength of reinforced concrete and steel structures is shown in a flowchart.

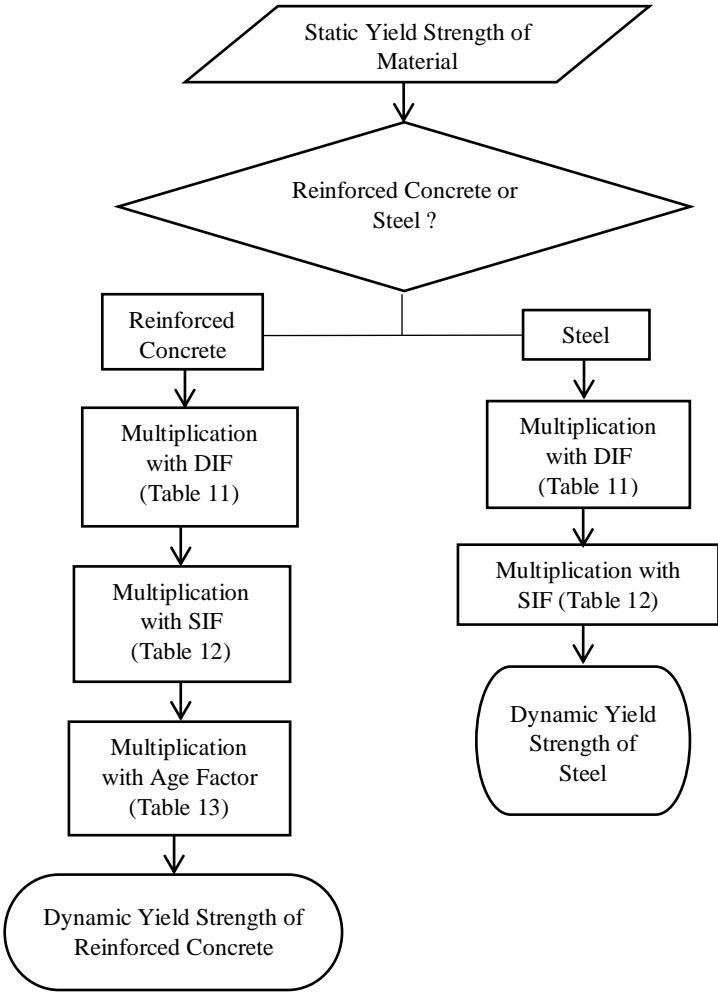


Figure 59. Calculation of Dynamic Strength

Once the dynamic strength of the structure is determined, structural response can be calculated. For this purpose, as the first step, net impulse is calculated, as described in Section 2.3. Net impulse is the external load applied to the SDOF system, in which mass, stiffness and loads are converted to the SDOF system by means of load and

mass factors. Calculation of the structural response is explained in the flowchart given in Figure 60.

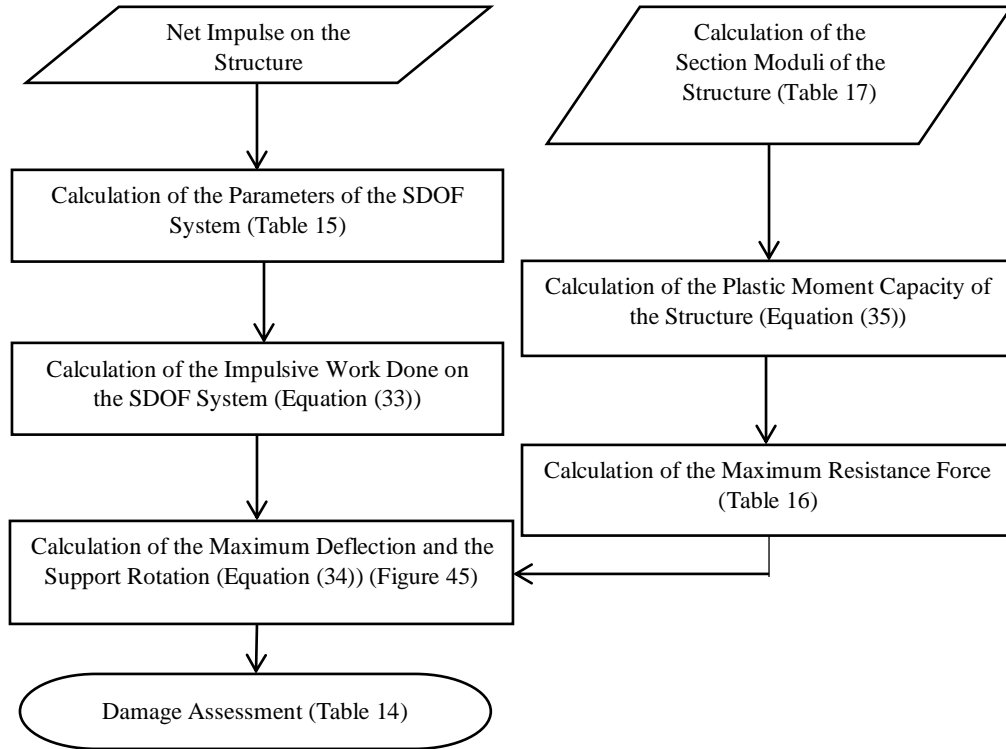


Figure 60. Calculation of the Structural Response

For the calculation of the structural response using the SDOF method, the load can be assumed to be either point load or uniform load. It should be noted that although the two cases do not cover all loading possibilities, especially for the far-field explosion, the loading tends to be uniform [12]. For the short stand-off distances, it is more accurate to use uniform loading than the point load. Hence, in the developed tool, uniform loading assumption is used. For the uniform loading assumption, a comprehensive study is performed and presented in Section 0.

Another assumption that is used to complete the process of the calculation of the structural response given in Figure 60 is that structure is assumed to be plastically deformed. The developed tool calculates the required mass of the explosive to destroy a given structure in the case studies. Since the developed code only aims to determine the limit explosive weight, one can assume that the structure has to be

plastically deformed. Thus, the tool uses plastic deformation cases presented in Table 15, Table 16 and Table 18. It should also be noted that, during the response analysis of the structure due to blast loading, the developed tool also calculates whether the structure is elastically or plastically deformed using Equation (37) for justification.

CHAPTER 4

RESULTS OF DAMAGE ASSESSMENT OF STRUCTURES SUBJECTED TO BLAST LOADING

In Chapter 3, the proposed method for the fast responding blast induced damage assessment tool is explained with flowcharts in detail. The tool is prepared in MS Excel spreadsheet and presented in Appendix A. The MS Excel spreadsheet has five regions.

In region 1 of the spreadsheet, the user gives the following as input:

- location of the explosive
- mass and the TNT equivalency of the explosive
- metal mass to explosive mass ratio
- location of the structure
- dimensions of the structure

With these input, in region 1 of the spreadsheet, following calculations are made:

- equivalent mass of the TNT explosive
- average stand-off and scaled distances with respect to the midpoint of the structure
- average side-on overpressure and dynamic overpressure value
- determination of whether the Mach Stem is formed or not
- Triple point height and Mach Stem pressure value

In region 2 of the Excel spreadsheet structure is divided into segments in order to calculate the impulsive loading accurately. Number of divisions that one can give as

input change from 1 to 10. In Section 4.1, a case study is performed in order to investigate the effect of number of divisions on the results. After the structure is divided into several zones, angles of incidence, scaled distances are calculated for all zones. The position vector for each zone is taken from the detonation point to the mid of the selected zone. After the calculation of the angle of incidence and scaled distance for each zone, side-on overpressure, positive phase duration, coefficient of reflection, face-on overpressure, dynamic overpressure, stagnation pressure, sound velocity and clearing time for each zone, are calculated respectively.

Thereafter, front and rear wall and net impulse/area are calculated for each zone. Impulse/area values are then multiplied by the loaded area of each zone and net impulse on each zone is determined. Finally, impulses on each zone are summed up and net impulse on the structure is determined.

In region 3 of the Excel spreadsheet, material and geometric properties of the structure is computed. In the first part of the region, the following are given as input:

- material of the structure (either reinforced concrete or steel)
- boundary condition (either fixed-fixed or simply supported)
- elastic and plastic section moduli
- moment of inertia
- static strength of the material

With these input, following calculations are made:

- dynamic increase factor and strength increase factor values
- load and mass factors
- dynamic strength of the structure

In region 4, structural response calculation by means of SDOF methodology is performed. In region 4, no external input is given but results of the calculations made in regions 1-3 are used in region 4 for the determination of the following:

- total force on the structure
- total impulse on the structure
- whether the structure is plastically deformed or not
- maximum deflection

In region 5, damage assessment of the structure is made. The output of region 5 is:

- maximum deflection
- hinge rotations
- whether the structure failed or not (according to the allowable hinge rotation criteria, see Table 14)
- If not failed, damage percent of the structure is given. Linear trend is assumed to determine damage percent. No blast load; i.e. no hinge rotation is regarded as “0% damaged” whereas 10° of hinge rotation for concrete materials, 20° of hinge rotation for steel materials are considered as “100% damaged”. For midranges, interpolation is performed.

4.1. Effect of the Number of Divisions on the Results

Since the scaled distance is the base point for determining the blast effect, scaled distance must be calculated for each zone in the structure which is divided into segments. In order to determine the optimum number of divisions, two different sample concrete columns, with dimensions of 0.5x0.5x5 m and 1x0.5x5 m are selected, as shown in Figure 61.

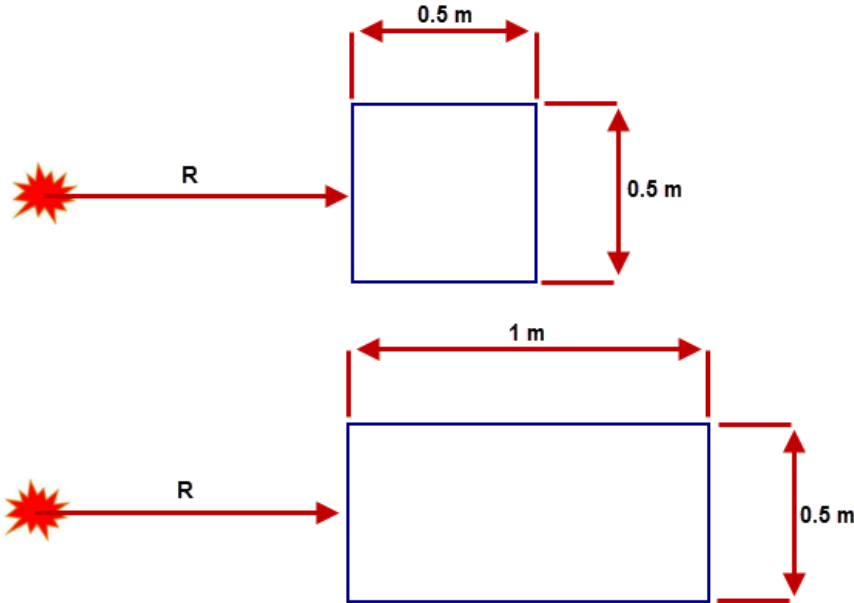


Figure 61. Cross Sections of Sample Columns

Columns are then exposed to the blast loading due to the explosion of TNT occurring at four different stand-off distances. Stand-off distances are taken as 1m, 2.5m, 5m and 10 m for the blast analysis of the two columns. For each analysis, mass of the TNT explosive required to cause 100% damage in the concrete column is determined. In other words, the required amount of explosive necessary for the concrete column to have 10° of hinge rotation is determined for each case. The sample columns are divided into 1, 2, 4, 6, 8 and 10 segments along the height of the columns. For example, if the sample column is divided into 10, each zone of the column is 0.5 m when Mach Stem is not formed. On the other hand, if Mach Stem is

formed, the column is divided into one Mach Stem region plus 10 segments, as shown in Figure 62.

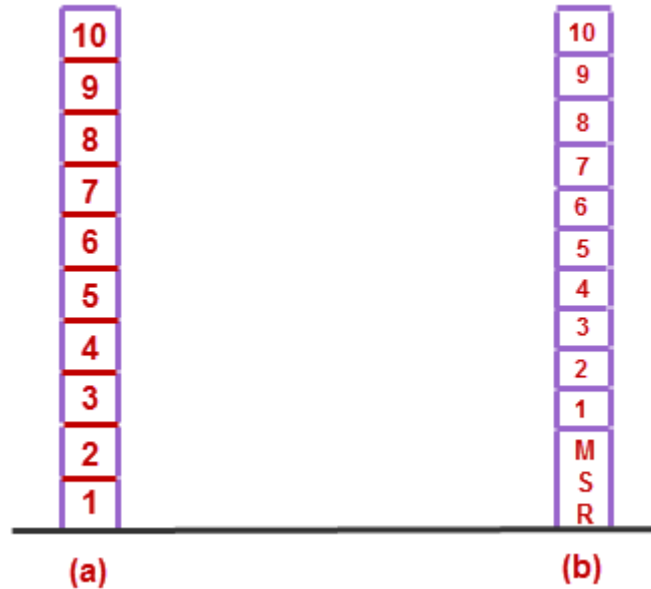


Figure 62. Sample Column Division with 10 Segments without/with Mach Stem Region (MSR)

For the 1 m stand-off distance, Figure 63 shows the variation of the TNT explosive mass required to fail the column with the number of divisions. It is seen that when the column is taken as one-piece, the required amount of TNT explosive is largely underestimated for the 1x0.5x5m column. For the 0.5x0.5x5m column, the scatter in the amount of explosive is less but still when the number of divisions is less, the amount of explosive to fail the structure is incorrectly estimated. For both columns, it can be said that convergence of the amount of TNT explosive is achieved at approximately 8 divisions.

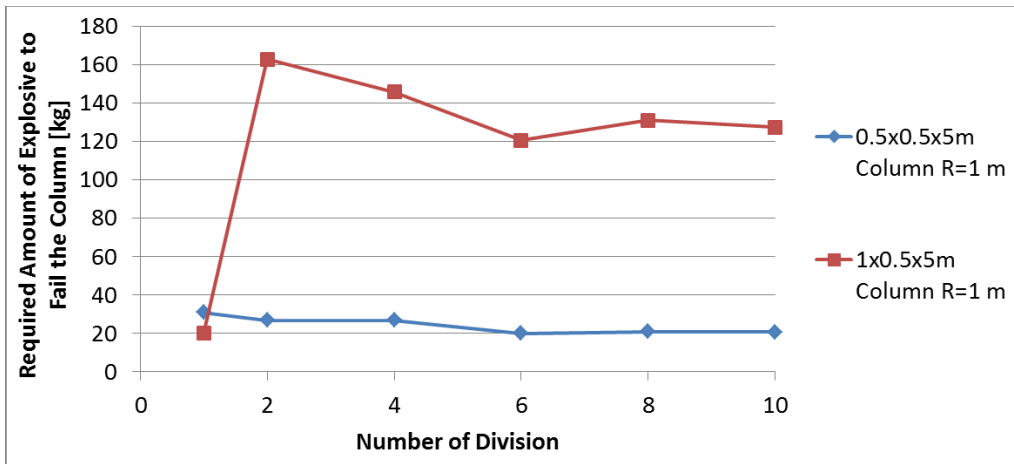


Figure 63. Variation of the Required Amount of TNT Explosive for the 1 m Stand-Off Distance to Fail the Sample Columns with the Number of Divisions

For the 2.5 m stand-off distance, Figure 64 shows the variation of the TNT explosive required to fail the column with the number of divisions. When the number of division is 1, explosion of 63.8 kg of TNT fails the 0.5x0.5x5 column, whereas explosion of 104.1 kg of TNT fails the same column when 10 divisions are used. For the 1x0.5x5 m column, explosion of 349.5 kg of TNT fails the column when only one division is used, while explosion of 626.6 kg of TNT fails the same column for when the number of divisions is 10.

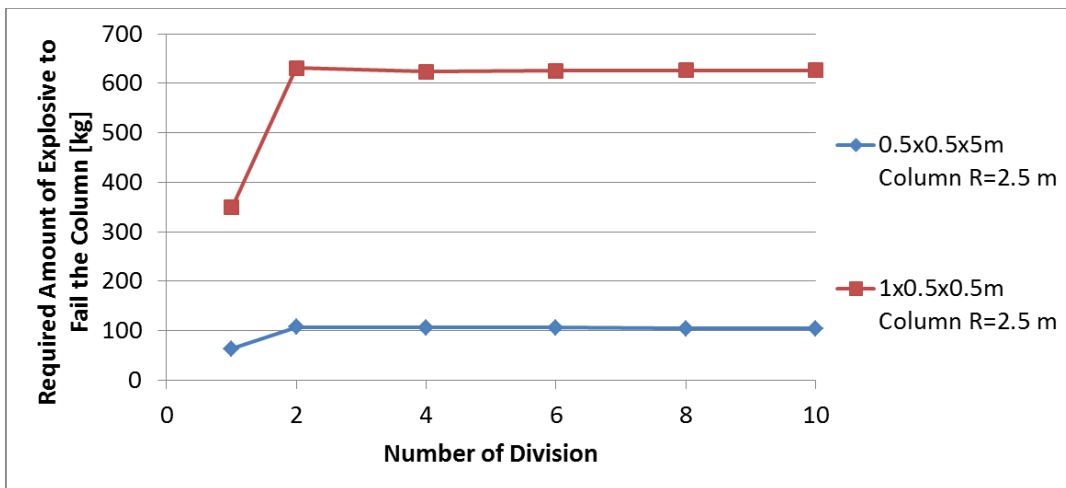


Figure 64. Variation of the Required Amount of TNT Explosive for the 2.5 m Stand-Off Distance to Fail the Sample Columns with the Number of Divisions

For the 5 m stand-off distance, Figure 65 shows the variation of the TNT explosive required to fail the column with the number of divisions. When the number of division is 2, explosion of 359.8 kg of TNT fails the 0.5x0.5x5 column, whereas explosion of 364.3 kg of TNT fails the same column when 10 divisions are used. For this case, there is no significant scattering. For the 1x0.5x5 m column, explosion of 2371.3 kg of TNT fails the column when 2 divisions are used while explosion of 2407 kg of TNT fails when 10 divisions are used.

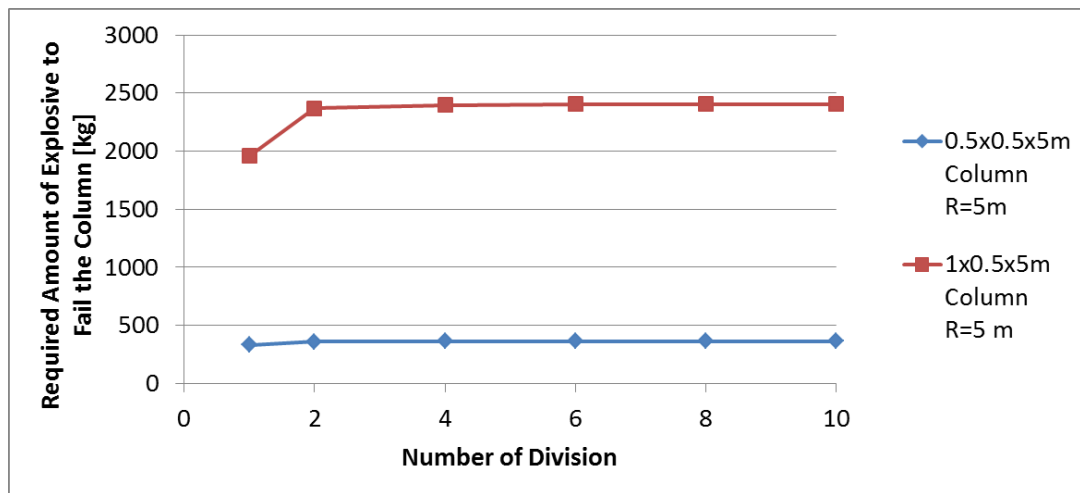


Figure 65. Variation of the Required Amount of TNT Explosive for the 5 m Stand-Off Distance to Fail the Sample Columns with the Number of Divisions

For the 10 m stand-off distance, Figure 66 shows the variation of the TNT explosive required to fail the column with the number of divisions. In this case, explosion of 721.7 kg of TNT fails the 0.5x0.5x5 m column when 1 division is used, whereas explosion of 727.2 kg of TNT fails the same column when 10 divisions are used. As seen in Figure 66, as the stand-off distance increases, the effect of the number of divisions used on the failure explosive mass becomes less and less. This is because the position vectors from the detonation point to the center of each zone do not differ much when the stand-off distance is increased. For the 1x0.5x5 m column, explosion of 9021.6 kg of TNT fails the column when one division is used, whereas explosion of 9421.5 kg of TNT fails the same column when 10 divisions are used.

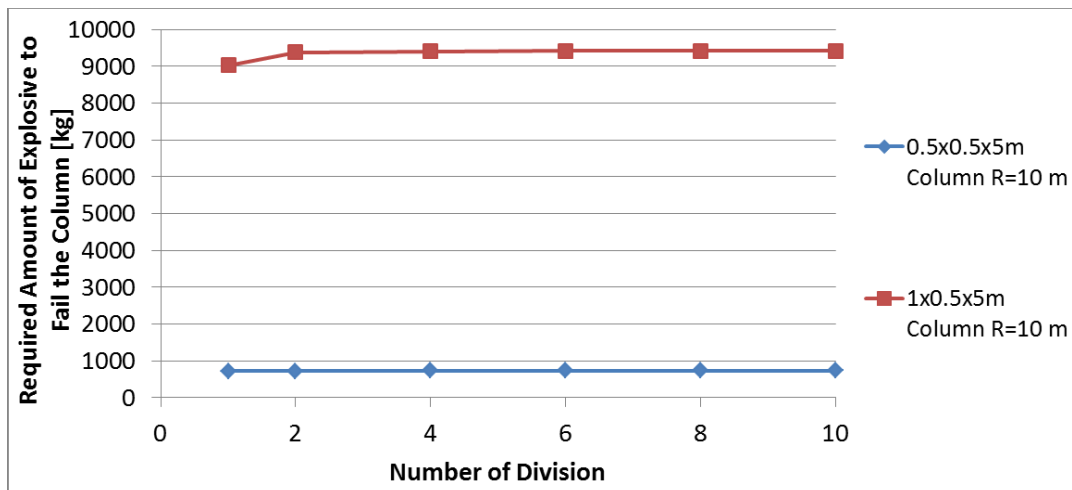


Figure 66. Variation of the Required Amount of TNT Explosive for the 10 m Stand-Off Distance to Fail the Sample Columns with the Number of Divisions

For all the cases studied, the required amount of TNT explosive required to cause failure is given in Table 22. For near-field explosions such as 1 m stand-off distance, explosive mass converges when the number of divisions is greater than 8. As stand-off distance increases, for less number of divisions, the convergence is obtained. For all possible cases, ten numbers of divisions is sufficient for convergence and therefore number of divisions to be used is selected as 10 in the developed damage assessment tool.

Table 22. Variation of the Required Amount of TNT Explosive Mass [kg] for Failure of Sample Columns with the Number of Divisions

Stand-off Distance [m]	Member Dimension	Number of Division					
		10	8	6	4	2	1
1	0.5x0.5x5	20.7	21	20	26.8	26.9	30.8
1	1x0.5x5	127.2	130.9	120.5	145.7	162.7	19.9
2.5	0.5x0.5x5	104.1	104.3	106	106.1	107.3	63.8
2.5	1x0.5x5	626.6	626.2	625.6	623.8	631	349.5
5	0.5x0.5x5	364.3	363.9	363.7	363.1	359.8	330.8
5	1x0.5x5	2407	2405.5	2403.7	2398.7	2371.3	1959.1
10	0.5x0.5x5	727.2	727.1	727.1	726.8	725.7	721.7
10	1x0.5x5	9421.5	9417.7	9414.8	9410.3	9385.1	9021.6

4.2. Blast Induced Failure Assessment Using AUTODYN

To check the accuracy of the fast responding tool developed, two independent analysis tools are also used to predict the failure explosive mass of concrete columns. RC BLAST is one of the analysis tools which uses the SDOF approach and gives quick results. RC BLAST [5] is explained briefly in Chapter 1. Another tool used for comparison is the finite element software AUTODYN [4]. In this chapter, the modeling of the blast analysis in AUTODYN is given in detail. As previously mentioned in Chapter 1, AUTODYN uses Euler-Lagrange coupling for fluid-structure interaction. In the blast phenomenon, after the detonation, explosive is converted into fast moving expanding gases, led by the shock front. This part forms the fluid part (Euler) of the analysis in AUTODYN. Before reaching to the structure, shock front and the expanding gas propagate through the air freely. To model the free propagation, 1-D wedge modeling of TNT explosive and the air is used as shown in Figure 67. 1 mm elements are used in the wedge modeling as shown in the enlarged view.

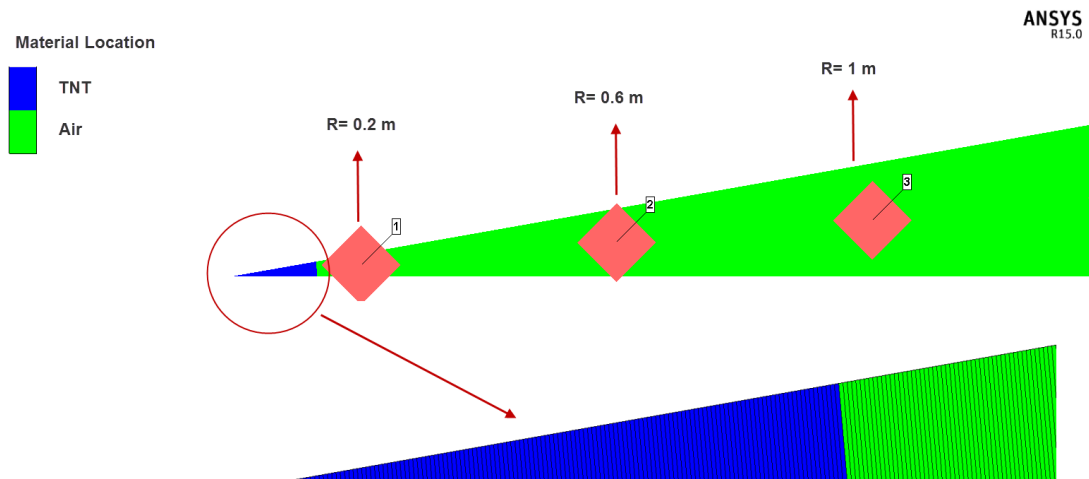


Figure 67. Wedge Modeling of TNT Explosive and Air

In the modeling, wedge domain is filled with air in order to solve free propagation up to 1 m away concrete column. The wedge domain is then filled with TNT explosive at time 0. TNT explosive is then detonated and very high pressurized gases, led by

wavefront, are formed as shown in Figure 68. Wedge modeling continues up to wavefront reaches 1 m stand-off distance.

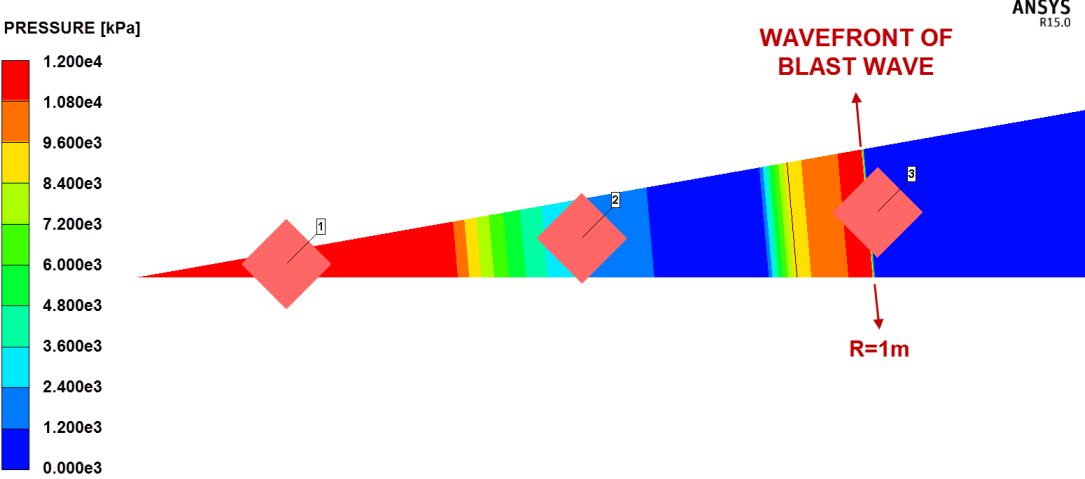


Figure 68. High Pressurized Gases and Wavefront in Wedge Modeling

In the analyses, different explosive masses are detonated and free propagation of the blast wave up to the structure is modeled and solved. Masses of explosive used in the analyses are listed in Table 23.

Table 23. Explosive masses used in the Wedge Method

Stand-off Distance [m]	Mass of TNT Explosive [kg]
1	15
1	30
1	45
1	60
1	75
1	90
1	100
1	150
1	250

In the sample AUTODYN analysis described, the structure is located 1 m away from the explosive and information in the wedge model is mapped into 3D Euler domain shown in Figure 69 after wavefront moves by 1 m away from the detonation point. Specifically, pressure and velocity information of the high pressurized expanding gas and wavefront in the wedge modeling is transferred to the 3D Euler domain and blast wave propagation continues on 3D Euler domain. Euler domain is modeled such that flow out boundary condition is defined at the $\pm X$, $\pm Z$ and $+Y$ surfaces. There is no flow out boundary condition defined at $-Y$ surface because reflection from ground is taken into account. Moreover, the column is fixed at both ends in the model for the particular example.

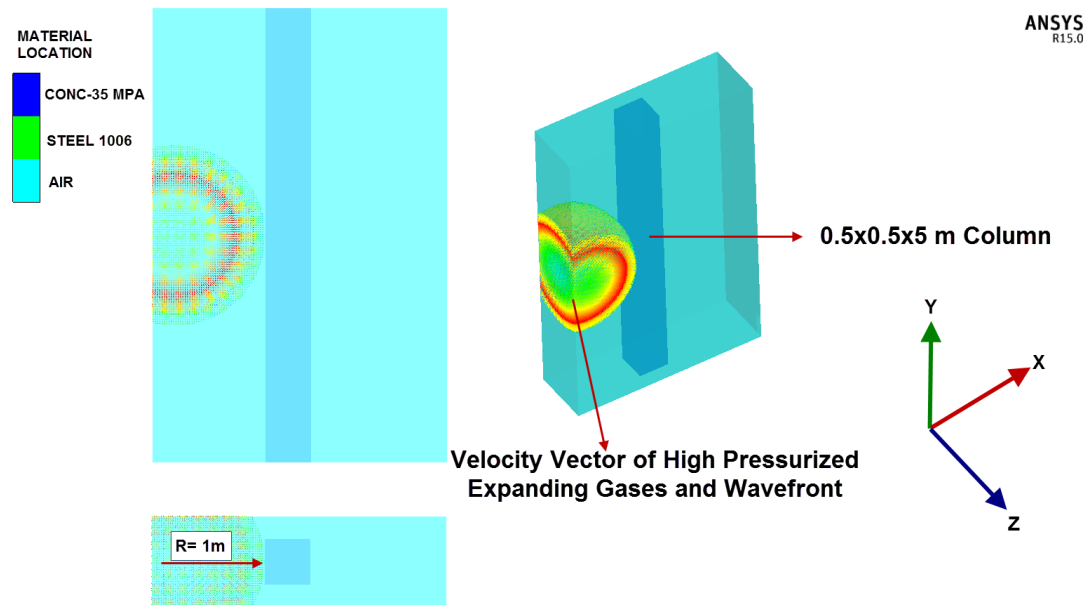


Figure 69. Mapping of the Pressure and Velocity Information of High Pressurized Gases into 3D Euler Domain

For modeling, element size is also important in the finite element method. For this purpose, air filled Euler domain and Lagrange concrete column are meshed according to some recommendations. In the reference [7], a 0.416x0.406x10 m sample concrete column is modeled for blast-structure interaction analysis. In this study, mesh dependency of the concrete column is also examined. Cubic elements

with 8 nodes are used in the analyses. Mesh density used in this study is given in Table 24.

Table 24. Mesh Density used in Modeling the Concrete Column [7]

Mesh Configuration	Number of Elements in Column
Coarse	360
Fine	4160
Very Fine	20000

By referring to Table 24, 0.5x0.5x5 m column is meshed with 10000 cubic elements with element dimension of 50 mm. Aspect ratio of the elements used in meshing the column is taken as 1 to improve the accuracy of the solution. For Euler-Lagrange interaction, Euler domain is modeled such that an Euler element size is one half of the Lagrange element size in order to prevent Euler leakage through the Lagrange part [4]. When elements of Euler and Lagrange domain are not sized properly, expanding gas and the wavefront do not pressurize the Lagrange domain fully. Hence, Euler domain is modeled as 25 mm cubic elements with 8 nodes according to the recommendation. Euler and Lagrange domains are shown in Figure 70.

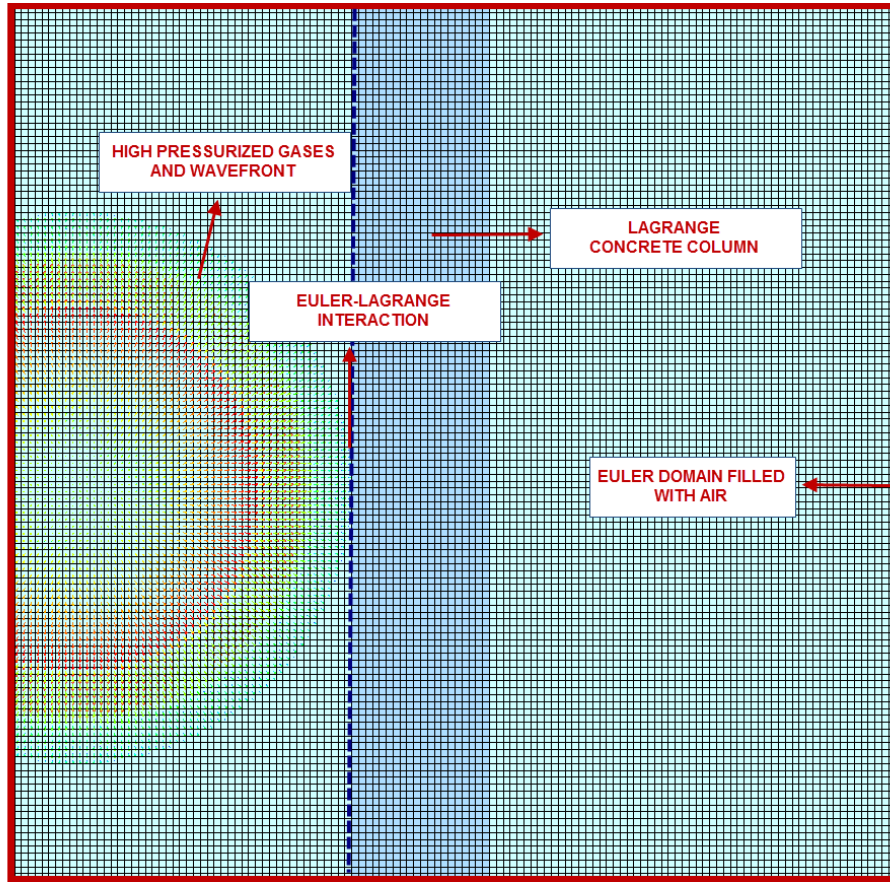


Figure 70. Euler and Lagrange Domain for the Interaction

For failure assessment, an erosion criterion is defined for the concrete model. Erosion could be defined in terms of user-defined elastic strain, plastic strain and failure mode of the elements. For elastic and plastic strain erosion criterion, elements are eroded when the elastic/plastic strain exceeds certain limit given as input by the user. In the erosion failure criterion, AUTODYN computes the damage factor of the elements by Equation (40) [45],

$$D = \sum \frac{\Delta \varepsilon^p}{\varepsilon^f} \quad (40)$$

where $\Delta \varepsilon^p$ is the accumulated plastic strain and ε^f is the failure strain which is given by,

$$\varepsilon^f = D_1 * \left(\frac{p}{f'_c} - \frac{p_{spall}}{f'_c} \right) D_2 \quad (41)$$

where f'_c is the static compressive strength of the concrete, p_{spall} is the spall strength of the concrete, p is the pressure exerted on the element, D_1 and D_2 are material constants as given in Table 25.

Table 25. Material Constants for Damage Factor Calculation

D_1	D_2
0.4	1

AUTODYN calculates the damage factor by Equation (40). When damage factor is greater than zero, the elements degrades and when it is equal to 1, the element is assumed to fail and therefore it is eroded.

Failure of the concrete column can be assessed using the erosion criteria. In this case, when an element is damaged; it starts to be degraded. When damage factor is equal to 1, element fails and eroded, thus visually one can see how the respective sections of the column fail by monitoring the level of erosion. Column failure is based on checking the non-eroded elements in any section. For instance, in Figure 71 structural integrity loss of the 0.5x0.5x5 m column subjected to the blast load due to the explosion of 75 kg of TNT is shown. In this case, element erosion method is used to visually inspect the evolution of the failure in the column. Figure 71 shows that erosion of the elements start at the hinge points at both ends of the column and at the mid span. At 20 ms, most of the elements in the end and mid span sections are eroded. At t=30 ms, all the elements in three sections, in the lower, upper end supports and in the mid span section, are eroded. This is an indication that column can not sustain any load anymore.

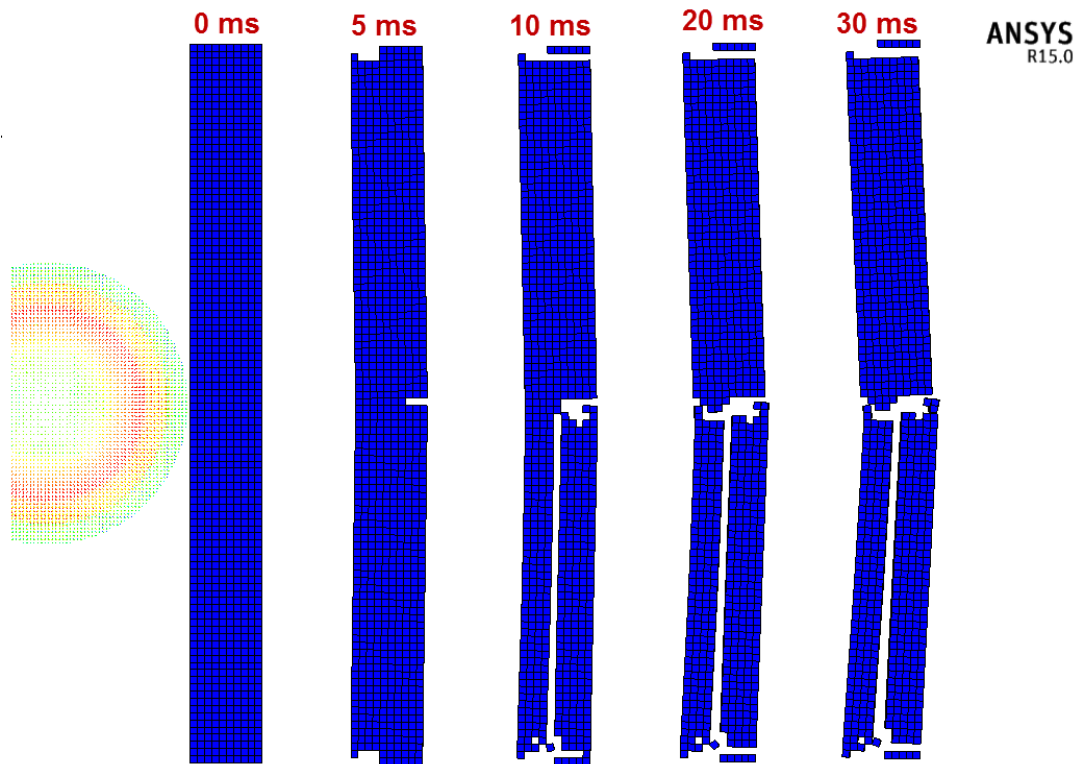


Figure 71. Loss of Structural Integrity Utilizing the Failure Erosion Criteria

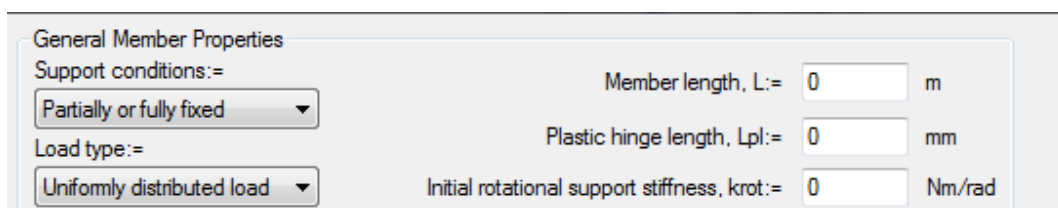
4.3. Blast Induced Failure Assessment Using RC BLAST

RC BLAST [5] needs 3 different types of input from the user for the analysis. These are

- Physical properties of structure
- Load-deformation curve
- Applied pressure

As for the physical properties of the structure, total mass [kg] and the loaded area [m²] have to be given as input. For the sample 0.5x0.5x5 m concrete column studied, total mass is 3000 [kg] and the loaded area is 2.5 [m²].

For load-deformation curve, there are some steps to be covered. Firstly, user should define the boundary condition, load type, which can be either uniform or point load, member length [m], plastic hinge length [m], explained in section 2.4, initial rotational support stiffness [N-m/rad] as depicted in the user interface of RC BLAST given in Figure 72. In the analysis, fixed boundary condition and uniform loading are selected as in AUTODYN analysis. For some desired parameters such as plastic hinge length, initial rotational support stiffness, the software gives some tips and suggestions. For the unknown or indefinite parameters for the analysis, recommendations are used.



General Member Properties	
Support conditions:= Partially or fully fixed	Member length, L:= 0 m
Load type:= Uniformly distributed load	Plastic hinge length, Lpl:= 0 mm
	Initial rotational support stiffness, krot:= 0 Nm/rad

Figure 72. General Member Properties for the Load-Deformation Curve

For step 2, the user defines a material model, cross-section of the member as seen in Figure 73. 0.5x0.5m cross section is given as input in RC BLAST. Later on, moment-curvature is formed by RC BLAST, as depicted in Figure 74.

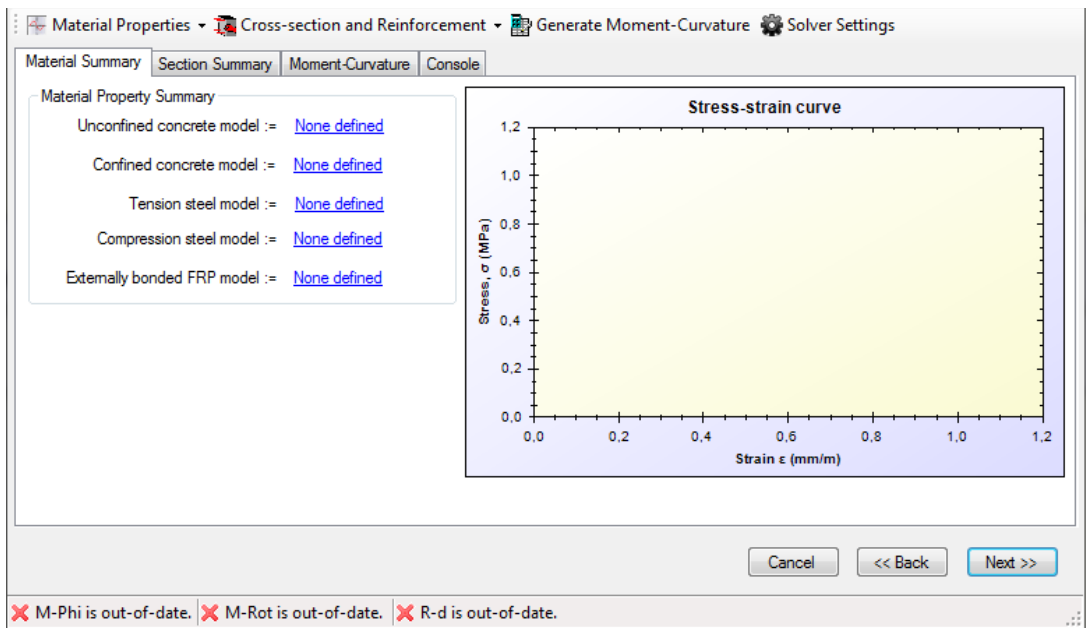


Figure 73. Material and Section Properties for the Load-Deformation Curve

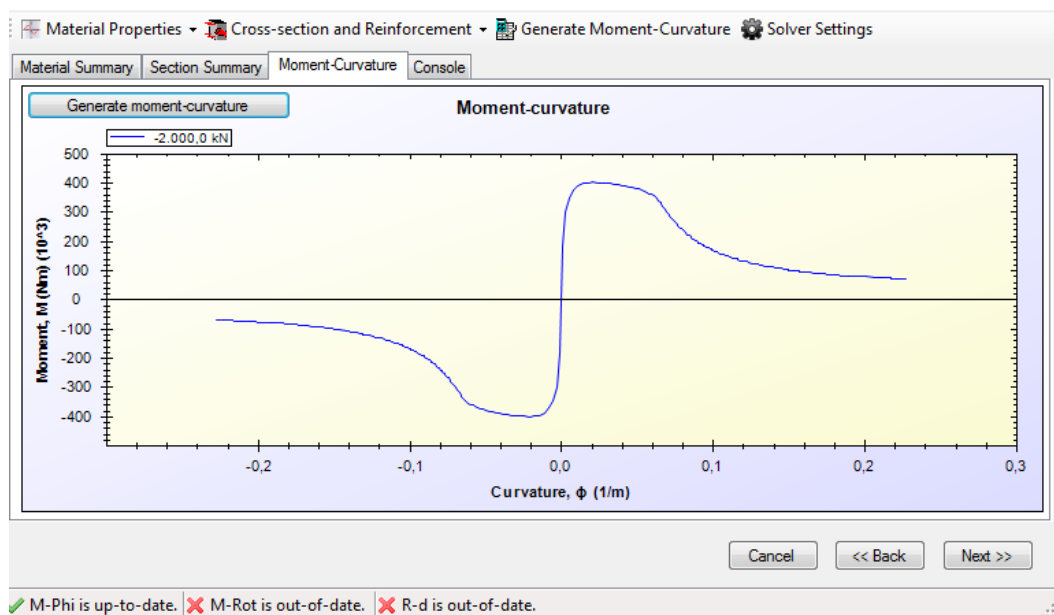


Figure 74. Sample Output of Moment-Curvature

Then, by using the generated moment-curvature curve, yield points and ultimate curvature points should be selected. The software suggests some tips for those points. For the analysis performed in this study, the suggestions of the software are used.

For the applied pressure input, user can select either blast parameters mentioned in section 2.1 (peak side-on overpressure, positive phase duration, peak negative pressure, negative phase duration) or explosive mass/stand-off distance so that blast parameters are automatically calculated. For the sample analysis performed in this section, 10 kg of TNT is detonated at 1 m stand-off distance.

After preparing all the input that is required by RC BLAST, the tool gives the displacement vs. time curve for the SDOF model of the structure exposed to blast loading. As seen in Figure 75, for the particular analysis performed, the displacement of the structure has an oscillating trend with a maximum displacement of 30 mm and the structure does not fail in this case.

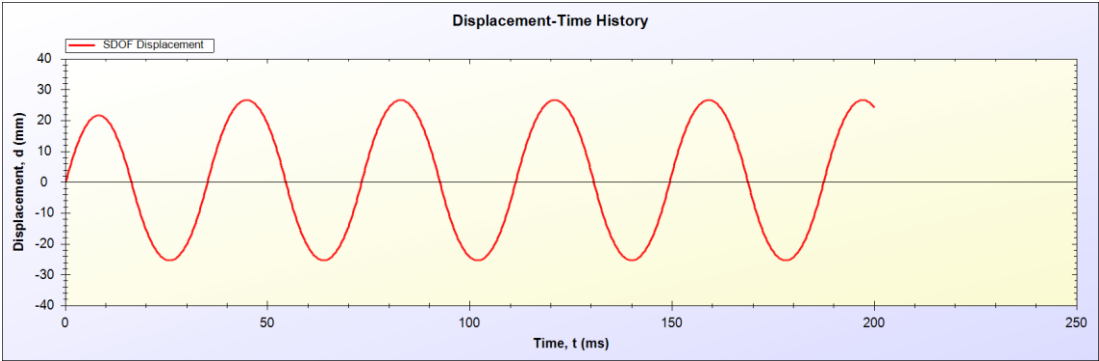


Figure 75. Displacement vs. Time History Curve as a result of explosion of 10 kg of TNT

When the mass of the TNT is increased to 20 kg, the structure has still an oscillating displacement curve as depicted in Figure 76. Maximum displacement is increased to 62 mm due to increase in the TNT mass.

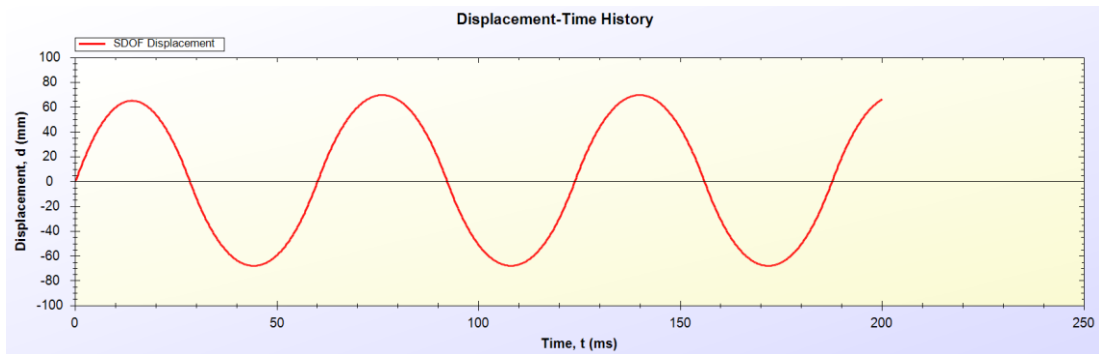


Figure 76. Displacement vs. Time History Curve as a result of explosion of 20 kg of TNT

In order to determine the failure mass of TNT, mass of TNT is increased to 25 kg and RC BLAST gives the output shown in Figure 77. In this case, the displacement curve is not an oscillating curve; rather it has an increasing displacement with decreasing slope and finally reaches 192 mm deflection at 37 ms.

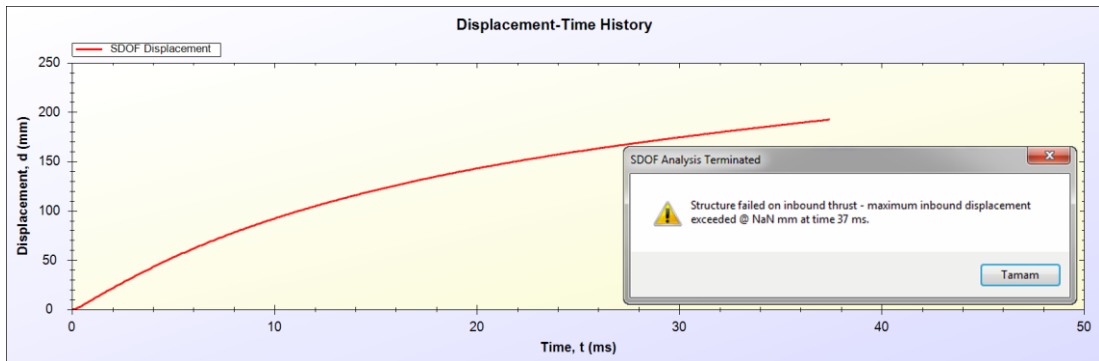


Figure 77. Displacement vs. Time History Curve as a result of explosion of 25 kg of TNT

Following the same procedure, failure mass of the explosive is determined for the 0.5x1x5 m concrete column as well and results are given in Table 26.

Table 26. Failure Mass of the Explosive Calculated by RC-BLAST

	Failure Mass of the Explosive [kg]	
	0.5x0.5x5 Column	0.5x1x5 Column
RC BLAST	25	134

4.4. Assessment of the Results

In order to test the accuracy of the fast responding tool developed in the thesis study, the failure assessment results obtained by the present code are compared with the SDOF solver RC BLAST and also with the explicit finite element solver AUTODYN. As mentioned in section 1.2, the aim of the tool is to give fast and accurate enough results for bridge-like-structures exposed to external blast loading. Since RC BLAST and the tool developed in the present study are fast-responding tools, once the required parameters are given as input, failure assessment results can be obtained in a few seconds. However, AUTODYN analyses last more than a day depending on the model. Determining the required amount of explosive to fail the bridge-like structures is not an easy process for AUTODYN. For each explosive mass, one has to perform AUTODYN analysis to make failure assessment and this process requires many reanalysis by changing the explosive mass. One of the significant advantages of the developed tool is that the approximate failure explosive mass can be determined very fast and predicted failure explosive mass can be used as the initial explosive mass in AUTODYN analysis. This way number of detailed AUTODYN analysis to be performed can be reduced significantly.

For comparison, two sample columns with the dimensions 0.5x0.5x5 m and 1x0.5x5 m are analyzed. For a stand-off distance of 1 m, structures are exposed to the blast loading due to the explosion of 15, 30, 45, 60, 75, 90, 100, 150, 250 kg of TNT. Table 27 lists the first set of analysis performed by AUTODYN.

Table 27. First Set of AUTODYN Analysis

Stand-off Distance [m]	Mass of TNT Explosive [kg]	Member
1	15	Column (0.5x0.5x5)
1	30	Column (0.5x0.5x5)
1	45	Column (0.5x0.5x5)
1	60	Column (0.5x0.5x5)
1	75	Column (0.5x0.5x5)
1	90	Column (0.5x0.5x5)
1	100	Column (0.5x0.5x5)
1	150	Column (0.5x0.5x5)
1	250	Column (0.5x0.5x5)
1	15	Column (0.5x1x5)
1	30	Column (0.5x1x5)
1	45	Column (0.5x1x5)
1	60	Column (0.5x1x5)
1	75	Column (0.5x1x5)
1	90	Column (0.5x1x5)
1	100	Column (0.5x1x5)
1	150	Column (0.5x1x5)
1	250	Column (0.5x1x5)

For the first set of analysis, two sample columns are examined whether they fail or not using the column failure criteria explained in Section 4.2 based on the erosion of the elements throughout the whole cross section. Starting from 15 kg of TNT explosive, mass of explosive is increased up to the failure of the structure. For the 15kg, 30kg and 45 kg of TNT, there exists no cross section throughout which all elements are eroded. In other words, the column has not failed yet. Figure 78 demonstrates effect of 45 kg TNT explosion on the 0.5x0.5x5 m concrete column. At the end supports, some elements start to be eroded at 5 ms. Although some elements eroded at the column ends, erosion throughout the whole cross section does not occur. Moreover, at the midspan, no erosion occurs and midspan does not deflect much.

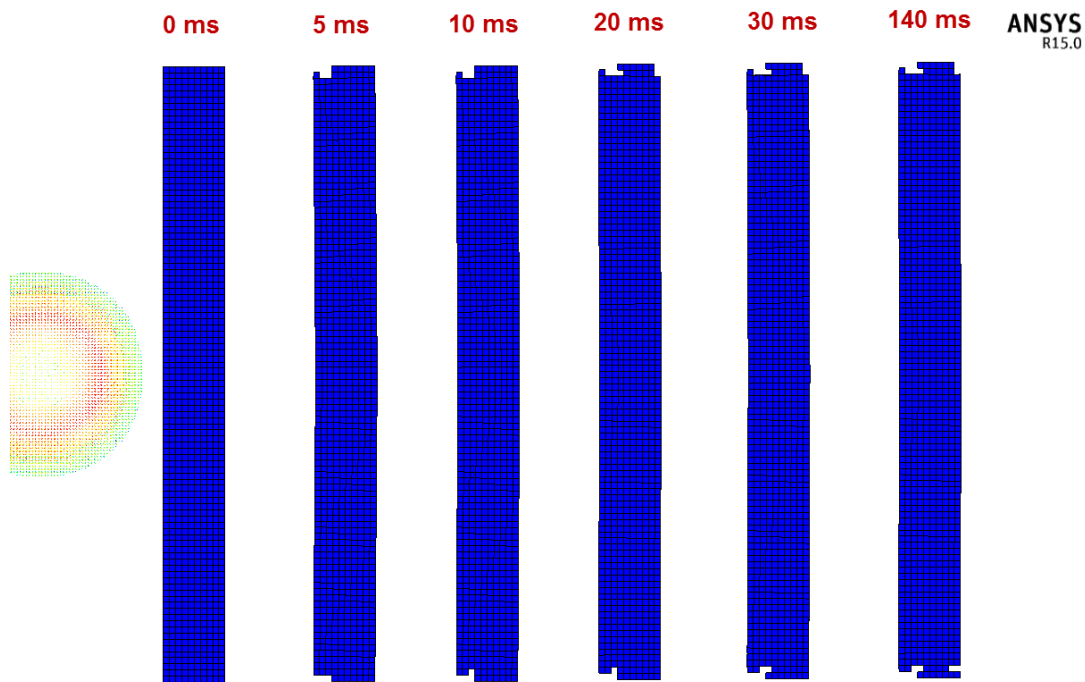


Figure 78. Effect of 45 kg TNT Explosion on the 0.5x0.5x5m Concrete Column

Since 45 kg TNT explosion is not enough to fail the concrete column, effect of 60 kg TNT explosion is investigated. Figure 79 shows the effect of 60 kg TNT explosion on the 0.5x0.5x5 concrete column. At 5 ms, some elements start to erode near the end supports. At 10 ms, midspan elements also start to erode as well. It is seen that at 30 ms, most of the elements near the end supports and the midspan erode. At 50 ms, throughout upper and lower end support, elements fully erode in the sections near the upper and the lower end supports. Compared to the explosion of 45 kg TNT, at 30 ms, most of the elements erode in the sections nears the end supports for the explosion of the 60 kg TNT. It is also seen that at the midspan, most of the elements erode as a result of explosion of 60 kg TNT whereas no erosion exists in the midspan for the explosion of 45 kg TNT.

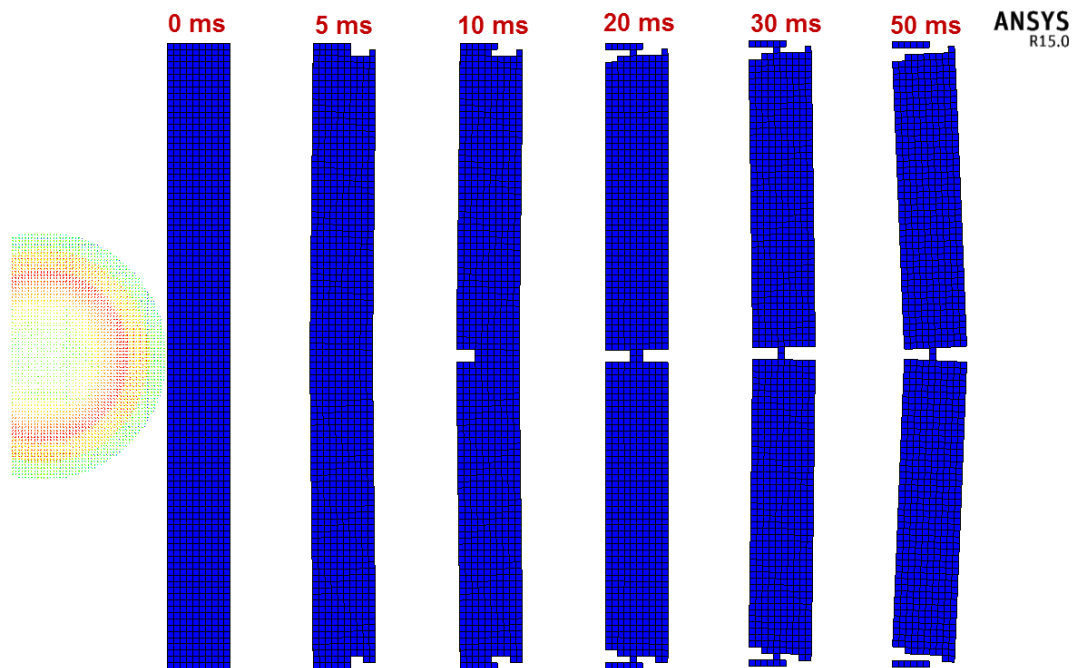


Figure 79. Effect of 60 kg TNT Explosion on the 0.5x0.5x5m Concrete Column

Table 28 summarizes the results of first set of analysis. After the first set of analysis, to narrow the range of the failure mass of TNT for 0.5x0.5x5 m column, second set of analysis is performed.

Table 28. Results of First Set of AUTODYN Analysis

Stand-off Distance[m]	Mass of TNT Explosive [kg]	Member	Column Failure?
1	15	Column (0.5x0.5x5)	No
1	30	Column (0.5x0.5x5)	No
1	45	Column (0.5x0.5x5)	No
1	60	Column (0.5x0.5x5)	Yes
1	75	Column (0.5x0.5x5)	Yes
1	90	Column (0.5x0.5x5)	Yes
1	100	Column (0.5x0.5x5)	Yes
1	150	Column (0.5x0.5x5)	Yes
1	250	Column (0.5x0.5x5)	Yes
1	15	Column (0.5x1x5)	No
1	30	Column (0.5x1x5)	No
1	45	Column (0.5x1x5)	No
1	60	Column (0.5x1x5)	No
1	75	Column (0.5x1x5)	No
1	90	Column (0.5x1x5)	No
1	100	Column (0.5x1x5)	No
1	150	Column (0.5x1x5)	No
1	250	Column (0.5x1x5)	Yes

The results given in Table 28 show that 0.5x0.5x5 m concrete column fails due to the explosion of 45-60 kg of TNT whereas 0.5x1x5 m concrete column fails due to the explosion of 150-250 kg of TNT. To narrow the range, a second set of analysis is performed and explosive masses causing the failure of the column are determined and presented in Table 29.

Table 29. Results of Second Set of AUTODYN Analysis

Stand-off Distance [m]	Mass of TNT Explosive [kg]	Member	Column Failure?
1	50	Column (0.5x0.5x5)	Yes
1	55	Column (0.5x0.5x5)	Yes
1	155	Column (0.5x1x5)	No
1	160	Column (0.5x1x5)	No
1	165	Column (0.5x1x5)	No
1	170	Column (0.5x1x5)	No
1	180	Column (0.5x1x5)	Yes
1	190	Column (0.5x1x5)	Yes
1	200	Column (0.5x1x5)	Yes
1	210	Column (0.5x1x5)	Yes
1	220	Column (0.5x1x5)	Yes
1	230	Column (0.5x1x5)	Yes
1	240	Column (0.5x1x5)	Yes

Figure 80 shows the effect of 50 kg of TNT explosion on the 0.5x0.5x5 m column. At 5 ms, elements begin to erode near the end supports. As time elapses, number of eroded elements increase. At 30 ms, most of the elements in the sections near end supports and at the midspan erode. However, erosion of all elements in the sections near the end supports and at the midspan takes place 100 ms later at 140 ms. This is an indication that 50 kg of TNT is certainly the limit on the failure mass of the TNT explosive. It should be recalled that for the 60 kg of TNT explosion, the column fails at 50 ms.

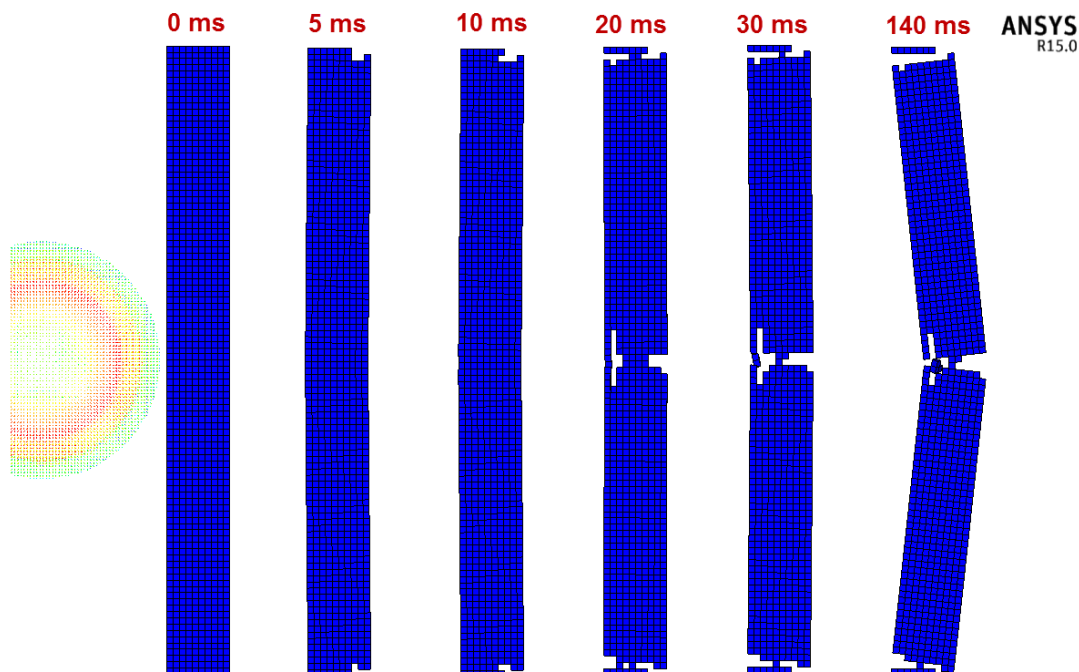


Figure 80. Effect of 50 kg TNT Explosion on the 0.5x0.5x5m Concrete Column

Failure response of the concrete columns determined by AUTODYN are compared to the test and analysis results of Williamson, shown in Figure 10, and great similarity is observed between the two simulations and tests. For concrete columns exposed to the explosion with small scaled distance, it is seen that concrete columns deflect such that as if they broken in the midsection. In other words, plastic hinges are seen, as shown in Figure 44. This similarity in a way demonstrates that flexural failure is modeled correctly in AUTODYN analyses.

The results of AUTODYN analyses show that considering the column failure criterion which is based on checking the non-eroded element in any section of the column, 0.5x0.5x5 m column fails as a result of explosion of 45 - 50 kg of TNT while 0.5x1x5 m column fails as a result of explosion of 170 - 180 kg of TNT.

For the same case, results of the fast-responding RC BLAST, results obtained by the developed tool and with the AUTODYN results are compared in Table 30. The results show that the tool and RC BLAST, which use SDOF methodology, give close results for both 0.5x0.5x5 m column and 0.5x1x5 m column. However, for both

columns failure masses of the explosive predicted by AUTODYN are higher than the failure masses of the explosives determined by the developed tool and RC BLAST.

Table 30. Comparison of Explosive Masses Calculated by the Present Study, RC-Blast and AUTODYN

	Failure Mass of the Explosive [kg]	
	0.5x0.5x5m Column	0.5x1x5m Column
Present study	20.7	120.7
RC BLAST	25	134
AUTODYN	45 - 50	170 - 180

To investigate the reason for the difference in the failure masses obtained by AUTODYN and predicted by the developed tool, side-on pressures obtained by the developed tool and AUTODYN are compared. For different scaled distances, peak side-on overpressures obtained by AUTODYN and the developed tool are compared in Table 31. The results show that the developed tool (Equation (9) and Table 4) overestimates the peak side-on overpressure compared to AUTODYN results.

Table 31. Comparison of Peak Side-on Overpressures Obtained by AUTODYN and the Developed Tool

Mass of TNT Explosive [kg]	Distance [m]	Scaled Distance [m/kg ^{0.33}]	AUTODYN Side-on Overpressure [kPa]	Tool Side-on Overpressure [kPa]	Difference [%]
15	0.5	0.20	13794	16794	17.86%
15	0.75	0.31	8042	9879	18.60%
15	1	0.41	5183	6631	21.84%
15	1.25	0.51	3536	4714	24.99%
15	1.5	0.61	2527	3474	27.26%
15	1.75	0.72	1897	2631	27.89%
15	2	0.82	1486	2037	27.05%
15	2.25	0.92	1184	1608	26.36%
15	2.5	1.02	957	1290	25.84%

After determining the difference in peak side-on pressures determined by the developed tool and AUTODYN, the side-on overpressure calculated by the tool are

decreased to match the side-on overpressure determined by AUTODYN. With the decreased side-on overpressure, failure masses of the explosive are calculated again by repeating the analysis for the two columns having dimensions 0.5x0.5x5 m and 0.5x1x5 m for the stand-off distance of distance of 1m. Table 32 gives the updated explosive mass calculated using the decreased side-on overpressure. From Table 32, it seen that with the updated side-on overpressure, failure explosive masses calculated by the developed tool are much closer to the AUTODYN results. It should be noted that in the present study side-on overpressure is based on the experimentally determined values and AUTODYN calculates it by analysis, therefore it is doubtful that side-on pressure calculated by AUTODYN analysis is absolutely correct. It is noted that the developed tool, which is based on SDOF approach, calculates lower failure explosive mass than AUTODYN. In this respect, the calculated failure explosive mass forms the lower bound for the AUTODYN analyses. It can be commented that the developed tool gives conservative values for the failure explosive mass.

It is also considered that present set of analyses by the developed tool and AUTODYN are performed for the stand-off distance of 1m which is small. In the developed tool, loading is assumed to be uniform along the structure. For small stand-off distances, distribution of the load along the structure may deviate from uniform loading and this could also account for the differences obtained for the failure explosive masses by the developed tool and AUTODYN.

Table 32. Comparison of Explosive Masses by the Present Study and AUTODYN

	Failure Mass of the Explosive [kg]	
	0.5x0.5x5m Column	0.5x1x5m Column
Present Study	20.7	120.7
Present Study with Updated Side-on Overpressure	36.5	181.9
AUTODYN	45 - 50	170 - 180

In this section uniform load assumption used in the developed tool is studied. Recall that in the developed tool, instead of point load, uniform loading assumption is done

for the SDOF conversion. In theory, it is not possible to represent the blast load by either uniform load or point load. However, uniform loading assumption is more reasonable since the loading is distributed along the structure.

To check the uniformity of the load, series of fast-responding analyses are performed. 0.5x0.5x5 m concrete column, shown in Figure 61, is sampled and divided as shown Figure 62 for the uniformity analyses. 60 kg of TNT is exploded at a height of burst of 2.5 m. Stand-off distances are taken as 1 m, 2m, 3m, 4m, 5m and 10 m.

At 1 m stand-off distance Mach Stem is not formed. Mach Stem is the 1st discrete zone in all graphs. Figure 81 shows the distribution of the face on overpressure along the structure for a stand-off distance of 1 m. As seen in Figure 81, load is maximized in the mid-region whereas it is minimum at the upper and the lower ends. Loading is symmetric since the height of burst is half of the column height. For small stand-off distance, blast load varies so much along the column.

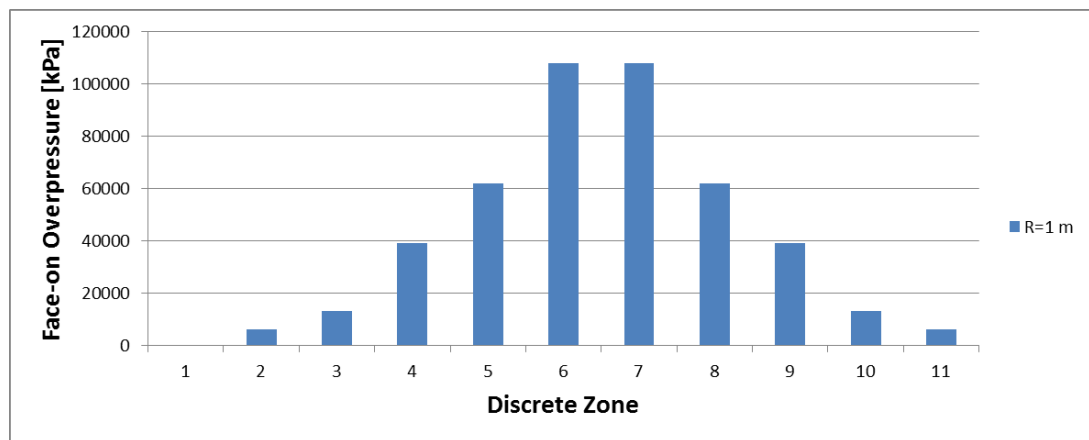


Figure 81. Distribution of the Face on Overpressure along the Structure for a Stand-off Distance of 1 m

Figure 82 shows the distribution of the face on overpressure along the structure for a stand-off distance of 3 m. For the stand-off distance of 3 m, Mach Stem forms and the triple point height ruins the symmetry. However, in this case load is more uniformly distributed along the structure compared to the 1 m stand-off distance case.

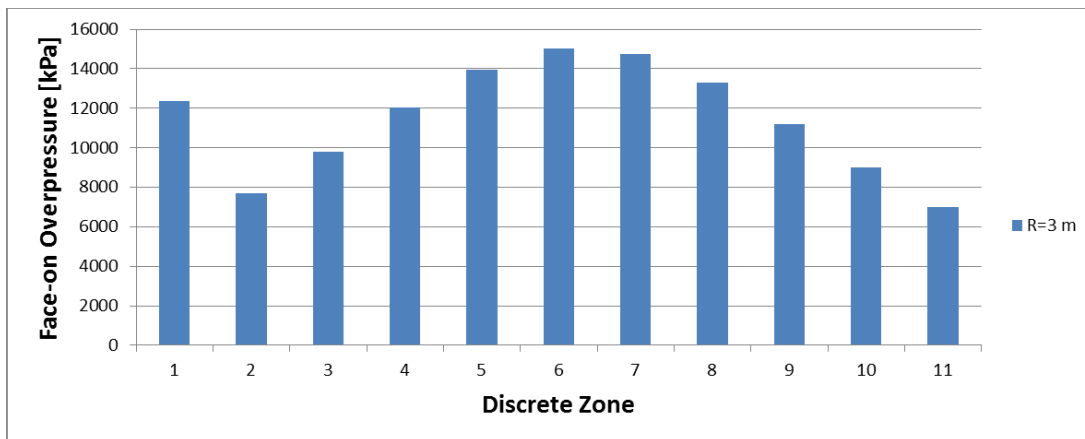


Figure 82. Distribution of the Face on Overpressure along the Structure for a Stand-off Distance of 3 m

Figure 83 shows the distribution of the face on overpressure along the structure for a stand-off distance of 5 m. For the stand-off distance of 5 m, Mach Stem again forms but its intensity diminishes since the stand-off distance increases and loading is more uniform.

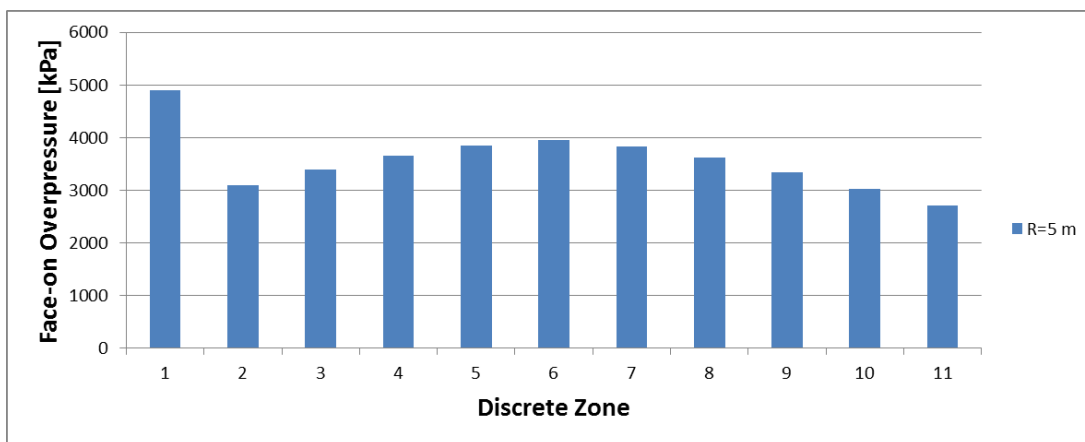


Figure 83. Distribution of the Face on Overpressure along the Structure for a Stand-off Distance of 5 m

Figure 84 shows the distribution of the face on overpressure along the structure for a stand-off distance of 10 m. For the stand-off distance of 10 m, loading is very close to uniform load disregarding the Mach Stem Region.

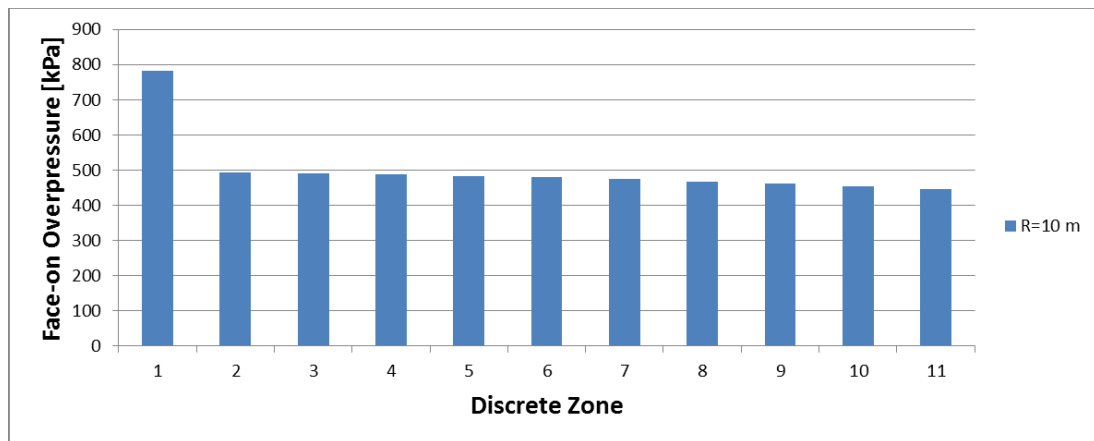


Figure 84. Distribution of the Face on Overpressure along the Structure for a Stand-off Distance of 10 m

In the overall, as the stand-off distance increases, uniform loading assumption becomes more reliable approach for blast analysis. For 1 m stand-off distance, loading is not uniform. For small stand-off distances, distribution of the load along the structure is not uniform and this could account for the differences obtained for the failure explosive masses by the developed tool and AUTODYN. To see the effect of uniformity of the loading at the stand-off distance of 5 m, where loading could be considered to be almost uniform, further analyses are performed in order to determine the failure masses of the TNT explosive by the developed tool and AUTODYN. For the 0.5x0.5x5 m concrete column, in the developed tool, failure explosive mass is computed as 460 kg of TNT . To trace this clue, in AUTODYN, 440-500 kg of TNT explosive range is scanned to determine failure mass of the TNT explosive.

For the 450 kg of TNT explosive at a stand-off distance of 5 m, time response of the column is shown in Figure 85. It is seen that damage starts at the lower end support at 5 ms. At 30 ms, many of the elements at the lower end support erode. Furthermore, some elements at upper end support also erode. At 85 ms, the column deflects considerably at lower end support and almost all elements erode. At 200 ms, all elements at lower end support erode and the column fails.

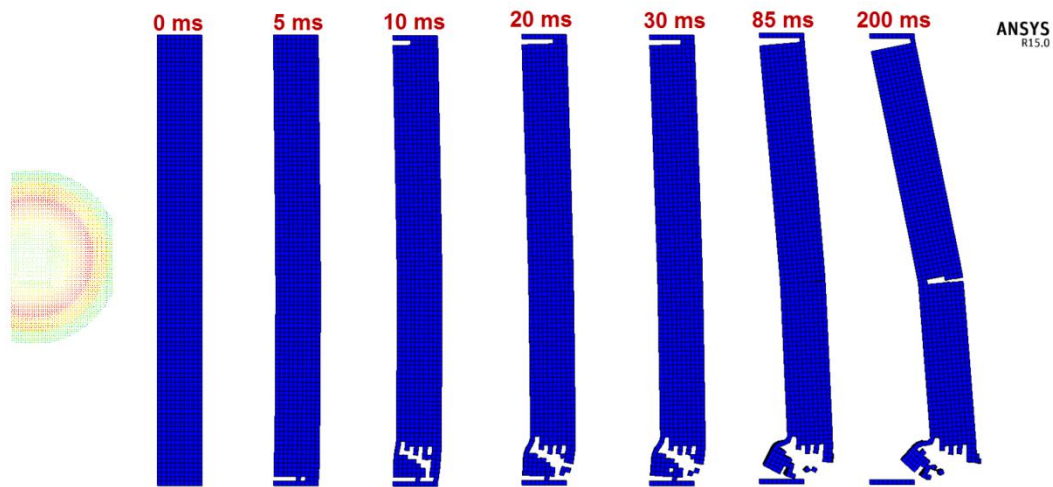


Figure 85. Effect of 450 kg TNT Explosion on the 0.5x0.5x5m Concrete Column

It is seen that lower end support is damaged much more than the other plastic hinge locations, which are at the upper end support and at the midsection. To investigate the reason behind this, face-on overpressure distribution along the column is analyzed by the developed tool as shown in Figure 86.

It is observed that Mach Stem is formed and impacts the target resulting in 27000 kPa approximately. On the other hand, other parts of the column are subjected to face-on overpressures between 11000 and 14500 kPa. Face-on overpressure at the Mach Stem region is almost 2.5 times the face-on overpressure on the other part of the column. Higher face-on overpressure in the Mach Stem segment of the column yields greater damage at the lower end support and column fails at the lower end of the column.

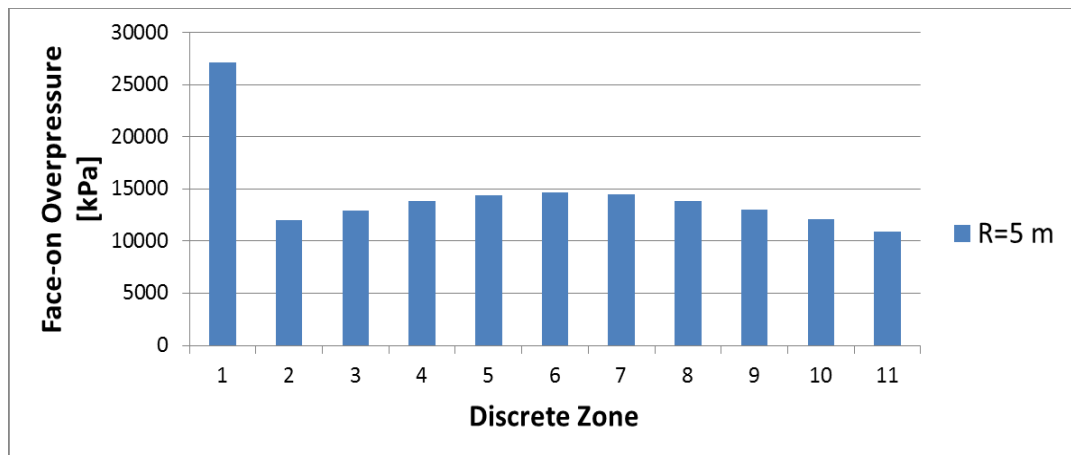


Figure 86. Distribution of the Face on Overpressure along the Structure Exposed to 450 kg of TNT Explosive for a Stand-off Distance of 5 m

In Table 33, the failure masses of explosives for the 0.5x0.5x5 m column are listed for the 1m and 5 m stand-off distances. At 1 m stand-off distance, the difference is 11 kg when average of 45 and 50 kg of TNT explosive is considered. At 5 m stand-off distance, the difference is 8.3 kg of TNT explosive. In terms of percent difference, at higher stand-off distances, the difference in the failure explosive mass calculated by the developed code and AUTODYN is much lower than the percent difference for the low stand-off distance case for which the loading less uniform. It is thus concluded that when the stand-off distance is increased, loading becomes more uniform.

Table 33. Comparison of Failure Masses of the TNT Explosive Calculated by AUTODYN and by the Developed Tool at Stand-off Distances 1m and 5 m

	AUTODYN	DEVELOPED TOOL
Failure Mass of TNT Explosive at Stand-off Distance of 1 m	45 - 50	36.5
Failure Mass of TNT Explosive at Stand-off Distance of 5 m	450 - 455	460.8

In addition to difference in the side-on overpressure calculated by the developed tool and AUTODYN, and uniform load assumption used in developed tool, other probable reasons for the differences between the failure explosive masses determined by the developed tool and AUTODYN could be listed as:

- The tool discretizes the structure into 10 segments. In reality, the structure is composed of infinite segments.
- The tool disregards negative phase loading. Negative phase diminishes impulse on the structure. The decreased impulse results in higher mass of the explosive necessary to fail the structure.
- Failure criteria used by AUTODYN, RC BLAST and the tool are different. There is no clue for failure criterion used in RC BLAST. Difference in failure criteria may result in different results.
- SDOF methodology requires several assumptions. In this method, a complex concrete model is simplified into lumped mass-spring system. The simplification is so sharp and this also causes differences between the results obtained by the developed tool and AUTODYN.

Although there are some differences between the failure explosive masses calculated by the developed tool and AUTODYN, failure explosive masses calculated by the developed tool are not very off from the failure masses calculated by AUTODYN. As it is mentioned before, the calculated failure explosive mass by the developed tool forms the lower bound for the expensive AUTODYN analyses. In this respect, the developed tool can be used for fast estimation of the failure explosive mass and for more refined analysis, failure explosive mass determined by the tool can be used as the lower bound for AUTODYN analysis and the number of AUTODYN analysis to be performed for the more accurate determination of the failure explosive mass can be reduced significantly.

CHAPTER 5

CONCLUSION AND FUTURE WORK

The main objective of the thesis study is to develop a fast responding tool which is accurate enough for the damage assessment in the columns of bridge structures subjected to blast loading. In order to achieve this goal, available studies in the literature are extensively examined to establish the background of the blast phenomenon and also to determine the methodology for the developed tool. The methodology of the fast responding blast induced damage calculation tool is explained by means of flowcharts presented in Chapter 3. Key points of the developed tool are the determination of the side-on overpressure up to the structure, determination of the impulsive work on the structure and calculation of the structural response. As for the determination of the side-on overpressure, Kingery's empirical formula is determined as the most accurate approach which gives the best fit to the experimental results. In fact in the literature, Kingery's empirical formulation is extensively used for the calculation of blast parameters, especially for the side-on overpressure. For the accurate calculation of the impulsive work on the structure, Mach Stem phenomenon is investigated in detail and effect of the Mach Stem is included in the developed tool. The most critical point on the determination of impulsive work on the structure is to model the spatial distribution of the face-on overpressure along the structure. For accurate calculation of the impulsive work on the structure, the structure is divided into several segments. Thus, variation of the stand-off distance and the angle of incidence along the structure is modeled precisely. Furthermore, in order to determine the effect of the ratio of the rear wall loading to the front wall loading, a study is performed and this ratio is determined as function of the scaled distance. It is shown that for small scaled distances, front wall loading is really dominant over the rear wall loading. Hence, for the scaled distance less than $0.5 \text{ m/kg}^{1/3}$, it is concluded that the rear wall loading is negligible. For the calculation of the response of the structure, material behaviour of concrete and steel structures is examined. Effects of dynamic increase factor,

strength increase factor, age factor are considered for determining the dynamic strength of the material. Single Degree of Freedom (SDOF) approach is utilized for the flexural response of the structure exposed to the blast loading. Biggs' tables are used for the conversion of the continuous system into discrete SDOF system. Maximum deflection and hinge (support) rotations are computed for damage assessment of the structure. For the damage assessment, failure criteria published by Department of Defense of the US army is used.

In addition to the studies performed to develop the fast responding analysis tool, commercial programs RC BLAST and AUTODYN are used to assess damage in structures subjected to blast loading for comparison purposes. As mentioned in Section 4.3, RC BLAST is also a SDOF solver and gives deflection versus time curve for the blast loaded concrete and steel structures. When sample structures are subjected to relatively small amount of TNT explosion at 1 m stand off distance, structures deflect with oscillation in a sinusoidal manner. Increasing the amount of TNT explosive raises the amplitude of deflection, but the deflection may still be in oscillating form. Once the amount of TNT explosive is increased above a certain limit, deflection of the structure increases with a decreasing slope and converge to the failure deflection limit of the structure. RC BLAST gives a warning window showing the failure mass of the TNT explosive and the time of failure. By using the developed tool and RC BLAST, failure responses of two sample concrete columns subjected to blast loading are determined. Failure response analyses of the same sample columns are also performed by AUTODYN which is an explicit dynamic finite element solver. Free propagation of the blast wave is solved using the wedge modeling approach. By mapping the pressure and velocity information of high pressurized expanding gas and the wavefront to the 3D Euler domain, interaction of the blast wave with the structure is analyzed. The damage and failure is assessed in two stages; element failure and the column failure. For the element level failure, damage factor calculated by AUTODYN is used to decide on the failure of the element and element is allowed to degrade when it starts to be damaged and element fails when the damage parameter becomes equal to one. Concrete column failure is based on checking the existence of non-eroded elements which have damage factor

less than one in any section of the column. When all the elements in a section of the column erode, it is considered that the column can not sustain load anymore. By applying the two stage failure criterion, series of AUTODYN analyses are performed and failure masses of the TNT explosive is determined for the two sample columns studied. Failure explosive mass results obtained by the developed tool, RC Blast and AUTODYN show that although the developed tool and RC BLAST yields close results, they differ from AUTODYN significantly. To find out the reasons behind this difference, side-on overpressure results obtained by AUTODYN and Kingery's formulation, which predicts test results very closely, as seen in Figure 53, are compared. It is seen that AUTODYN yields lower side-on overpressure than obtained by the Kingery's formulation which is used in the developed tool. As a follow-up study, side-on overpressure predicted by the developed tool is reduced to match the side-on overpressure determined by AUTODYN. With the reduced side-on overpressure, failure masses of the TNT explosive are recalculated. It is seen that failure explosive masses determined by the updated side-on overpressure determined are much closer to the AUTODYN results. For further investigation of the possible source of the differences between the failure masses predicted by the developed tool and AUTODYN, uniformity of the load as a function of the stand-off distance is examined. It is seen that for the sample columns studied, the load is not uniform when the stand-off distance is 1 m, and load becomes more and more uniform when the stand-off distance is increased. For the 5m stand-off distance, failure masses of the TNT explosive calculated by AUTODYN and the developed tool are compared and it is seen that at high stand-off distance the difference in the failure masses diminishes due to the enhanced load uniformity. Despite some differences between the failure explosive masses calculated by the developed tool and by AUTODYN, they are not very off from each other. When the computational time spent is considered, the developed tool is very efficient compared to AUTODYN.

It is noted that the developed tool, which is based on the SDOF approach, calculates lower failure explosive mass than AUTODYN. In this respect, the calculated failure explosive mass forms the lower bound for the AUTODYN analysis. It can be

commented that the developed tool gives conservative values for the failure explosive mass. Thus, the developed tool can be used for fast estimation of the failure explosive mass and for more refined analysis, failure explosive mass determined by the tool can be used as the lower bound for AUTODYN analysis and the number of AUTODYN analysis to be performed for the more accurate determination of the failure explosive mass can be reduced significantly.

In conclusion, the developed tool can be used for the design of bridge-like structures in two main ways. Column dimensions can be optimized to withstand possible detonation threats. By taking advantage of the very fast analysis capability of the tool, preliminary design of the column can be performed. More refined analysis can be performed by AUTODYN, if necessary. In addition, the explosive mass and the detonation point to cause failure of the structure can be optimized by performing parametric analysis and examining the effective blast parameters.

Regarding the future work, single column analysis can be extended to the blast analysis of the whole bridge structure. Furthermore, the developed code can be improved to estimate the damage of the whole bridge structure for various detonation locations with the goal of determining the optimum detonation point to fail the whole bridge. Moreover, graphical user interface can be developed for the fast responding blast analysis tool. With such a graphical user interface, the ease of use of the tool can be substantially increased.

REFERENCES

- [1] Nago, T., Gupta, A., Ramsay, J., (2007). Blast Loading and Blast Effects on the Structures: An Overview. *Electronic Journal of Structural Engineering*. Volume 10 (EJSE Special Issue). Retrieved from <<http://www.ejse.org/Archives/Fulltext/2007/Special/200707.pdf>>.
- [2] Agrawal, A.K., Yi, Z. (2009). *Blast Load Effects on Highway Bridges*. New York, NY: American Society of Civil Engineers.
- [3] AASHTO. (2002). National Needs Assessment for Ensuring Transportation Infrastructure Security. < <http://security.transportation.org/sites/security/docs/NatlNeedsAssess.pdf>>.
- [4] Autodyn [Computer Software]. (2016). Retrieved from <<http://www.ansys.com/products/structures/ANSYS-Autodyn>>.
- [5] RC Blast [Computer Software]. (2016). Retrieved from <<http://www.rcblast.ca>>.
- [6] Collins, G., S., (2002). *An Introduction to Hydrocode*. Claeys, New York: Springer.
- [7] Sherkar, P., Whittaker, A.S., Aref, A.J. (2010). *Modeling the Effects of Detonations of High Explosives to Inform Blast-Resistant Design* (Technical Report MCEER-10-0009). New York, NY: MCEER Thrust Area 3, Innovative Technologies.

- [8] LS-Dyna [Computer Software]. (2016). Retrieved from <
<http://www.lstc.com/products/lstc-dyna>>.
- [9] Williamson, E.B., Bayrak, O., Davis, C., Williams, G.D. (2011)
“Performance of Bridge Columns Subjected to Blast Loads II: Results and
Recommendations” *J. Bridge Eng.*, pp. 586-594. 10.1061/(ASCE)1084-
0702(2011)16:6(586).
- [10] Fujikara, S., Bruneau, M., Lopez-Garcia, D. (2008). Experimental
Investigation of Multihazard Resistant Bridge Piers Having Concrete Filled Steel
Tube under Blast Loading. *Journal of Bridge Engineering*. Volume 13 (6). 586-
594. 10.1061/(ASCE)1084-0702(2008)13:6(586).
- [11] Matthews, T., Elwood, K. J., Hwang, S. J. (2007) *Explosive Testing to
Evaluate Dynamic Amplification during Gravity Load Redistribution for Reinforced
Concrete Frames*. 2007 ASCE Structures Congress, ASCE, Reston, VA.
- [12] Tokal-Ahmed, Y.M. (2009). *Response of Bridge Structures Subjected to Blast
Loads and Protection Techniques to Mitigate the Effect of Blast Hazards on Bridges*.
The State University of New Jersey, New Jersey, USA.
- [13] ELS [Computer Software]. (2016). Retrieved from <
<http://www.extremeloading.com>>.
- [14] Chock, J.M. (1999). *Review of Methods for Calculating Pressure Profiles of
Explosive Air Blast and its Sample Application*. Virginia Polytechnic Institute and
State University, Blacksburg, Virginia, USA.

- [15] Nastran [Computer Software]. (2016). Retrieved from <
<http://www.mscsoftware.com/product/msc-nastran>>.
- [16] Matthews, D.S. (2008) *Blast Effects on Prestressed Concrete Bridges*.
 Washington State University, Washington DC, USA.
- [17] Oswald, C., Bazan, M. (2014) *Comparison of SDOF Analysis Result to Test
 Data for Different Types of Blast Loaded Components*. Structures Congress 2014: pp.
 117-130. DOI: 10.1061/9780784413357.012 .
- [18] Driels, M., R., (2013). *Weaponneering: Conventional Weapon System
 Effectiveness Second Edition*. Reston, VA: Greenham.
- [19] Williamson, E.B., Bayrak, O., Williams, G.D. (2010) *Blast-Resistant
 Highway Bridges: Design and Detailing Guidelines* (NCHRP Report 645).
 Washington, D.C.: Transportation Research Board.
- [20] Smith, P.D., Hetherington J.G. (1994). *Blast and Ballistic Loading of
 Structures*. Shrivenham, England: CRC Press.
- [21] Remennikov, A. (2007). *The State of the Art of Explosive Loads
 Characterisation*. University of Wollongang, Australia.
- [22] U.S. Department of the Army (1990) *Structures to Resist the Effects of
 Accidental Explosions* (Technical Manual 5-1300). Alexandria, VA: Department of
 the Army, the Navy and the Air Force.
- [23] Dusenberry, D.O. (2010). *Handbook for Blast-Resistant Design of Buildings*.
 Hoboken, NJ: John Wiley & Sons Inc.
- [24] Needham, C.E. (2010). *Blast Waves*. New York, NY:Springer-Verlag.

- [25] Kinney G. F., Graham K.J. (1985). *Explosive Shocks in Air*. Berlin, Germany: Springer.
- [26] Brode H.L. (1955). *Numerical Solution of Spherical Blast Waves*. New York, NY: Springer.
- [27] Newmark, N.M., Hansen R.J. (1961). *Design of Blast Resistant Structures: Shock and Vibration Handbook*. New York, NY: McGraw Hill.
- [28] Mills, C.A. (1987). *The Design of Concrete Structures to Resist Explosions and Weapon Effects*. Proceedings of the 1st International Conference on Concrete for Hazard Protections, Edinburgh, UK, pp.61-73.
- [29] Kingery, C.N. (1966). *Air Blast Parameters versus Distance for Hemispherical TNT Surface Bursts* (Technical Report No: 1344). Aberdeen, Maryland: Ballistic Research Laboratories.
- [30] Boris, G. (2004). *Translation from Russian to English the Book: Blast Effects Caused by Explosions* (Technical Report N62558-04-M-0004). London, England: European Research Office.
- [31] Glasstone, S., Dolan, P.J. (1997). *The Effects of Nuclear Weapons*, 3rd Edition. Washington DC: United States Department of Defense.
- [32] U.S. Army Corps of Engineers (2008). *Structures to Resist the Effects of Accidental Explosions* (UFC 3-340-02). Washington, DC: Air Force Civil Engineer Support Agency.

- [33] Altunlu, K. (2008). *Safety Assessment of R/C Columns Against Explosive Attacks by Vehicle or Human from Exterior*. Middle East Technical University, Ankara, Turkey.
- [34] Karlos, V., Solomos, G. (2013) *Calculation Of Blast Loads For Application To Structural Components* (Jrc Technical Reports 32253-2011). Ispra, Italy: Joint Research Center.
- [35] Payne, C.M. (2010). *Principles of Naval Weapons Systems*. Annapolis, MD: US Naval Institute Press.
- [36] Bulson, P.S. (1997). *Explosive Loading of Engineering Structures*. New York, NY:Chapman and Hall.
- [37] Miller, P. (2004). *TowardstheModelling of BlastLoads on Structures*. University of Toronto, Ontario, Canada.
- [38] Rahman, S.,Timofeev, E. (2007). *PressureMeasurements in Laboratory-ScaleBlastWaveFlowFields: Review of Scientific Instruments*, Vol. 78.
- [39] U.S. Army Engineer Research and Development Center (2003). *Bridge and Tunnel Vulnerability Workshop* sponsored by the Federal Highway Administration Office of Bridge.
- [40] Tedesco, J. (1999). *Structural Dynamics: Theory and Approach*. Menlo Park, CA: AddisonWesleyLongman.
- [41] Malvar, L.J., Crawford, J.E. (1998). *Dynamic Increase Factors for Concrete*. 28th Department of Defence Explosives Safety Seminar.

- [42] American Society of Civil Engineers (1997). *Design of Blast Resistant Buildings in Petro-chemical Facilities*. Reston, Virginia: ASCE.
- [43] Biggs, J. (1964). *Introduction to Structural Dynamics*. New York, NY: McGraw Hill.
- [44] Budynas, R.G., Nisbett, J.K. (2013) *Shigley's Mechanical Engineering Design*. New York, NY: McGraw Hill.
- [45] Brannon, M. R., Leelavanichkul, S. (2009). *Survey of Four Damage Models for Concrete* (Technical Report SAND2009-5544). Livermore, CA: Sandia National Laboratories.
- [46] Shin, J., Whittaker, A., Aref, A. (2015). Near-field Blast Assessment of Reinforced Concrete Components. *International Journal of Protective Structures*. Volume 6(3). pp. 487-508.

APPENDICES

A. VIEW OF THE DEVELOPED TOOL

Detonation and Exp. Information											
X [m]	Y [m]	Z [m]	Weight [kg]	Weight [kg]	TNT Equivalency	M/C	Equivalent Weight [kg]	Equivalent Weight [kg]	Equivalent Weight for M.S.R. [kg]	Equivalent Weight for M.S.R. [kg]	Critical Height for M.S.R. [m]
0	0	10	90.1885483	189.16	1	0	90.1885483	189.1569533	148.0592735	128.613932	23.809014

Member Position															
X [m]	Y [m]	Z [m]	Delta_X [m]	Delta_Y [m]	Delta_Z [m]	Average Stave-off [m]	Average Scaled Distance [m/kg ^{0.33}]	Average Scaled Distance [m/kg ^{0.33}]	Average Scaled Distance [m/kg ^{0.33}]	Average Side-on Pressure [kPa]	Average Dynamic Pressure [kPa]	Epsilon	Alpha_Critical	Angle of Incidence for Bottom	Mach Stem Formed?
1	0	0	2	2	20	1	0.22623748	0.371802558	14707.85611	15078.67704	0.0068401	18.8821148	3.7102811	NO	

Material and Geometry Prop.																				
Reinf. Conc = 1;	Flexural = 1;	Shear = 2	Mass of Member [kg]	Weight of Member [kN]	Elastic Section Modulus [m ³]	Plastic Section Modulus [m ³]	Moment of Inertia [m ⁴]	Plastic Moment [kNm]	DIF for Yield	DIF for Ultimate	SIF	Age Factor for Concrete	Static Yield Strength of Conc [psi]	Dynamic Yield Strength of Conc [psi]	Dynamic Yield Strength of Conc [Pa]	Young Modulus of Conc [Pa]	Static Yield Strength of Steel [Pa]	Dynamic Yield Strength of Steel [Pa]	Dynamic Yield Modulus of Steel [Pa]	Young Modulus of Steel [Pa]
1	1	1	182000	211.8214407	4.333333333	5.333333333	7.248407	1.25	1.25	1.1	1.1	5000	790815	54476593	3.48E+10	3.00E+08	4.13E+08	58889.37561		

Loading and F.C.			
Beam & Column = 1;	Fixed = 1;	Load Factor	Mass Factor
Shear = 2	S.S = 2	0.64	0.0

SHEAR STRENGTH												
Reinf. Radius [mm]	Offset in Depth [mm]	Offset in Width [mm]	Effective Depth [mm]	Spacing [mm]	Reinf. Bar Area [m ²]	Shear Str. Of Concrete [kN]	Shear Str. Of Reinf. Bars [kN]	Shear Str. Of Reinf. Conc. [kN]	Shear Str. Of Steel [kN]	Uniform Load Intensity [kN/m ²]	Dynamic Reaction [kN]	Shear Failure ?
10	50	50	1800	1800	50	0.4864784	893.0792139	1107.823864	2102.897208	1278.122	3087.413387	YES

Total Force on Member [N]																				
Total Force on Member [N]	Total Force on Member [N]	Total Impulse on Member [N-s]	Total Impulse on Member [N-s]	Max. Elastic Deflection [mm]	Ryield [N]	Ryield SOOF [kN]	Ryield SOOF [kN]	Stiffness [N/mm]	Stiffness SOOF [N/mm]	Stiffness SOOF [kN/m]	Period of Member [s]									
3.90E+08	3.77E+08	8.48E+04	1824628.145	1187763	7.10E+08	3.24889387	2.81E+07	1.88E+07	4178.382019	7.12E+06	4.57E+06	2.61E+04	0.028793	FALSE	334.25419	381.97888	117.32383328	2.18791485	0.218751468	1

Number of Division of Member											
Mach Stem Region [TPM]	Angle of Incidence for M.L.1	Angle of Incidence for M.L.2	Angle of Incidence for M.L.3	Angle of Incidence for M.L.4	Angle of Incidence for M.L.5	Angle of Incidence for M.L.6	Angle of Incidence for M.L.7	Angle of Incidence for M.L.8	Angle of Incidence for M.L.9	Angle of Incidence for M.L.10	Angle of Incidence for M.L.10
10	0	81.8280283	81.8888874	78.6900875	71.5620212	43	43	71.5620212	78.6900874	81.8888874	81.8280283

Force on Each Disc Member [N]											
Impulse [N-m]	Impulse/Area [kN-m/m ²]	Force on Each Disc Member [N]	Impulse [N-m]	Impulse/Area [kN-m/m ²]	Force on Each Disc Member [N]	Impulse [N-m]	Impulse/Area [kN-m/m ²]	Force on Each Disc Member [N]	Impulse [N-m]	Impulse/Area [kN-m/m ²]	Force on Each Disc Member [N]
3275427.28	71.14689.99	16078436.9	48782159.5	91281177	93261177	49782159.5	16078436.9	16078436.9	3275427.28	71.14689.99	16078436.9

B. DERIVATION OF MASS AND LOAD FACTORS

In the study of Biggs [43], load and mass factors are given in Table 15. In Appendix B, derivation of load and mass factors are given for the plastic regime. Uniformly loaded structure fixed at both ends is shown schematically in Figure B1.

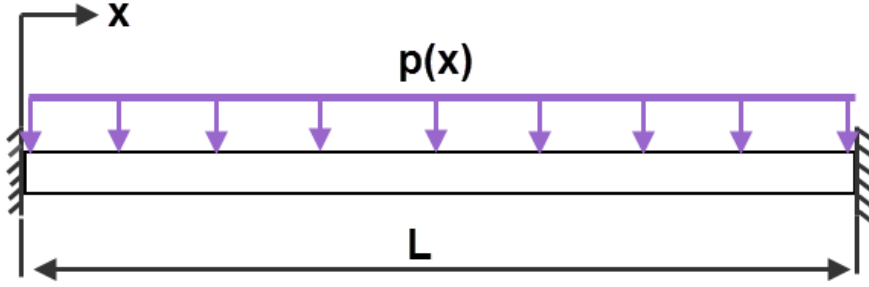


Figure B1. Uniformly Loaded Structure Fixed At Both Ends

LOAD FACTOR FOR THE UNIFORMLY LOADED FIX-FIX BEAM

Load factor is given by [43],

$$K_L = \frac{F_E}{F} \quad (B1)$$

where K_L is the load factor, F_E is the equivalent force on structure and F is actual force on structure. Equivalent force is given by,

$$F_E = \int_0^L p(x)\phi(x)dx = \int_0^L p_0 \phi(x)dx \quad (B2)$$

where $p(x)$ is force per unit length along the structure, $\phi(x)$ is shape function. Shape function is given by Equation (B3),

$$\phi(x) = \frac{\Delta(x)}{\Delta_{max}} \quad (B3)$$

For a structure in the plastic regime, deflected shape is given in Figure B2.

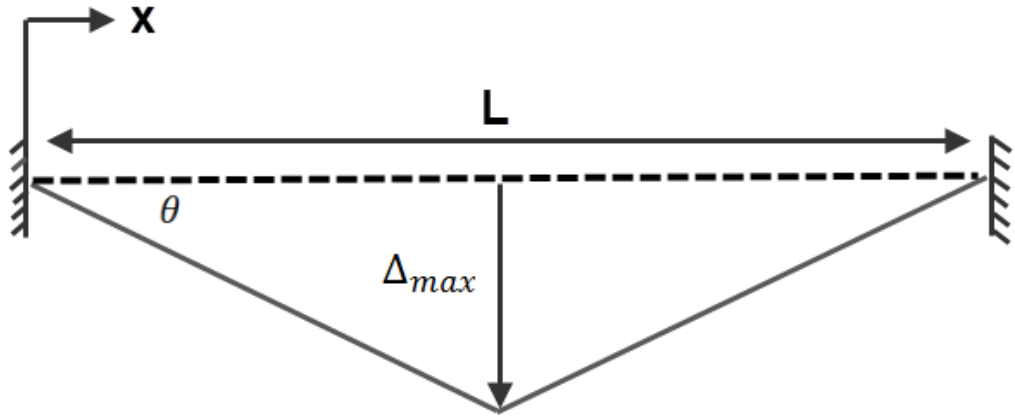


Figure B2. Deflected Structure in the Plastic Regime

$\Delta(x)$ is given by Equation (B4)

$$\begin{aligned} \Delta(x) &= x \tan \theta \quad \text{for } x \leq L/2 \\ \Delta(x) &= (L - x) \tan \theta \quad \text{for } x \geq L/2 \end{aligned} \quad (B4)$$

and Δ_{max} is given by Equation (B5).

$$\Delta_{max} = \frac{L}{2} \tan \theta \quad (B5)$$

Thus, shape function $\phi(x)$ is computed as,

$$\begin{aligned}\phi(x) &= \frac{\Delta(x)}{\Delta_{max}} = \frac{x \tan \theta}{\frac{L}{2} \tan \theta} = 2 \frac{x}{L} \quad \text{for } x \leq \frac{L}{2} \\ \phi(x) &= \frac{\Delta(x)}{\Delta_{max}} = \frac{(L-x) \tan \theta}{\frac{L}{2} \tan \theta} = 2(1 - \frac{x}{L}) \quad \text{for } x \geq \frac{L}{2}\end{aligned}\tag{B6}$$

Load factor is given by Equation (B7)

$$K_L = \frac{F_E}{F} = \frac{\int_0^{L/2} p(x)\phi(x)dx + \int_{L/2}^L p(x)\phi(x)dx}{p_0L} = 0.5\tag{B7}$$

MASS FACTOR FOR UNIFORMLY LOADED FIX-FIX BEAM

Mass factor is given by [43],

$$K_M = \frac{M_E}{M}\tag{B8}$$

where K_M is the mass factor, M_E is the equivalent mass of structure and M is the actual mass of structure. Equivalent mass is calculated as,

$$M_E = \int_0^L m(x)\phi^2(x)dx\tag{B9}$$

where $m(x)$ is the mass per unit length along the structure and $\phi(x)$ is the shape function given by Equation (B6). Hence, mass factor is calculated as,

$$K_M = \frac{M_E}{M} = \frac{\int_0^{L/2} m(x)\phi^2(x)dx + \int_{L/2}^L m(x)\phi^2(x)dx}{mL} = 0.33\tag{B10}$$